Energy Environment and Sustainable Development

Research Infrastructures

Scientific correspondent : Gilles Ollier

DGLab

The Deep Geodynamic Laboratory - Gulf of Corinth Project

Contract nb EVR1-CT-2000-40005

www.corinth-rift-lab.org

Final Report; November 2003

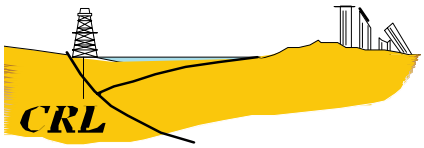

Period covered : June 1st, 2002 – June 30, 2003

Coordinator F.H. Cornet ; Institut de Physique du Globe de Paris
4 place jussieu, 75 252, Paris cedex 05, France ; Email cornet@ipgp.jussieu.fr-

Participants information:

N°	Institution/Organisation	Street name and number	Post Code	Town/City	Country Code	Title	Family Name	First Name	Telephone N°	Fax N°	E-Mail
1	Institut de Physique du Globe de Paris (IPG-P) Lab. de Mécanique des roches	4 Place Jussieu	75252	Paris	F	Dr	Cornet	François Henri	(33-1) 44 27 38 97	(33) 144 27 38 94	cornet@ipgp.jussieu.fr
2	National and Kapodistrian University of Athens (NKUA), Seismological Laboratory	Panepistimioupolis, Zografou	157 84	Athens	EL	Dr	Papadimitriou	Panayotis	(30-1) 7247445	(30-1)7243217	ppapadim@geol.uoa.gr
3	Université de Droit, d'Economie et de Sciences d'Aix Marseille, CEREGE-Dept of Geophysics	Rd 543, Bp 80	13545	Aix-en-Provence	F	Dr	Pezard *	Philippe	33(0)4-67-14-93-10	33(0)4-67-14-93-08	pezard@dstu.univ-montp2.fr
4	GeoForschungsZentrum Potsdam (GFZ-Otsdam) Geomechanics and Geotechnology"	Telegrafenberg	14473	Potsdam	DE	Pr	Borm	Günter	+49 331 288 1500	+49 331 288 1502	gborm@gfz-potsdam.de
5	Institut Français du Pétrol (IFP)e, Division Géologie et Géochimie	1&4 Avenue de Bois Préau	92852	Rueil Malmaison	F	Dr	Moretti	Isabelle	++33-1 47 52 61 91	++33-1 47 52 70 67	Isabelle.Moretti@ifp.fr
6	Università di Catania (U.Catania), Dipartimento di Scienze Geologiche	Corso Italia 55	95129	Catania	I	Pr	Cancarini Ghisetti	Francseca	+39-095-7195722	+39-095-7195728	ghisetti@tin.it
7	University of Patras (UPSL), Seismological Laboratory	Rio, University Campus	261 10	Patras	EL	Pr	Tselentis	Gerasimos	+3061997556	+3061990639	Tselenti@upatras.gr
8	The University of Edinburgh, (U. Edin) Department of Geology and Geophysics	West Mains Road	EH 93 JW	Edinburgh	UK	Pr	Main	Ian	0131-650-4911	0131-668-3184	ian.main@glg.ed.ac.uk
9	Ecole Nationale des Ponts et Chaussées – CERMES	6 et 8, Avenue Blaise Pascal	77455	Marne-La-Vallée	F	Dr	Sulem	Jean	+33 1 64 15 35 65	+33 1 64 15 35 62	sulem@cermes.enpc.fr

*Now at : Université de Montpellier 2, Laboratoire de Tectonophysique, ISTEEM/cc49, 34095 Montpellier cedex 5

SECTION 1

MANAGEMENT AND RESOURCE USAGE SUMMARY

1.1. OBJECTIVES OF THE REPORTING PERIOD

The DGLab project is part of a set of projects clustered under the generic name "Corinth Rift Laboratory", some of them being funded by the European Commission (DGLab, CORSEIS, 3F-Corinth, AEGIS, ASSEM) some other ones by national funds (PLOUTON for Greece, GDR-Corinth for France, GRECO for Germany). In particular, DGLab has contributed to the development of the regional CRL seismic network, while CORSEIS and the French (CNRS supported) GDR-Corinth provided the necessary funds for the maintenance of this network. The drilling operation for the 1000 m deep well AIG10 was mostly funded through DGLab, but received significant support from the International Continental Drilling Program (ICDP) and some from 3F-Corinth.The core analysis, borehole logging and Vertical Seismic Profiles, as well as the hydraulic reconnaissance have been co-funded by DGLab, 3F-Corinth and the German (DFG supported) GRECO project.

This reporting period, June 1st 2002-June 30 2003, is the last one of the DGLab contract. It covers the drilling and coring of the active Aegion fault, the petrographic and structural analysis of retrieved cores together with the performing of various in situ and laboratory observations meant to determine the hydro-mechanical characteristics of the material intersected by the well. It presents finally the installation of permanent monitoring equipment and discusses the sharing of data.

A major result of drilling the Aegion fault is the identification of the role of the fault as a hydraulic barrier and the existence of a karstic aquifer, below the fault, from 780 m down to at least 1000 m. These results have induced significant changes in the original plans and generated unforeseen difficulties, because of the flow produced by the karst. Yet the interstitial pressure below the fault and the acoustic activity are presently being monitored. Results demonstrate the importance of such permanent monitoring facilities and the necessity to keep them running for at least 4 to 5 years. Indeed, given the regional seismic activity, such a period of observation should deliver data for a few magnitude 4 earthquakes and possibly for one magnitude 5.

This section summarizes the major operations run in the various workpackages, for the current reporting period. For each workpackage we outline required adaptations imposed by site conditions as well as interactions with other ongoing projects. In fact, it is only thanks to the clustering of the various projects that important results have been obtained despite unforeseeable conditions associated with the geological uncertainty of the project. Also, this has required some difficult management decisions, as outlined in each of the workpackage presentations.

Presently, a unique European research facility is being developed for an in situ investigation on Earthquake sources and seismic hazard mitigation, but also on interactions between faults and regional flow. It involves both the development of the local facility itself but also the build up of an efficient database common to all CRL participants, accessible by all concerned institutions. It has generated a forum where the various concerned European teams discuss their results. It provides data and support for Ph.D students and Postdoc fellows from at least six different European countries.

1.2. SCIENTIFIC/TECHNICAL PROGRESS MADE IN THE DIFFERENT WORKPACKAGES ACCORDING TO THE PLANNED TIME SCHEDULE:

As explained in the second report, the success of the DGLab project, rested on the successful drilling of a 1000 m deep well intersecting the Aegion fault within mesozoic carbonate rocks, below the quaternary conglomerates. Preliminary geophysical and geological reconnaissance outlined the necessity to drill further to the north of the originally targeted public land. Very fortunately, the Koronaki family, owner of a large piece of land where an old soap

factory was destroyed during the Aegion earthquake, accepted to give some of their land for the project. Given the uncertainty on the geological and geophysical data and given some simple reasoning on fault geometry, it was considered safer to place the drilling on land available, i.e. some 130 m closer to the fault, rather than precisely in the area initially recommended by the geophysical and geological reconnaissance (but where no land was available). It is recognized today that the drill site could not have been situated in a more optimum location because of both, the geological and the surface site conditions.

1.2.1. Work Package 1: Reconnaissance of Aigion and Heliki Faults (Univ. of Patras, IFP and IPGP)

This phase was completed during the first two reporting periods. In particular, it was proposed that the dip of the fault would be somewhere between 60 and 65 °, when a value of 61° has been effectively observed. Similarly, on the footwall (south compartment) the top of the carbonate rocks had been planned to be somewhere between 720 m (according to seismic reflection analysis) and 660 m (according to seismic refraction data) below ground surface, when the VSP run in the well, a posterirori, have given a value of 500 to 520 m from sea level (620 m from ground level). So it may be concluded that preliminary reconnaissance was somewhat successful. Yet drilling results have outlined the existence of radiolarite formations and their very significant impact on the regional hydrogeology. This aspect had not been put forward by the teams in charge of the initial DGLab reconnaissance but had been outlined by some of the geological reconnaissance work conducted by other teams working for CRL.

This is certainly one of the important management conclusions for CRL: It is essential that the various teams working within the CRL structure share their data and do not work independently. Each project may have its own self-supporting logic and resources. But it is absolutely necessary to set-up a permanent technical and administrative structure for integrating the outcome of the various independent projects in order for the whole CRL consortium to benefit fully from the various independent efforts.

1.2.2. Work Package 2 : Drilling & Coring through Aigion Fault (GFZ-Potsdam & IPG-P)

Because the drilling operation was central to both, the DGLab project and the 3F-Corinth project, it was decided to combine drilling resources from both projects in order to fulfil the program objectives. Yet, 250 000 Euros were still missing in January 2002 and an application was prepared for getting ICDP support. No letter of formal agreement had been received from ICDP, when it became urgent to start the AIG10 drilling (April 2002). Only a phone call to F.H. Cornet, indicated that the proposal had been successfully examined. However, the review committee considered that the preliminary geophysical and geological reconnaissance was far from being conclusive and they recommended granting the support of 250 000 dollars only after the project would have proven successful.

This raised a very delicate management situation, for someone had to take the risk of failure, i.e. cover costs not covered by ICDP in case of failure. A group of three persons discussed at regular intervals and every time it was necessary, during the follow up of the drilling operations. This group included : G. Borm (partner in charge of WP2 within DGLab and Principal Investigator for the ICDP contribution), F.H. Cornet (coordinator of DGLab, partner in charge of drilling projects in 3F-Corinth and director of GDR-Corinth), Isabelle Moretti (coordinator of 3F-Corinth and partner in charge of WP4 in DGLab). It was decided to use the French GDR Corinth yearly funds together with the funds available for other drilling activities in 3F-Corinth, to cover this risk. This provided enough funds for GFZ to launch an initial drilling job order for an

uncored, rotary drilled, 900 m deep well. If the drilling would be successful and intersect the fault within the carbonate rocks before reaching 900 m, then the ICDP funds would be secured and the drilling contract would be extended in accordance. In case of failure, there would not be any cored section and a new decision would have to be taken.

Upon reaching the limestone at 696 m below sea level, the initiation of the coring activity was decided to start at 710 m. When the fault was intersected at 761 m, it became clear that the ICDP funds would be secured. This left enough funds to core an extra 40 meters and then resume rotary drilling down to 940 m.

It was then decided to deepen the well from 940 m down to 1000 m, to conduct the complete set of planned logs and to conduct a water production test on the whole uncased well length. This necessitated an additional 98 000 Euros, which were shared between DGLab and 3F-Corinth (mostly IPG-P funding) :

1. The drilling of the second well AIG5 was cancelled, because of lack of funds.

2. The drilling of AIG7, planned in the 3F-Corinth project, was also cancelled

3. All monitoring equipment planned for AIG7 was moved into the well TRI-5, planned in Trizonia Island, on the northern shore of the rift.

Finally, the total drilling costs for AIG10 reached about 860 000 Euros, when only 450000 had been planned originally. It is outlined here that it is only through the combining of resources from DGLab, 3F-Corinth and GDR-Corinth, that the drilling of AIG10 has been successful. Without the CRL cluster, DGLab would never have been able to fulfil its original objectives.

The discrepancy between available funds and funds effectively required for completing the drilling operation has been the cause for most of the delay of the project. This discrepancy came from the default of the Greek drilling company that had helped to prepare the cost estimate for the drilling operation, during the initial budget preparation. Clearly, for future work, a more detailed preliminary cost appraisal will have to be prepared when deep drilling operations are involved. This will require a specific budget.

1.2.3. Work Package 3 : Logging & Downhole Measurements - run jointly by DGLab-Corinth (GFZ-Potsdam, IPG-P and CEREGE), 3F-Corinth (IPG-P), and German GRECO (GFZ & Univ. Karlsruhe)

Because the well AIG-5 has been cancelled, the logging planned for partner 2 (CEREGE) in this well, was displaced to well TRI5, in Trizonia island. Indeed only an electrical imaging log had been planned initially in TRI5, for this well was designed only for stress measurements.

Partner 4 (GFZ-Potsdam) and Univ. of Karksruhe have run their logs and hydraulic reconnaissance tests, as funded by the German GRECO program. In addition, GFZ was able to secure some extra funds from the German DFG for running a temperature log, one year after drilling, when the temperature had stabilized in the well.

Partner 5 (IFP) was able to run jointly with partner 7 (UPSL) and partner 1 (IPG-P) the planned vertical seismic profiles. These confirmed results from seismic refraction reconnaissance run in winter 2001.

Partner 1 (IPG-P) commissioned the company Schlumberger for running various imaging logs, under 3F-Corinth funding. Then he ran a 3 days water production test, while the drill rig was

still on site with the drill string assembly inside the casing. It was decided then, to postpone the planned stress measurements so as to conduct these tests just before installing the permanent monitoring system described in workpackage 6. Indeed, the stress measurement system is planned for operating in water rather than in mud. Rather than adapting the system to mud conditions, it was considered more appropriate to wait that the well be filled with water.

But these stress measurements could not be run later because flow conditions in AIG10 well did not match preliminary measurements. Flow was so fast (larger than 400 m^3/h) that it carried solid particles of various sizes, reaching 10 cm in diameter for the largest. This rendered completely insecure the lowering of the stress measuring device.

1.2.4. Workpackage 4 : Core analysis : Petrofabric, Geochemistry implications and Physical properties; run jointly by DGLab (IFP & Univ. of Catania) and 3F-Corinth (IFP)

IFP and GFZ-Potsdam participated in the continuous geological follow up of the AIG10 drilling activity. Continuous geological logs have been established. IFP was more specifically in charge of the coring program. 100 m of nearly continuous cores have been retrieved, including within the fault gauge. They have been archived. Interested teams from the various CRL participating groups have received samples for their respective petrofabric and structural analysis.

1.2.5. Workpackage 5 : Core Analysis : Mechanical and Hydraulic Characterization (Univ. of Edinburg & CERMES)

The continuous coring of the fault material has provided samples of excellent quality for laboratory work. These have been tested in the laboratory for both their mechanical (CERMES) and their hydrological (Univ. of Edinburgh) properties. This set of tests completed the series run on samples collected from surface outcrops and provide necessary data for later numerical modelling. They clearly show the role of hydraulic barrier for the fault. They raise the interesting question of possible thermo-mechanical coupling during dynamic slip.

1.2.6. Workpackage 6 : Downhole Instrumentation and Continuous Data Acquisition – run jointly by DGLab (IPG-P (with the support of DT-INSU), Univ. of Patras & Univ. of Athens) and CORSEIS (IPG-P and Univ. of Athens)

The DGLab participation to the development of the Corinth Rift Laboratory research infrastructure includes :

Participation to the set up of the CRL seismic monitoring network;

Installation of a permanent downhole monitoring facility across the Aegion fault, in well AIG10.

During this reporting period, partner 2 (NKUA) has participated to the maintenance of the CRL seismic network and to the analysis of the results (part of the database includes time records of seismic events, determination of hypocenters, magnitudes and focal mechanisms). This work is integrated with that conducted by CORSEIS and GDR-Corinth.

The second main activity of WP6 involved the development and installation of the downhole permanent monitoring equipment. This encompassed the following activities :

1. Site development (installation of shelters with water, electricity and phone line, together with water evacuation system for accommodating flow

produced by the well in case of unforeseen failure of the wellhead assembly)

2. Cleaning and conditioning of the well AIG10
3. Installation of equipment in the well and verification of its performances
4. Demonstration of the efficiency of the permanent monitoring system.

The cleaning and conditioning of the well was considered to be a fairly simple operation. It was combined with the drilling of well TRI5, in Trizonia. For organisational reasons, it was considered more efficient to start with the drilling in Trizonia and to follow up with the cleaning in Aegion. Unfortunately, the drilling in Trizonia encountered difficulties that resulted in the borehole being finished only in mid June 2003. This prompted an application for a one month extension of the DGLab contract. But when the drilling in Trizonia was terminated, the driller did not move to the Aegion site as planned in the contract, so that work was postponed till September 2003, after the DGLab contract had officially been terminated.

In September 2003, despite some difficult conditions associated with the large water production of the well, it has been possible to install a dynamic and a static pressure transducer together with a hydrophone and a 3 components accelerometer within the upper top section of the casing in well AIG10. This insures a continuous monitoring of the downhole pressure (casing is cemented down to 708 m) together with that of local instabilities. Hence, the system provides means to monitor the pressure around the Aegion fault and to correlate it with the microseismic activity as monitored with the CRL network.

The combination of tools provides a unique way to monitor pressure variations with frequencies ranging from the continuous signal up to 1 Khz. Given the presence of the karstic system in the lower section of the well, it is anticipated that very original data will be gathered with this system, if it can be maintained for at least 4 to 5 years in order to cover properly seasonal variations. However, the downhole seismometer and accelerometer have not been installed yet, nor has the fault been isolated, hydraulically speaking. Hence it is hoped that it will be possible to pursue, in an accompanying program, the well completion so as to conduct the stress measurements which are still lacking and to install the complete monitoring system, as originally planned.

1.3. MILESTONES AND DELIVERABLES OBTAINED

1.3.1. WP1- site reconnaissance

Deliverables D1.1, D1.2, D1.3 were produced at the end of the first reporting period, together with site location recommendation.

Milestones: Results from the drilling operation have confirmed results from seismic refraction analysis on the depth of carbonate rocks for the southern compartment of the fault. They have also confirmed the fault dip. However, estimates of the fault offset based on local geological observations have not been confirmed yet. Present results provide only a minimum value for the offset which has been found equal to150 ± 20 m.

1.3.2. WP2 – Drilling and coring

Deliverable D2.1. The drilling of the 1001 m deep AIG10 well has been successfully completed. The Aigion fault has been intersected at 761 m, within the targeted carbonate formation. Coring through the fault has been successful (see next section)..

Deliverable D2.2 Well AIG5 has been cancelled because of absence of funds after the drilling of well AIG10. It would be interesting to consider drilling this well, in a future project, so as to conduct interference tests in the material above the fault, and possibly within the fault itself.

Milestones : A unique set of continuous cores through an active fault has been made available to the scientific community**.** The well AIG10 is ideally located for permanent monitoring of interstitial pressure below the Aigion fault

1.3.3. WP3 Logging and downhole measurements

Deliverable D3.1 A quite complete set of logs has been obtained for the well AIG10. It includes borehole imaging (acoustic and electrical) and Dual Sonic Imager (DSI) logs in the uncased section of the well together with electrical and sonic logs for the complete well length. A thermal log has been obtained one year after the completion of the drilling operation. Unfortunately partner 3 (CEREGE) could not conduct any geophysical logs in well TRI5 because of borehole stability difficulties

Deliverable D3.2 University of Karlsruhe conducted hydrological reconnaissance tests .IPGP ran a 3 days water production test within the complete open hole section of the well, when the drill string assembly was still in place in the well. It was followed by various production periods with the well completely free. These tests demonstrate the role of hydraulic barrier for the Aegion Fault.

Deliverable D3.3. Stress measurements were planned to be conducted just after drilling. But, after conducting the water production test in the uncased section of the well, the water was displaced with mud. Since the initial hydraulic reconnaissance had evidenced a water production flow rate equal to 50 m^3/h, it was felt more appropriate to wait that the well be placed again in water production conditions for the stress measurements. But when the well was placed back to water producing conditions, it turned out that the flow rate was larger by a factor of 9 as compared to that measured a year earlier. This prevented any measurement.

Deliverable D3.4 Vertical seismic profiles have provided a satisfactory verification of refraction data gathered in WP1. They also yield an estimate of the fault offset which demonstrates the present activity of the fault and justify a posteriori the choice of the Aegion fault for installing our permanent monitoring equipment.

Milestones ; Electric and acoustic boreholes images have been obtained in the very same intervals covered by coring and this provide a unique data set for calibrating these logging methods. In addition, the DSI was run under various borehole pressure conditions and this provided another unique set of data on the non-linear response of carbonate rocks. Finally images of the karstic fractures below the fault are the only source of information presently available on this unique hydrological situation. A detailed seismic velocity profile has been established for the upper 1000 m of the hanging wall of Aegion fault. It yields an accurate estimate of the fault offset.

1.3.4. WP4. Core analysis : Geology, Geochemistry and physical properties of fault material

Deliverables D4.1 and D4.2 Cores have been scanned and archived. Thin sections have been prepared and analysed. Data are available from partner 5 (IFP). Together with the borehole imaging logs, this set provides a unique set of data for better understanding the interaction between faults and fluids. Cores are still being analysed by various teams from GDR Corinth.

Milestones : The set of data retrieved from the cores provides a new insight on fault and fluid interactions. It demonstrates the existence of repeated shear and healing phases with progressive sealing of the fault gauge after slippage occurred.

1.3.5. WP5 : Core analysis – Mechanical and hydraulic characterization

Deliverables D5.1 **and D5.2** The new permeameter, which combines measurements of fluid pressure and chemistry has been built and commissioned. The Triaxial cell for mechanical testing is operational and the testing procedure has been validated on both analogue and cored material. Both equipments have provided unique data on the mechanical and hydro-mechanical behaviour of the various materials which act as flow barriers. They also have outlined interesting characteristics with respect to thermo-mechanical coupling.

Milestones : The hydro-mechanical characteristics of the Aegion fault gauge has been obtained. These results outline the role of compaction has well as a potentially interesting thermo-mechanical coupling effect. The hydraulic properties of main hydraulic seals have been determined.

1.3.6. WP6: Downhole instrumentation and continuous data acquisition

Deliverable D6.1 The subsurface seismic monitoring network is operational,.

Deliverables D6.2 and D6.3 The complete set of downhole permanent monitoring instruments have been built and tested, together with the data acquisition system. However, given the high production flow rate, only one packer equipped with dynamic and static pressure transducers, 3component accelerometer, a compass and a hydrophone, has been set up within the top of the casing. Today, the downhole pressure is continuously monitored together with acoustic activity. This provides unique data on the hydraulic response of the karst to various mechanical stimulations, including earth and ocean tides, as well as local earthquakes. It has already provided an interesting example of unstable motion followed up by a more pronounced stable volume variation. Data will be stored in the data base to be developed by MediaFrance, in Toulouse.

Milestone: A local seismic network together with a downhole interstitial water pressure monitoring system is operational. The downhole pressure monitoring concerns an extensive artesian karstic aquifer below the Aegion fault. Present results indicate that the facility provides a unique opportunity for monitoring both signals within the solid and within the fluid components. It is expected to provide unique data on diffusion phenomena covering various time domains ranging from seasonal periods up to the kilohertz.

Efforts are still underway to build up a data base common to all CRL projects were these data will be freely accessible to the concerned community. This remains a key objective which, hopefully will get implemented progressively. The AEGIS project provides already a significant educational support that helps in the design and development of this database.

1.4. DEVIATIONS FROM THE WORK PLAN OR/AND TIME SCHEDULE AND THEIR IMPACT TO THE PROJECT

While it was originally planned to install the downhole monitoring equipment by the end of year one (October 2001), in practice only some part of this monitoring equipment (although the most important part of it) was installed by September 2003, i.e. with a two years delay. This delay resulted in part from the geological reconnaissance which indicated that the fault dip was closer to 60° than the initially anticipated 70°. This required the search of private land which implied a four

month delay. The main cause of delay, however, was the failure of the Greek drilling company to provide a technically acceptable drilling scheme for the budget originally proposed during contract preparation. This implied an extra year delay because of the necessity of looking for additional funding. The final delays resulted from the unexpected flow conditions encountered in the carbonate rocks intersected by the well below the fault. This implied leaving the well filled with mud for stability considerations and the necessity to bring a work over rig for cleaning the well before installing the permanent monitoring equipment. It also resulted in the necessity to build up a water evacuation system. This added another 8 months delay, given the necessity to satisfy rules of French administration for public calls for tender.

However, today most of the milestones of the project have been reached. Further, these unexpected delays gave plenty of time for the design and testing of the permanent monitoring equipment. So far (two month operation) the data acquisition system is functioning as expected.

1.5. CO-ORDINATION AND COMMUNICATION ACTIVITIES

Web site : Circulation of information between partners and with other CRL projects is being achieved through an integrated web site (fttp:// www.Corinth-Rift-lab.org). In particular, conclusions of technical DGLab meetings are available there, for authorized participants, together with proceedings of workshops, list of participants, etc…

In addition, during the drilling operation, the ICDP web page was used for transmitting daily drilling reports. It has proven of great help for communication between participants. It still provides an address where drilling reports and well logs can be accessed. Interestingly the ICDP web site is maintained daily by dedicated personnel. In contrast, although the CRL web-page is maintained also by one specific person, CRL participants have not integrated the concept of sending on a routine basis their reports, papers and other on-going activity. Clearly, there is still some kind of cultural gap within the CRL community for routine exchanges through the web. One of the purposes of the E.U. supported AEGIS project is precisely to help feel this cultural gap. It is planned to develop, through various workshops, the tool (efficient dynamic web site with access to data base)for a better integration of the various groups.

Workshops are being held in Aegion, between all CRL participants on a two years basis (Sept. 29-Oct 4 2001 ; June 2-7, 2003) . The meetings are attended by about 80 participants from seven different European countries. They include students and post-docs presentation together with specific coordination meetings. In addition to exchanges between concerned scientists, the last workshop provided an opportunity for a session with local authorities and the general public from the Aegion area in order to familiarize them with seismic risk analysis and techniques for mitigating seismic hazard. Proceedings are available on CRL web site. Geological field trips have been organized during the workshops in order to discuss matters directly on site.

Independently, frequent meetings have been held between the coordinators of the other European projects, and sometime with some of the partners, in order to assess the progress of each project and insure adequate coordination between the various activities.

EGS-AGU-AAPG meetings-Dedicated sessions have been organized during European Geophysical Society yearly meetings (EGS, Nice 2002; AGU-EGS Nice, 2003). Sessions included both oral and poster sessions. General talks have been given at American geophysical Union (AGU fall meeting, 2003) and petroleum geologists yearly meetings (AAPG-Barcelone-2003; EAEG-Tunis 2003).

CRAS-Geosciences. A special issue of Comptes-Rendus Académie des Sciences– Geosciences is being prepared in order to gather all results obtained so far within the CRL project. This special issue is due for print for February 2004.

General Public communication. Information to the general public was provided through the television "Archimede" program on ARTE as well through radio discussions ("Tout s'explique", France Inter, one hour talk; micromega; 10 minutes discussion on Radio France International).

1.6. DIFFICULTIES ENCOUNTERED AT MANAGEMENT AND CO-ORDINATION LEVEL AND PROPOSED/APPLIED SOLUTIONS

The main difficulty encountered in this Research infrastructure project have been linked with administrative aspects : Public Administrations are not prepared to organize call for tenders for work outside their own country. The language is a strong barrier, each country insisting in using his own language for the preparation of the call for tender. This has been a source of delays as well as unfair treatment of some potentially concerned companies.

Dealing with VAT when ordering work in another country is another source of difficulty that many companies or public administrations do not know how to solve. It would be very helpful that existing rules be recalled in all contracts, with reference to proper legal texts for the various concerned countries.

Another important difficulty is the lack of technical personnel on site, for the maintenance of the CRL permanent monitoring network. If the present investment is to be productive, solutions will have to be found so as to insure proper maintenance of the facility with easy access to all concerned groups. This will require a European consortium to cover corresponding costs, including that of maintaining the database.

Table 1. Comparison between planned and used manpower and financial resources, by workpackages and partners.

	Contractant	Budgeted cost	Effective costs	Budgeted man-hours	Effective man-hours
WP1	UPSL*	110 000	109 501	2 263	3 786
Site reconnaissance	IPGP	10 000	2 832	676	85
	IFP	9 913	22 569	135	436
	Catania**	0	10 679	0	3 483
WP2					
	GFZ	505 000	837 024***	2 028	1 690
Drilling and coring	IPGP	78 500	66 016	338	85
WP3	UPSL*	95 000	112 900	2 300	2 882
	IPGP	128 970	89 665	2 028	6 084
	Cerege	34 880	42 211	1 014	1 014
Logging and temporary in-situ measurements	GFZ	15 000	13 838	2 028	2 704
	IFP	15 598	14 909	287	286
WP4	Cerege	0	0	507	0
Core analysis	IFP	20 910	9 434	304	123
	Catania	20 000	0	3 380	0
WP5	UEDIN	179 046	168 718	4 056	4 649
Core analysis:	CERMES	49 800	48 273	2 535	3 211
Mechanical and hydraulic characterisation	GFZ	0	0	2 028	338
	UPSL	17 400		169	
WP6	IPGP	191 680	233 916	4 732	16 224
Downhole instruction and continuous data acquisition	NKUA	26 000	24 863	1 690	2 625
TOTAL		**1 507 696,00**	**1 807 347*** **	**32 499**	**49 702**

* UPSL was planned to participate in WP6. However because of delays in setting up the permanent monitoring equipment in WP6, UPSL concentrated its activity in WP1 and WP3.

** Univ. of Catania was planned to work only in WP4. But, because of the lack of proper geological map, it was decided to ask Univ. of Catania to concentrate its activity in WP1 (site reconnaissance), as explained in the first progress report

*** as explained in the management report, chapter 1.2.2, additional funding were obtained from ICDP (250 000 US $), in order to cover the required drilling costs.

Table 2. Comparison between initially allocated funds and adjusted fund allocation

Contractant	Total costs accepted 1st year	Total costs accepted 2nd year	Total costs submitted 3rd year	**TOTAL costs**	**Budgeted costs**
IPGP	58 993,94	168 298,36	165 136,14	**392 428,44**	**409 150**
Coordination	14 376,29	14 313,48	30 244,58	**58 934,35**	**104 760**
TOTAL IPG	73 370,23	182 266,00	195 380,72	**451 362,79**	**513 910**
NKUA	10 219,73		14 643,05	**24 862,78**	**26 000**
CEREGE		2 907,24	39 303,55	**42 210,79**	**34 880**
GFZ	12 848,83	230 992,76	607 020,01	**850 861,60**	**520 000**
IFP	22 568,50	9 434,18	14 909,13	**46 911,81**	**46 420**
Catania	7 979,25	2 700,00		**10 679,25**	**20 000**
UPSL	109 501,34	81,04	112 818,56	**222 400,94**	**222 400**
EDIMBURGH	27 692,74	28 944,22	112 080,94	**168 717,90**	**179 044**
CERMES	29 933,41	3 468,67	14 871,35	**48 273,43**	**49 800**
	294 114,03	460 794,11	1 111 027,31	**1 866 281,29**	**1 612 454**
				1 807 346,94	without coordination

In order to complete the work planned during the drilling operation, it has been necessary to reallocate funds (73 500 Euros) to GFZ. This fund reallocation remains smaller than 20 % of the total of each concerned partner (62 500 E taken from IPG-P, 1 100 E taken from NKUA, 9 100 taken from Univ. Catania and 800 E taken from CERMES). This necessity of fund reallocation was declared to the scientific officer, prior to their becoming actually effective. It is reminded here that GFZ has obtained in addition, from ICDP, 250 000 US $, for covering its extra drilling costs.

SECTION 2 ACTIVITY REPORTS FROM WORKPACKAGES

The objective of DGLab is to contribute to the development of a European Research infrastructure, namely the Corinth Rift Laboratory (CRL). This Euroepan research infrastructure provides necessary facility and data for investigations on fault mechanics, on interactions between fluids and active faults and on seismic hazard mitigation. The DGLab contribution to CRL development has been more particularly concerned with the drilling through the active Aegion fault for the continuous monitoring of its activity, but it has also been involved with the local seismic network development.

It encompasses six different workpackages :

Workpackage 1 - Site reconnaissance

Workpackage 2 - Drilling and coring

Workpackage 3 - logging and temporary in situ measurements

Workpackage 4 - Core analysis : petrofabric

Workpackage 5 - Core analysis : mechanical and hydraulic characterization

Workpackage 6 - Downhole instrumentation and continuous data acquisition

Accomplishments achieved in these various workpackages are presented hereafter.

1. WORK PACKAGE 1 – PRELIMINARY SITE RECONNAISSANCE (UPSL, IFP, IPG-P & UNIV. CATANIA)

A preliminary site reconnaissance was run in order to constrain the location of the 1000 m deep well meant to core the Aegion fault within the mesozoïc formation. The understanding of local structures resulting from this preliminary site reconnaissance has been significantly improved by the drilling of the well and the various geophysical logs and measurements conducted in the well thereafter. We present here only the results from the preliminary reconnaissance. The updated understanding of the local structure produced by combining the results from workpackage 1 with those of workpackage 2 and 3, are presented in workpackage 3. The geological work was conducted by Institut Français du Pétrole (IFP together with the department of geology from the University of Catania. The seismic wok was conducted by Univ. of Patras Seismic Laboratory (UPSL) together with a team from IFP. Magneto telluric data gathered by IPG-P were also examined during the preliminary bibliographical work and helped define the precise geometry of the seismic profiles.

1.1. GEOLOGICAL FIELD DATA (IFP, UNIV. CATANIA)

Geological reconnaissance has been carried out in order to provide the missing local geological map and to undertake detailed studies of the most significant quaternary faults of the area.. A meeting in Paris, between F. Ghisetti and IFP, resulted in the preparation of a geological map and a report (Ghisetti et al., 2001) distributed to the various partners.

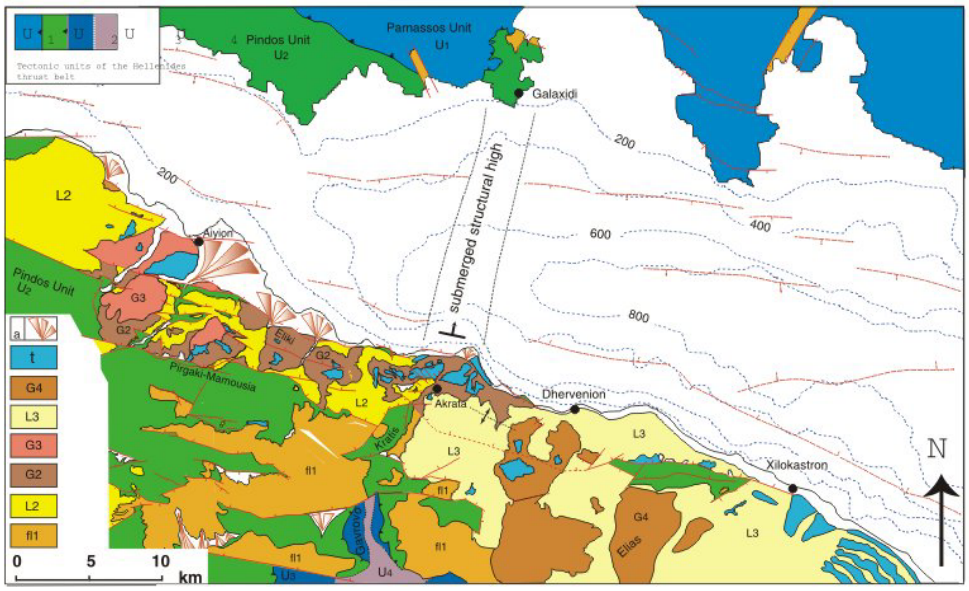

Fig. 1: Geologic map of the south shore of the Gulf of Corinth (Ghisetti and Vezzani, 2003). The Plio-Pleistocene sedimentary sequence developed above the carbonate substratum (in green) in the Aiyion and Dhervenion basins is subdivided in formations belonging to 4 depositional sequences (indexed with numbers from 1 to 4), separated by unconformities. Letters refer to lithology, with, from bottom, fl: alluvial fans and braided fluvial plan deposits; L: lacustrine-lagoonal sands, marls and clays interfingered with conglomerates and marine deposits; G: Gilbert fan deltas; t: continental and marine terraces, a: alluvial covers and alluvial fans.

Field work has also been carried out to interpret the seismic campaign and to study the deformation associated with the faults as well as the fractures and the fault related fluid flow.

Measured values
Helike fault dip versus surrounding facies

Site1: 70° (Intermediate fault plane through limestones)
Site2: 55° (Conglo\conglo, main fault plane – road Helike - Diakofto)
Site3 : 58° (Carbo\conglo - main fault plane – Freeway, south

IFP (I. Moretti, JM Daniel, L Micarelli and J. Schmitz) made a long field survey from beginning of May 2001 to June. The main objective was to study the fracturation in the fault vicinity in the frame of project 3F-CORINTH. The map and regional geology needed to be checked: for instance, the exact position of the Aigion fault has been studied by specific field record; the fault appears to be localised north from the railway at the level of the harbour.

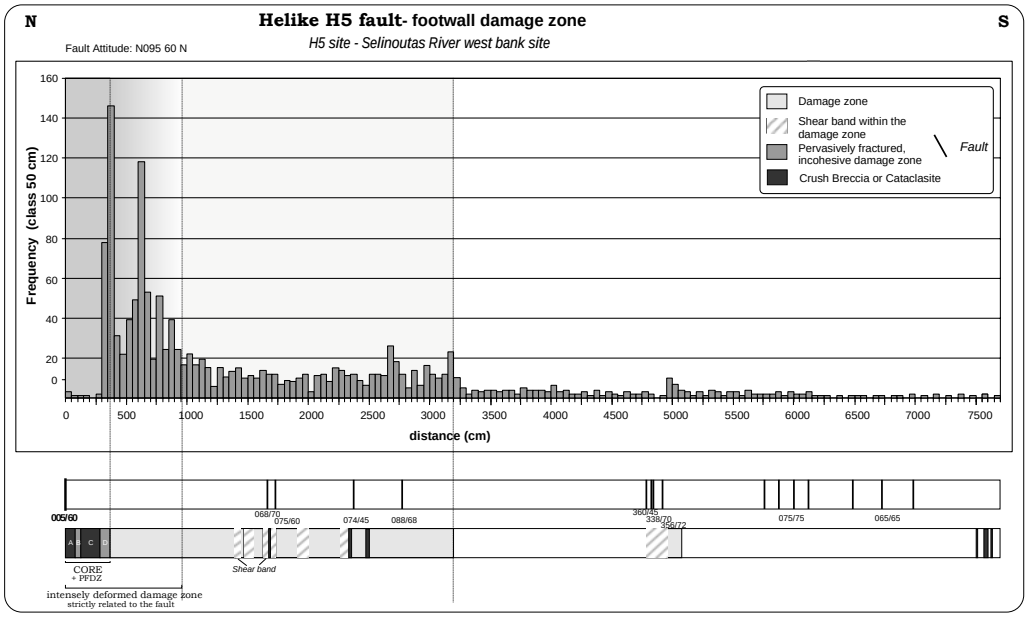

Fig.2: The core and damaged zone of the Helike fault.

The fault characteristics have been quantified in term of gouge, thickness, damaged zone. The macro-scale features has been studied and the results published in Micarelli et al. (2003). Interpretation of the reflection profiles and Well implantation

1.2. SITE RECONNAISSANCE BY SEISMIC PROFILES (UPSL, IFP,IPG-P)

1.2.1 Definition of seismic profiles geometry

The initial field scouting has been done in November 2000 by Andrea Sotiriou (UPSL), Ch Naville and I. Moretti (IFP) and F Cornet (IPGP), in order to define the location of the 4 seismic lines. The profiles have been selected according to the final goal: to image the Aigion fault with 2D-profiles accessible with vibrator trucks.

The Aigion fault escarpment on the Aigion harbour

Profile 1 follows the Meganitas River and intersects both the Aigion and Helike fault.

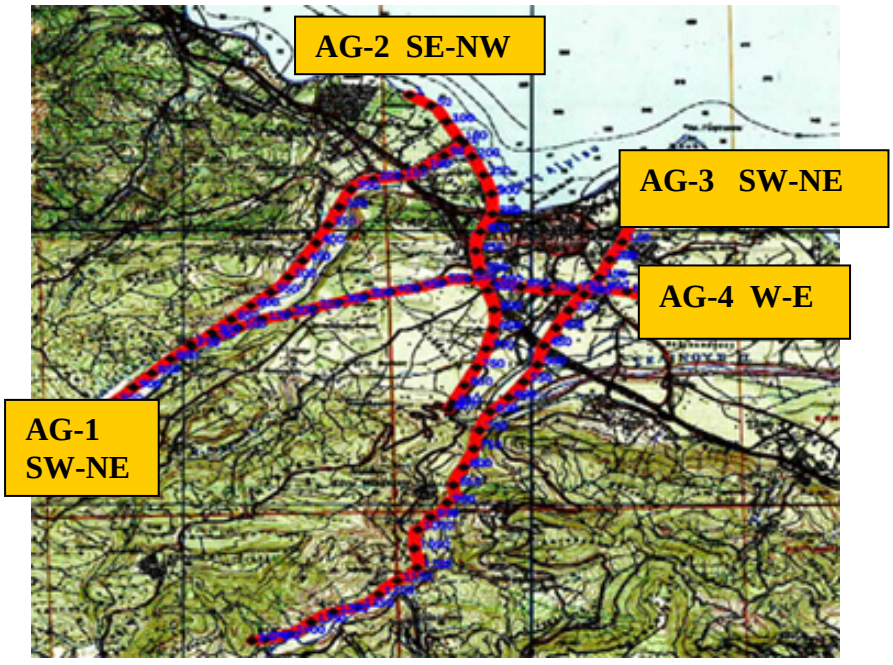

Location of the 4 seismic lines

Profile 2 starts north of the Meganitas River, follows the coast and crosses the Aigion fault at the level of the ferry port . The south end stops on the Helike fault.

Profile 3, East of Aigion, oriented about N20 in the Selounitas river, crosses the 3 faults: Aigion, Helike and Pirgaki-Mamousia

Profile 4 is a strike line in the plain between the Aigion and Helike faults, designed to intersect the three other lines.

The acquisition took place from January 29th to March 10th 2001. C. Naville and I. Moretti IFP, visited the crew on Jan 30 – Feb 6, 2001. One 50,000lbs vibrator was used as a source, stack of 3 sweeps 8-80Hz per VP, with 120 receiver traces, 15m apart, asymmetric split spread. This field operation has been filmed for the German/French TV Channel ARTE and presented on the scientific broadcast ARCHIMEDE.

1.2.2. Processing

During the spring 2001, the 4 seismic lines have been processed by Patras University /UPSL with the industrial PROMAX seismic software. IFP validated the choice of processing parameters.

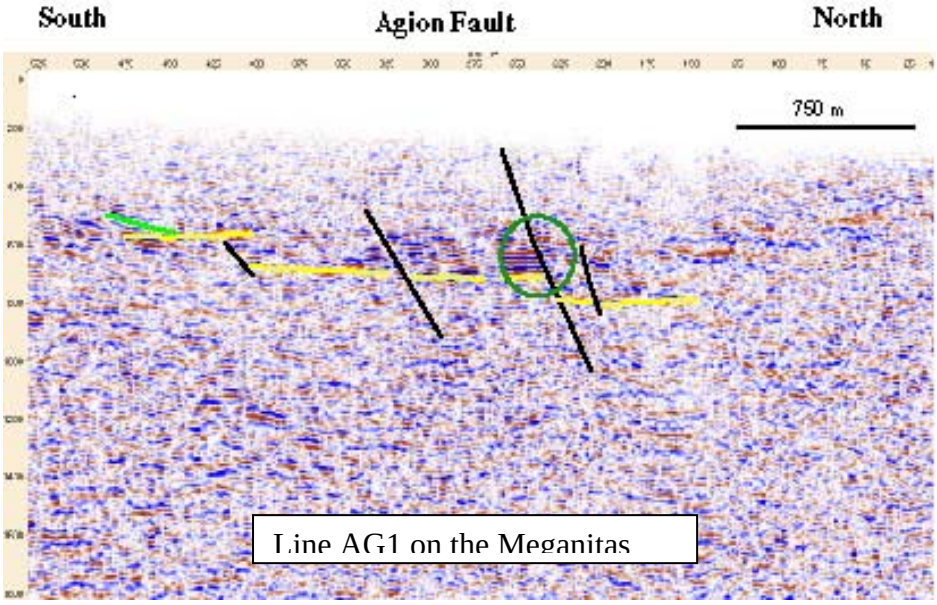

Fig.3. Reflection stack section on line AG01-01: expected top of carbonates horizon in yellow

Despite of the variable quality of seismic results from one line to the other, a few positive results can be derived from the seismic stack images: for instance, on line AG1 (seismic section below), the Aigion fault is rather flat up to 1 km with a dip of 60°N, the base of the syn-rift (top of the Carbonate) is at 720 m south from the Aigion fault and the Helike block (between the Helike and the Aigion faults) is almost flat. The apparent tilt is dipping northward on AG1.

In conclusion, the conventional processing was not very easy as the stack results are quite poor on lines IG-1 and AG-2, expressing laterally coherent reflection line-ups on short distances corresponding to blocks of a few hundred meters only. Stacks on Line AG-3 and AG-4 are extremely poor, so that line crossing controls are not even possible. Nevertheless, the quality of the seismic acquisition is not the cause of the poor stack results obtained. These results on stack sections express the structural complexity of the subsurface in the Aigion area and in such context, so that migrating these sections was not justified.

Worse, on the seismic line AG2 across Aigion city, no result could be obtained in the northern compartment of the Aigion fault, either from reflection or refraction seismic methods.

Consequently, the southern compartment was briefly studied by IFP, using the refracted arrivals of a 4000m/s marker probably corresponding to the top of the carbonate layer located in depth around the substratum of interest.

The sketch below summarises the final depth results from measurements on refracted arrivals in the Southern compartment, using the Gardner method with a 3 layer velocity model. In the Northern compartment of Aigion fault, the sketch derives from a "best interpretative guess".

This short refraction study is detailed in the IFP report # 56241, as part of the first. DG-LAB progress report and is discussed in Naville et.al. (2003)

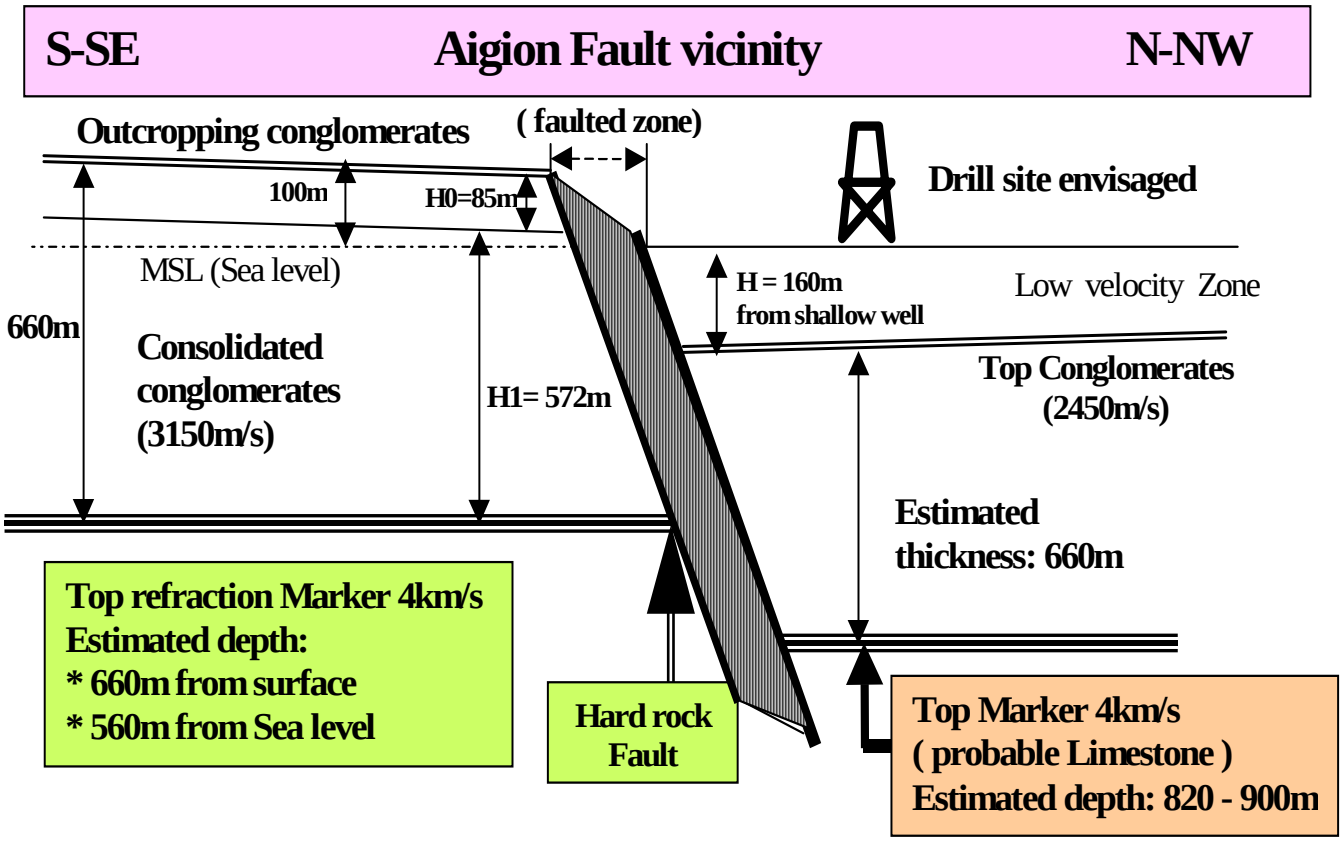

1.3. SITE LOCATION RECOMMENDATION (IFP)

The interpretation of the few coherent markers has been done as well as the time/depth estimations based on the seismic velocity deduced from the refraction data and/or known by the seismologists in the area (CORSEIS project) .

As the reflection seismic results of the 4 reflection lines, a rapid evaluation of the refracted arrivals on raw records was attempted and resulted in the structural sketch shown in the "***processing***" chapter above: As a conclusion, if we assume that the total thickness of the conglomerate formation is the same on both sides of the Aigion fault, and that the outcropping conglomerates in the southern compartment have not been eroded, we obtain a minimal depth

of 160 + 660 = 820m for the top of the Carbonate 4000m/s marker on the North side of Aigion fault (the top of conglomerates has been reached at 160m depth with a shallow well drilled for the CORSEIS project).

Based on field data from the Helike fault and from the seismic image, it was proposed that:

(1) the Aigion's fault has a dip of 60°N,
(2) the carbonates depth is about 660 meter from surface on line 2 based on the refraction analysis.

This work led IFP, in 2001, to propose drilling the well Aig-10 in the northern fault compartment at a distance of 575±50 meters from the Aigion fault trace identified, on ground surface, with the railway track.

2.WORKPACKAGE 2 : DRILLING OF WELL AIG10 (GFZ-POTSDAM; IPG-P; IFP)

2.1 FINAL SITE SELECTION (IPG-P)

Once the site had been defined on the base of both geological and geophysical considerations, scouting of local available land was undertaken in order to identify a suitable drilling location. The final choice was made when the Koronakis family donated a part of their land to the project (see blue arrow on the figure).

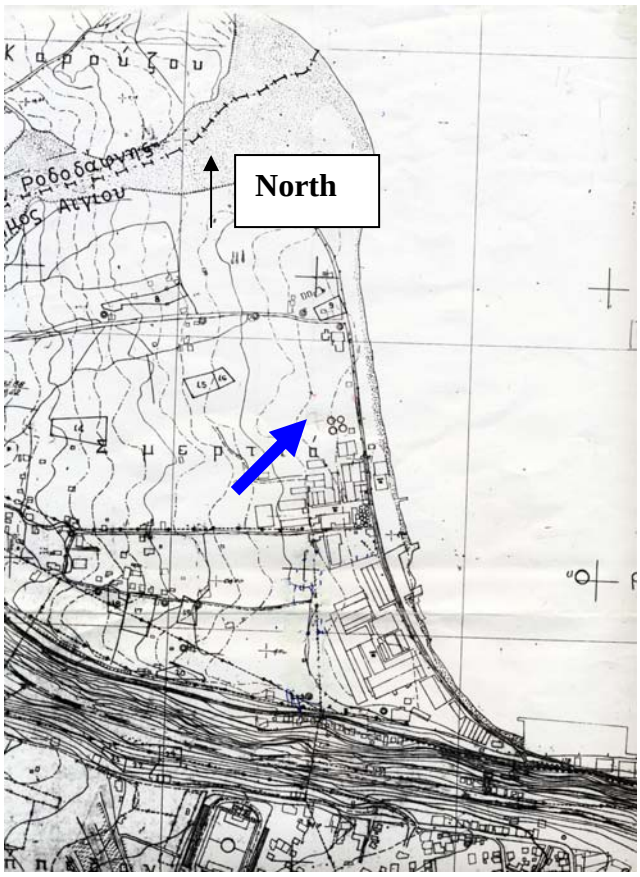

Fig.1. Final AIG10 well site location. It is about 420 m north to the Aigion fault. The fault can be identify by the escarpment to the south of the map (lower part)

2.2 DRILING AND CORING OPERATIONS (GFZ-POTSDAM, IPG-P & IFP)

The drilling concept for the AIGION well (AIG-10) was developed under the constraints of a strict budget plan without contingency capabilities, a drilling depth capacity of appr. 1000 m depth and the scientific requirement of continuous high-quality coring in the so called "Aigion fault zone".

The well was projected and operated under the leadership of the ICDP Operational Support Group at GFZ. The AIG-10 well was drilled between July 7, 2002 and September 23, 2002. Prior to drilling, an interim report on the geologic-tectonic and hydrogeological conditions in the area of the deep borehole AIG10 was made in order to support the planned drilling activities and further scientific research was made by the University of Karlsruhe (Applied Geology, AGK) (Rettenmaier et al., 2002). In this study, possible hazard indicators and technical problems of drilling due to the specific geological conditions were discussed and merged to general risk assessment at this borehole site. This report was made available to interested project partners, such as the Operational Support Group Potsdam (OSG) and the drilling company.

The borehole was drilled by a German contractor with a B5R drilling rig in combination of Rotary Drilling and Wireline Diamond Coring technique in order to allow for both, a 12 ¼" and 9 5/8" drilling diameter (0 – 708,8 m) and high-quality coring in the fault section of the borehole (708,8 – 787,4 m, 101 mm core diameter). The relatively large diameter was chosen to enable later full instrumentation.

Thirty core runs yielded 71% core recovery; losses in the upper coring section were due to highly sheared strata. Nevertheless, the main fault zone was fully cored without any loss of material. Coring operations were performed with a Bentonite-Polymer-Freshwater mud (1.05-1.1 kg/l) at pump rates of 140 to 260 l/min, with 20 to 30 kN weight on bit (WOB) and topdriven 130 to 150 rotations per minute (RPM). The lowermost part of the well between 787.4 m and the final depth of 1001 m was rotary drilled (6 ¾"). The well was cased and cemented to 708,4 m (7 5/8"). See Table 1 for technical details and Figure 3 for the drilling and casing scheme. The inclination of the borehole was less than 3° at 330° azimuth, and the bottom hole temperature did not exceed 31°C.

The well site preparation was prepared by a domestic company (Figure 2 and 3).

All digital data sets including technical drilling parameters, initial scientific sample descriptions were distributed during the course of the operations via Internet and stored in the ICDP Drilling Information System serving the global community of cooperating scientists as basic information service

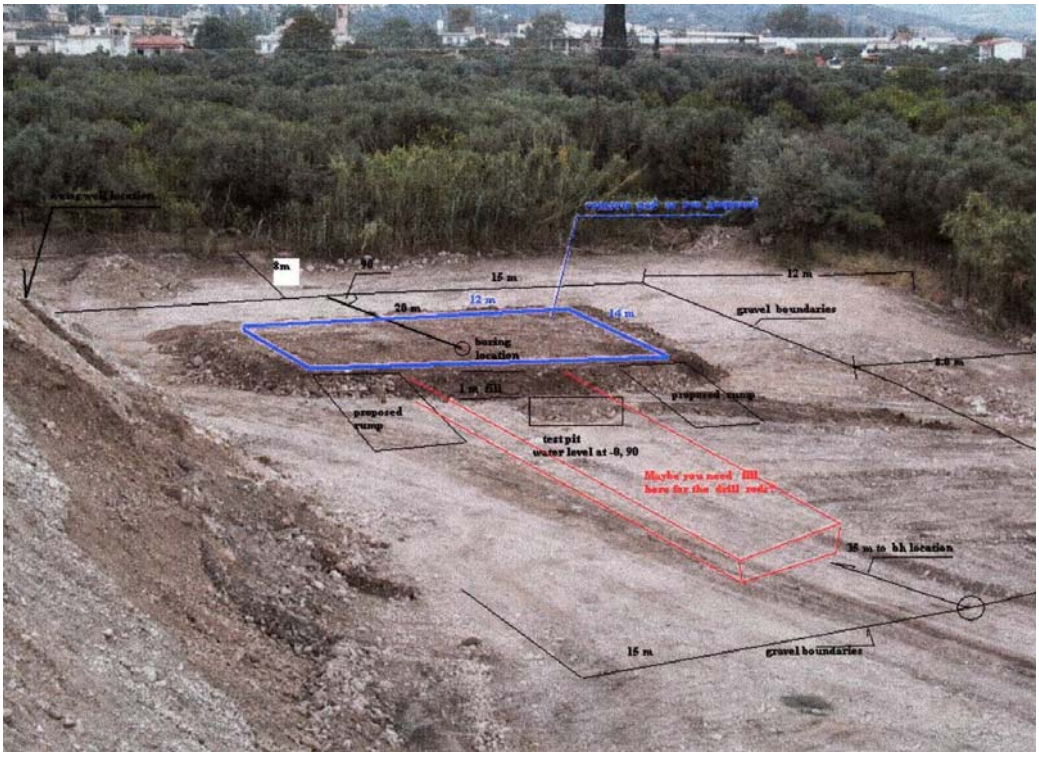

Fig.2. Planning of the well site

Fig.3. Drillsite during operations

Table 1: Technical characteristics of the AIG-10 drilling

Rotary Drilling Phase	Wireline Coring Phase
1) 0 – 708,8 m depth 2) 787,4 – 1001 m depth	708,8 m – 787,4 m depth
1) Drilling diameter: 311,15 mm (12 ¼ “) 244,5 mm (9 5/8”) 2) Drilling diameter: 171,5 mm (6 ¾”)	Drilling diameter: 171,5 mm (101 mm core)
2-1-7, 5-1-7, 5-3-7 IADC-Insert Bit rate of penetration (ROP) 1,8-2,8 m/h 20 – 60 kN weight on bit (WOB) 60 – 120 rotations per minute (RPM) 120 – 300 pumprate in liter per minute (l/min)	171,5 mm diamond core bits (ballaset) ~1,5 m/h ROP 15-30 kN WOB 120-150 RPM 140-260 l/min
Freshwater-based bentonite mud 1) Density: 1,08 – 1,21 kg/l 2) Density after the end of the drilling operations, dated 23.09.2002: 1.17 kg/l	Freshwater-based polymer bentonite mud Density: 1,05 – 1,10 kg/l
Rig characterisitics: 490 kN hook load capacity, 150 kW drawworks, 280 RPM topdrive with 12.000 Nm torque, 1 x 85 kW pump unit, standard mud circulation system, 3000 psi blowout preventer	
Timing of drilling operations: Juli 7, 2002 - September 23, 2002 (76 days) Final depth: 1001 m Coring range: 708,8 m – 787,4 m 30 core runs of 6 m nominal length Core recovery: 71%	

Most of the operations including drilling, coring, casing and cementing were executed according to the planning. However, the very instable sections caused enhanced drilling time and loss of drilling mud circulation due to fault zones.

After the end of the drilling operations the borehole was completed. The cellar with wellhead above the surface is covered with steel plates, secured by a lock.

The borehole was completed with following wellhead: 7-1/16” drilling spool with two 2” outlets, connecting spool to Flange DIN 2545 DN 350 with 3” outlets, DIN Gate Valve DN 350, PN 25 (Figure 5).

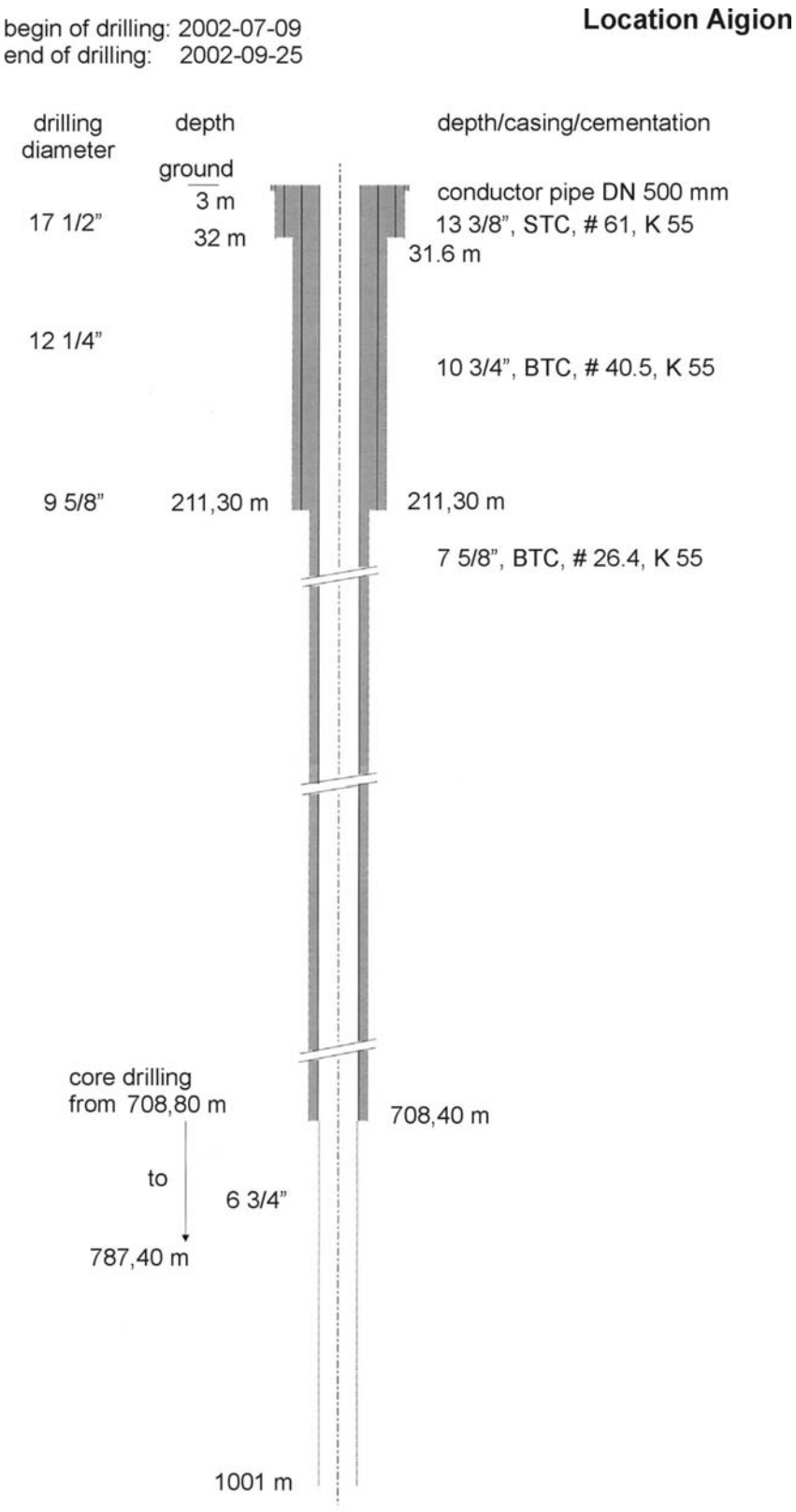

Fig.4: Drilling and casing scheme of the AIG-10

Fig. 5. Wellhead of the AIG-10

2.3. LITHOLOGIC AND STRATIGRAPHIC DESCRIPTION OF THE AIG-10 BOREHOLE

Recognition of stratification encountered in the AIG10 borehole (Figure 6) is based on an online analysis of well cuttings (0-708.8 m and 787.4-1001 m), core descriptions (708.8-787.4 m), monitoring of drilling parameters, as well as a preliminary geophysical well-log interpretation (0-1001 m) made during the drilling activities. The litho-log and cutting analyses are part of publications by LEMEILLE ET. AL. (2003) and RETTENMAIER ET. AL. (2003a, b).

Recognition of stratification of units encountered in the AIG10 borehole is based on an analysis of well cuttings (0-708.8 m and 787.4-1001 m), online core descriptions (708.8-787.4 m), monitoring of drilling parameters, as well as a preliminary geophysical well-log interpretation (0-1001 m).

The Corinth graben as recorded in the AIG10 borehole is filled from the top by a 3.5-m thick argillaceous sandy **soil**, Holocene and Pleistocene clays, marls, and the **Meganitas river deposits**. The latter down to 127 m are characterized by sandy, medium- to fine-grained gravels, intercalated with silty and clayey layers, which can act as aquicludes.

From 127 m to 388 m, the expected Eocene- Pleistocene **"Gilbert-Type" delta conglomerates** were encountered. These conglomerates, constituting the main part of the post-Alpine unit, are 261-m thick and consist of well-rounded limestone, marl, and sandstone detritus as well as subangular radiolarites and cherts of the Olonos-Pindos unit.

A clayey and sandy transition to marine sediments occurs below this unit, which is underlain by a dark-gray **marine clay** to a depth of 496 m. The Pleistocene calcareous, plastic fat clay is less silty and contains fossils and nannoplancton. This marine syn-rift deposit could be related to a marine high stand in late Pleistocene (LEMEILLE ET AL. 2003). The dark-gray clay is underlain by a reddish clay sequence.

The **Radiolarite formation** of sharp-edged green and red radiolarites of gravel size in the **Olonos-Pindos nappe** then is encountered at 496 m. This change in lithology also is obvious on the geophysical logs as well as from drilling time by the increase of the Rate Of Penetration (ROP). A dense radiolarite of a minimum thickness of 10 m is underlain by a radiolarite intercalated with silicious marls. With increasing depth, the lithology then repeatedly changes from limestone to radiolarite and marlstone. Because of this heterogeneity of the sequence between the depth of 506 m and 696 m, it can be assumed that several tectonic contacts (faults and thrust faults) exist, for example at 506 m, 578 m, 602 m, and 615 m depth.

These results are confirmed by observations made on outcrop south of Aigion, where thrust-fault zones may show several alternating thrust planes; well-logging data at these particular depths also support this interpretation. At approximately 696-698 m, a main thrust-fault zone was observed along which the Jurassic radiolarites were overthrusted on Cretaceous limestone.

Below this thrust-fault zone, the **Olonos-Pindos platy limestone formation** was identified by cuttings of light-brown or greenish-gray limestone and marlstone as well as red marl and silicious marlstone. The first core taken at a depth of 708.8 m confirms the typical character of the well-fractured, slab-shaped Olonos-Pindos platy limestones. The dip of bedding of the platy limestone is SE and E indicating a NW-verging thrust progradation. Two additional thrust planes were observed in core at 726 m and 742 m, which could be related to this tectonic movement.

Below 745 m, the Olonos-Pindos platy limestone shows several cataclastic bands. The first band (at 745.7 – 746.5 m) is characterized by a well-cemented cataclastic zone with healed calcite veins. Calcite crystals show features of pressure solutions and pressure shadows, whose textures can be interpreted as microkinematic indicators. We interpret this as dip-slip displacement/normal faulting. Another 70-cm thick cataclastic band with less good healed veins and shear structures was identified in core at 748 m. In contrast to the first two bands, the third band from 754-755 m shows open fractures, voids, and geodic cavities, which are filled only partly with calcite. It can be assumed that this cataclastic band is younger than the two previously described. These shear bands and cataclastic zones obviously are part of a major normal faul zone, assumed to be the **Aigion fault**. The fourth cataclastic band was encountered at 756 m and is at least 4-m thick. This band separates well-fractured platy, micritic limestone from the highly fractured radiolarite. At 760 m the contact between the **hangingwall (limestone)** and the **footwall (radiolarite)** dips approximately 55-60° N, which is coherent with the dip of the outcropping Aigion fault plane on the surface and at a distance of 470 m from the outcrop to the well. The angle between the bedding of the stratigraphic sequences, dipping SE and E, and the fault plane, dipping N, is between 80-100°.

After crossing the fault zone, an increase of water pressure from 5 bar up to 10 bar was measured (see GIURGEA ET AL. 2003). The highly fractured and brecciated radiolarites as well as the high influx of water caused core losses so that the transition from radiolarite to the underlying limestone could not be located in the cores. However, the geophysical logs indicate the contact with the **limestones** is at 770 m. The cores from 774 m to 787.4 m (end of coring) show that these limestones differ from the limestones of the upper parts of the drilled sequence. The limestones from 770 m downward are light gray with a high content of well-developed calcite crystals. Intercalations of marl and marlstone are rare. Only some thin, black, and marly intercalations were observed. The rock is porous and has open fractures,

large voids, cracks, and dissolution structures. The cores and the hydraulic behavior of the deeper intervals down to 1001 m suggest karstification and karstic water-flow conditions. Because of the high influx of water into the well and the high water pressure, the coring had to be stopped at 787.4 m and rotary drilling was continued to a total depth of 1001 m. Because of the hydraulic behavior and the strong increase of water pressure, it has to be assumed that the fault zone acts as a hydraulic boundary (GIURGEA ET AL., 2003). Cuttings from the last depth interval did not reveal any difference in lithology.

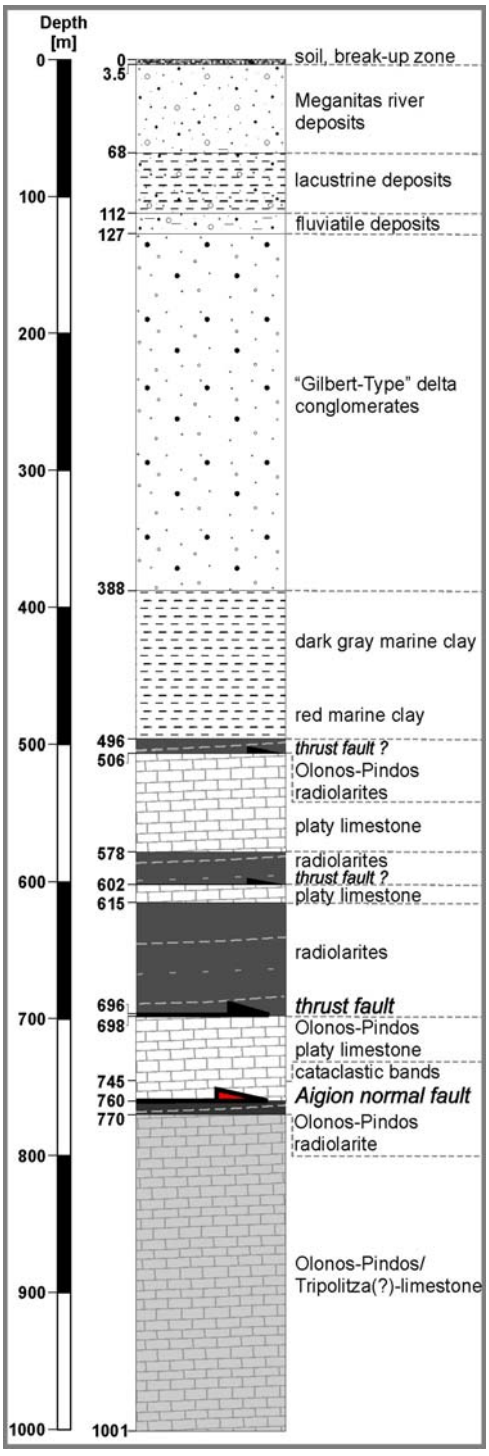

Fig.6.Generalized litho-log of the AIG-10 borehole

3. WORKPACKAGE 3 : GEOPHYSICAL LOGGING AND TESTING (IPG-P, GFZ-POTSDAM, CEREGE, IFP,UPSL)

A series of geophysical well logs were obtained by both the ICDP support group and the Schlumberger Company. In addition, hydraulic tests were performed followed, later on, by Vertical Seismic Profiles (VSP). This work benefited from support from DGLab, but also from the sister project 3F-Corinth, from ICDP, as well as from the German DFG.

All activities reported here belong to some regard to DGLab WP 3 (Logging and temporary in situ measurements) but they exceed what was proposed in WP3. For example additional pump tests were made in shallow water wells in the area to study more fully the regional aspect of hydraulic characterization. To fine-tune a conceptual regional hydraulic model, the chemistry of formation waters (also those from the pump test waters) was incorporated (cooperation with participant 10 of 3F). In addition, to establish the geological base for this flow model, a reconnaissance field to study geologic formations and geological structure was made and the litho-log of the AIG10 developed from cutting and core analysis (not planned in any WP).

The work involved the GFZ and university of Karlsruhe group, Schlumberger, IFP and IPG-P.

3.1 GEOPHYSICAL LOGS

3.1.1. Geophysical logging in the AIG10 borehole run by ICDP support Group (GFZ-Potdam)

A series of geophysical well logs was obtained in the AIG 10 borehole by the ICDP Operational Support Group (OSG) located at GFZ Potsdam (responsibility of EU project participant 4). The logging was partly funded (travel expenses for logging crew) by the German Science Foundation by its ICDP priority program.

The logs were obtained in two campaigns (Table). First logs were recorded when drilling reached 708 m (casing); the second series was obtained when the borehole reached the final depth. Standard GFZ logging tools (Mud Parameter, Spectral Gamma, GR-BCS-DIL and MSFL) were employed to collect data on borehole conditions and on wall-rock petrophysics. The data are available at GFZ Potsdam on request (contact: for@gfz-potsdam.de) and are in the process of being processed and interpreted.

The combined indications, mainly from resistivity, sonic and caliper logs, supported also by the GR and Potassium logs show the main fault zone between 755 m and 770 m. Well-log indications strongly point to at least three separate fault planes within the 15 m wide fault complex. The apparent thickness of this steeply dipping fault system appears wider than in the core analysis as these logging tools read deeper into the rock.

Later on, in September 2003, a series of temperature logs was obtained with the funds of the German Science Foundation and the GFZ Potsdam for a repetition measurement of thermal conditions in the well. Because the logs this time were obtained in a heavy drill mud, which prevents artesian water flow, the thermal conditions are supposedly close to static formation condition. A Distributed optical Temperature Sensing tool (DTS) was used which allows the measurement of temperature simultaneously along a profile in short time intervals of minutes.

This logging regime enables us to determine whether some parts of the well are under dynamic conditions. In the parts of the well where temperature is under static conditions, heat flow will be calculated, which is a prerequisite for calculating temperatures at deeper depth where earthquakes are generated.

Table 1: Well-logging runs performed by ICDP-OSG

Log	Date	Range (m)	Parameter
MP	08/18/2002	0 - 708	mud temperature and resistivity, total gamma
SGR	08/17/2002	705 - 150	K, U, Th, total GR
BCS-DIL-GR	08/17/2002	703 - 184	sonic, induction resistivity, total GR
MSFL-GR	08/17/2002	704 - 230	micro resistivity, 1-arm caliper, total GR
SGR	09/18/2002	688 - 1002	K, U, Th, total GR
BCS-DIL-GR	09/18/2002	703 - 1001	sonic, induction resistivity, total GR
MP	09/19/2002	0 – 1003	mud temperature and resistivity, total gamma
MSFL-GR	09/19/2002	725 - 1000	micro resistivity, 1-arm caliper, total GR

3.1.2 Geophysical logs run with Schlumberger (under IPG-P coordination)

Two borehole imaging logs (Formation Micro Imager-FMI and Ultrasonic Borehole Imager-UBI) and a Dipole Sonic Imager (DSI) were run with the Schlumberger Company, from 1000 m to 711 m, i.e. in the open-hole section of the well. The objective of both FMI and UBI logs was to obtain data on the fault structure and its surrounding. They were also meant to detect failure features if they occurred. Indeed these yield useful information on the regional stress field.

On the UBI log, a zone with significantly increased borehole diameter is identified between 756.5 m and 772.5 m, where the cores have clearly shown the presence of fault gouge. Hence, the fault zone vertical extension is at least 16 m. Since the well is vertical and since the mean dip of the fault is 61° (see WP3-3, Vertical seismic profile), the thickness of the fault is found to be equal to about 7.8 m. It includes in particular a clayish layer at 762 m, about 50 cm thick, which corresponds to the material shown on figure 1 of WP5.2.1.

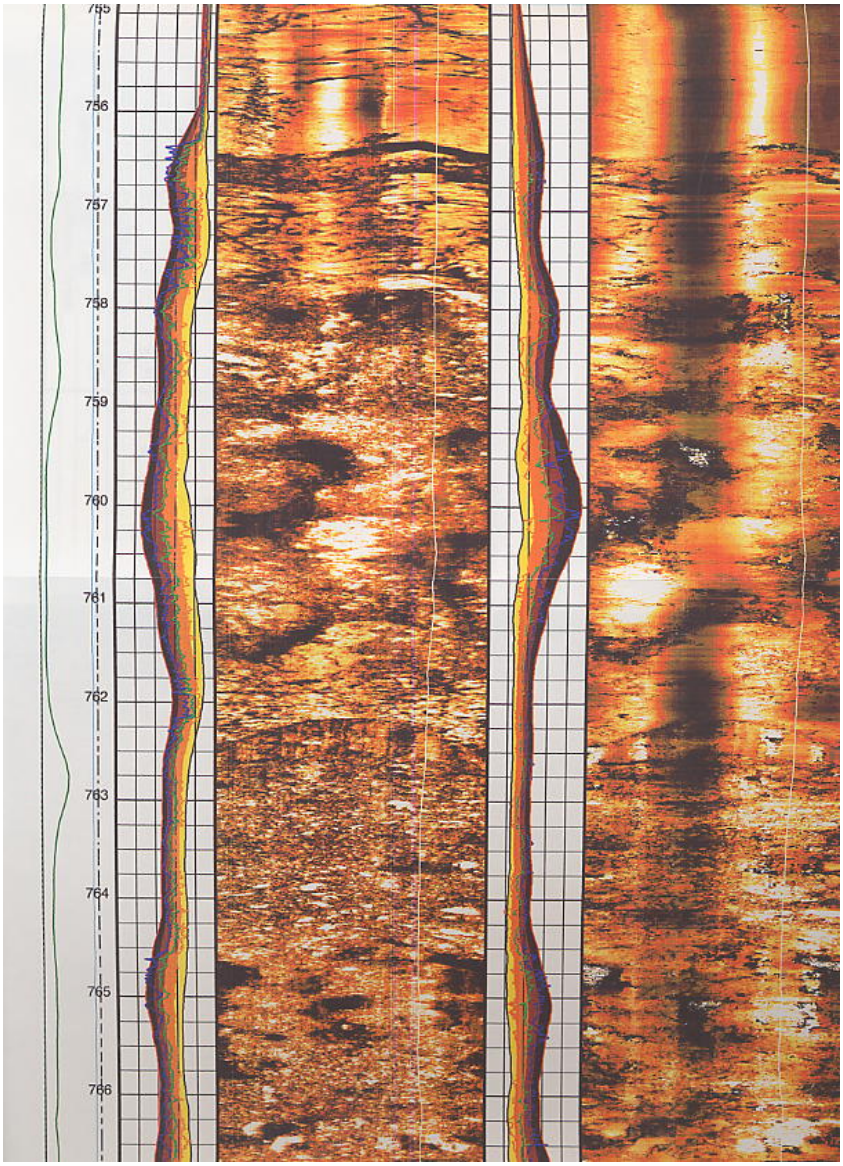

Fig. 1: Ultrasonic Borehole Imaging showing the clay zone within the fault zone at 760 m (Schlumberger depth); left image obtained from processing the signal amplitudes; right image obtained by processing the travel times.

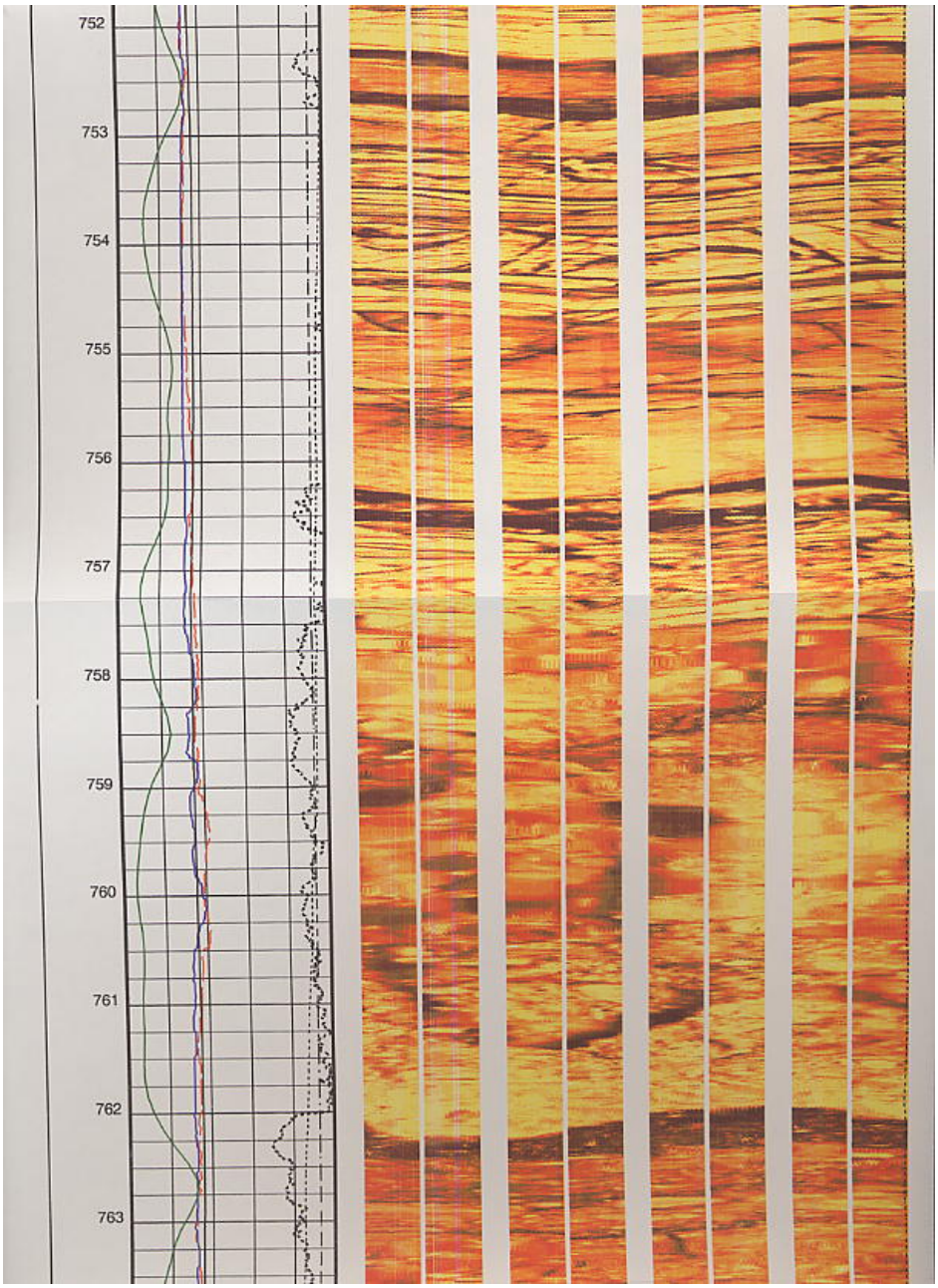

Fig.2: Electrical image (FMI) of the fault zone, showing the clayish layer within the fault zone (Schlumberger depths)

In addition, the borehole imaging logs have outlined zones, within the limestone, where significant borehole enlargements are observed. They are interpreted as corresponding to karstic zones . An example is given on figure 3. It may be observed that below and above the karstified zone, the well is well gauged. No breakouts are observed. Similar katstified zones have been encountered down to 934 m, i.e. about 500 m below the bottom of the sea; to the west of the site.

Interestingly, no temperature gradient is observed between 760 m and the bottom of the well, at 1000 m. The measured low temperature (32°) is taken as the proof of a significant downward flow.

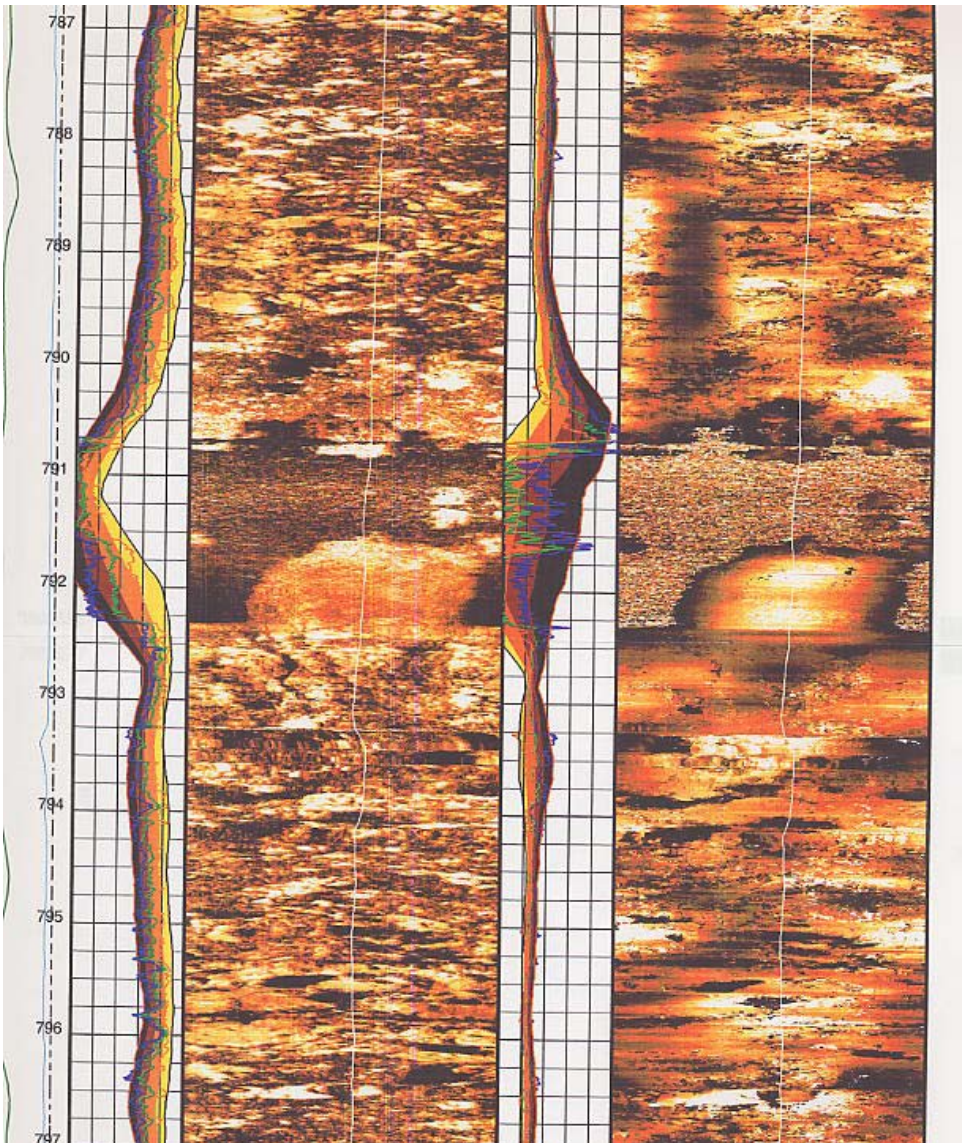

Fig. 3: Example of karstic zone identified with the UBI log (left amplitude image, right travel time image)

No pervasive borehole wall failure (tensile induced failure and breakouts) was observed and efforts have been undertaken to retrieve principal stress directions from the Dipole sonic log (DSI).

The DSI yields arrival times for P waves, S waves and Rayleigh waves. In addition, they have been used to retrieve the maximum horizontal principal stress direction (Prioul et al., 2003). The log has been acquired during three passes of a sonic logging tool at three different borehole

fluid pressures (0.1, 2.3, and 3 MPa). Specific sections of the well reveal clear characteristics of moderate-to-large azimuthal anisotropy (9-25 %) below the Aigion Fault, i.e., 779-784 and 809-816 m, with a fast-shear direction along direction N75°W, or homogeneous isotropic medium (i.e. 735-753 m) above the Fault. The presence of the Fault is coincident with the identification of lower velocities over an interval of approximately 12-14 m. Analysis of the data reveals that the formation is not acoustically stress-sensitive to the 3 MPa differential pressure applied. Interpretation of the sonic data with complementary image logs suggests the anisotropy is due to intrinsic fractures and bedding, and the fast-shear direction N75°W is consistent with the regional horizontal maximum principal stress (see figure 4).

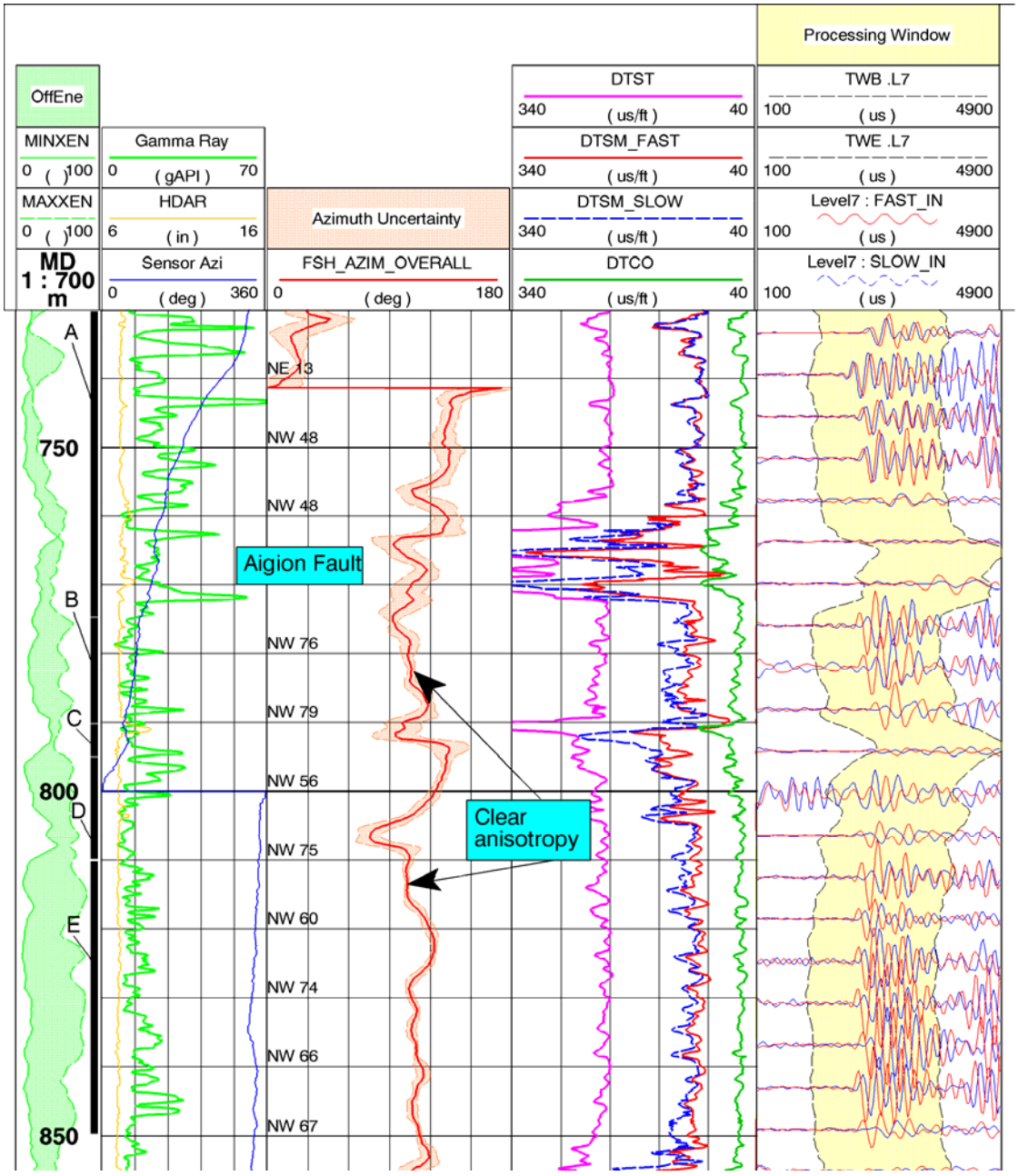

Fig.4: Dipole sonic logs for the AIG 10 well for depth interval 730-855 m (Prioul et al., 2003)

The green shaded area in the first depth track denotes differences between the maximum and minimum energies in the cross-component. The second track contains gamma ray (green line), average borehole diameter (yellow line), and the sensor azimuth (blue line). The next three tracks show, respectively, the fast-shear direction with uncertainty, the slowness logs (Stoneley,

compressional, fast-shear, and slow-shear), and the rotated waveforms with the processing window used to obtain the shear slowness.

3.1.3 Geophysical measurements in the tri-5 and aig-10 holes, Corinth Rift laboratory (CEREGE- Univ. of Montpellier)

Summary of Operations

Hole TRI-5 was made available for logging in the last four days of the first addendum period of the « DG-Lab Corinth » EC contract. With a nominal diameter of 7.0 inches (about 178 mm) for hole TRI-5, it was anticipated that downhole geophysical sensors designed for 3.0 to 4.0 inches diameter holes would have difficulties providing data with optimum quality. In the case of « DG-Lab Corinth » operations, this slimline set of sensors sensors was assembled to provide data in the 4.0 inches diameter AIG-5 hole initially planned in the DoW, later abandonned, and somewhat replaced *in fine* by TRI-5. The latter was targeted to reach 600 m, well into the footwall of an active normal fault projected from surface mapping to be cut at 200 to 300 m into the hole.

Hole TRI-5 was occupied twice for logging:
- on May 28th, 2003 were 2 logging runs failed to reach open hole, and
- on May 29th, 2003 when 5 logging runs recorded data above 206 mbrf only.

Hole AIG-10 was occupied once for a temperature logging run on Saturday May 31st, 2003.

Logging operations were aborted on May 31, 2003, as the end of the EC contractual period was reached.

3.1.3.1 Operations in Hole TRI-5

Depth reference : Depth in open borehole are conventionally measured just after drilling and from the drill floor, designated as mbrf (meters below rig floor). Rig floor position with respect to other references were measured and are summarised in Figure 1.

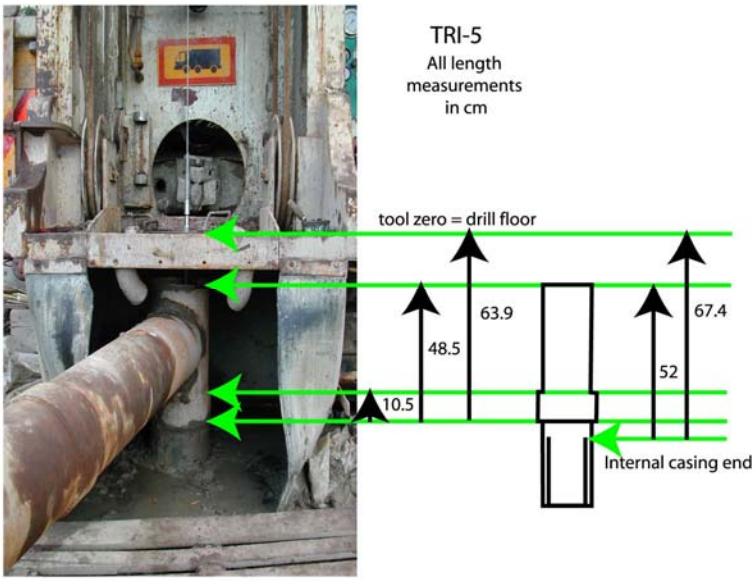

Fig. 5: Depth definition for Trizonia well

Hole conditions : Hole was cased down to 141 mbrf with a 7" (17.8 cm) diameter casing, and open at the time of logging operations down to a total depth of 355 mbrf.

First logging attempt (May 28, 2003)

The GLOG sonde which measures electrical resistivity was sent down in the first run for safety reasons as it is one of the more rugged sonde of the suite planned to be deployed. Data were recorded on the way down to check the integrity of the casing. The tool descent stopped at 141 mbrf, that is just upon entering open hole, due to an obstruction. Working the cable did not improve the situation and therefore the run was aborted and the tool brought back up to surface.

The SGR sonde which measures the natural gamma radioactivity around the hole was sent down in a second run. It was thought that this heavier sonde had more chance to pass the obstruction. Data were recorded on the way down. The tool also stopped upon reaching open hole at 143 mbrf, despite working the cable. A repeat log was then recorded through casing on the way up.

Logging operations were aborted after these two attempts and the hole made available for the drillers to ream it and attempt to reopen it. The drill pipe did encounter an obstruction at 141 mbrf that was overcome through rotary drilling. It was cleaned to total depth then made again available for logging.

Second logging phase (May 29, 2003)

The GLOG sonde for electrical resistivity was sent down again in the first run. Data were recorded on the way down. The tool stopped at 144 mbrf but, after working the cable, resumed its descent down to 151 mbrf, a level that could not be passed. A second log was then recorded on

the way up. It should be noted that electrical resistivity values are normally meaningless in sound casing, and can be degraded in open hole over 10 to 20 m in the vicinity of the casing shoe.

The SGR sonde for natural gamma radioactivity was sent down in the second run. Data were recorded on the way down. The tool also stopped at 151 mbrf, despite working the cable. A second log was then recorded on the way up, yielding a few more meters than what was recorded during the previous attempt. The overall signal is weak and compatible with carbonates down to about 108 mbrf (Figure 2), below which larger values are recorded to total depth, with a maximum near 120 mbrf corresponding to more clay-rich horizons.

The FWS sonde for acoustic velocities (Vp and Vs) was sent down in the third run. For this, two receivers are located respectively 76 (RX-1) and 116 cm (RX-2) away from a 20 kHz transmitter. Data were recorded on the way down. The tool went down to 206 mbrf. It was assumed that the greater tool length could possibly help passing below 151 mbrf, which worked. A second log was then recorded on the way up. Strong P and S casing arrivals are obtained in casing down to 141 mbrf (Figure 3). A weaker signal was recorded below in the 7.0 inch diameter open hole.

The FAC40 sonde for acoustic imaging of the borehole surface was sent down in the fourth run. Data were recorded on the way down with a low resolution to keep nominal descent speed. The tool went down to 202 mbrf. Data monitoring on the way down revealed a crucial technical difficulty. The borehole diameter, being close to 7 inches and larger, corresponded to a two way travel time very close to the second tool internal reflection on the teflon window through which the images are obtained, close to 144 µs. This meant that weak borehole wall reflections were systematically overcome by an internal reflection, the tool triggering system picking of course the larger of the two, instead of the borehole wall arrival. Original logging plans were made for a 100 mm diameter borehole (AIG-5), and TRI-5 with a 178 mm diameter, is far beyond the tool specifications. To alleviate this problem, two arrival time windows were set to exclude the internal reflection arrival time.

A first upgoing pass was recorded with a [150, 216] µs window, 144 measurement points per turn and 6 mm vertical offset. This pass was designed to image the hole enlargements. It was recorded from 202 to 141 mbrf. The FAC40 tool was then sent back down and a second upgoing pass was recorded from 202 to 141 mbrf with a [86, 142] µs window, 144 measurement points per turn were obtained with a 6 mm vertical sampling rate. This pass was designed to image the hole restrictions and was stopped upon entering casing at 136 mbrf.

The FAC40 tool was then lowered to 141 mbrf and a third pass was recorded within the casing with the same [86, 142] µs window as before but a lower resolution (72 measurements per revolution and a10 mm vertical sampling). This pass was also made to verify casing integrity. This pass is not correctly oriented because of the casing influence on the magnetic field triaxial measurements. The log terminates at 13 mbrf, where the tool came out of the water.

The IDRONAUT hydrochemical sonde was finally sent down in the fifth run. This sonde measures simultaneously borehole fluid temperature (°C), electrical conductivity (mS/cm), pH, Eh (mV), and pressure (dbar), from which fluid (here mud) density can be derived (Figure 2).

The data were recorded on the way down, as usual for borehole fluid measurements. The tool met an obstruction and stopped at 151 mbrf, where the down log was terminated. A maximum temperature of 20°C was obtained near total depth (151 mbrf), and fluid conductivity averages 40 mS/cm through the hole. Fluid density in the hole decreases gradually from 1.15 g.cm^{-3} near surface to about 1.05 g.cm^{-3} at the base of the logged interval.

The logging operations were terminated at TRI-5 when the IDRONAUT came back on the rig floor.

Data summary for TRI-5

The data recorded in Hole TRI-5 are summarized in Figure 2 for natural gamma ray, fluid properties, borehole wall acoustic images and inclinometry from magnetometer data. Figure 3 summarizes the sonic waveforms obtained in TRI-5. Note that hole inclination reaches a maximum of 10° at 141 mbrf. This may explain some of the difficulty encountered during tool descent.

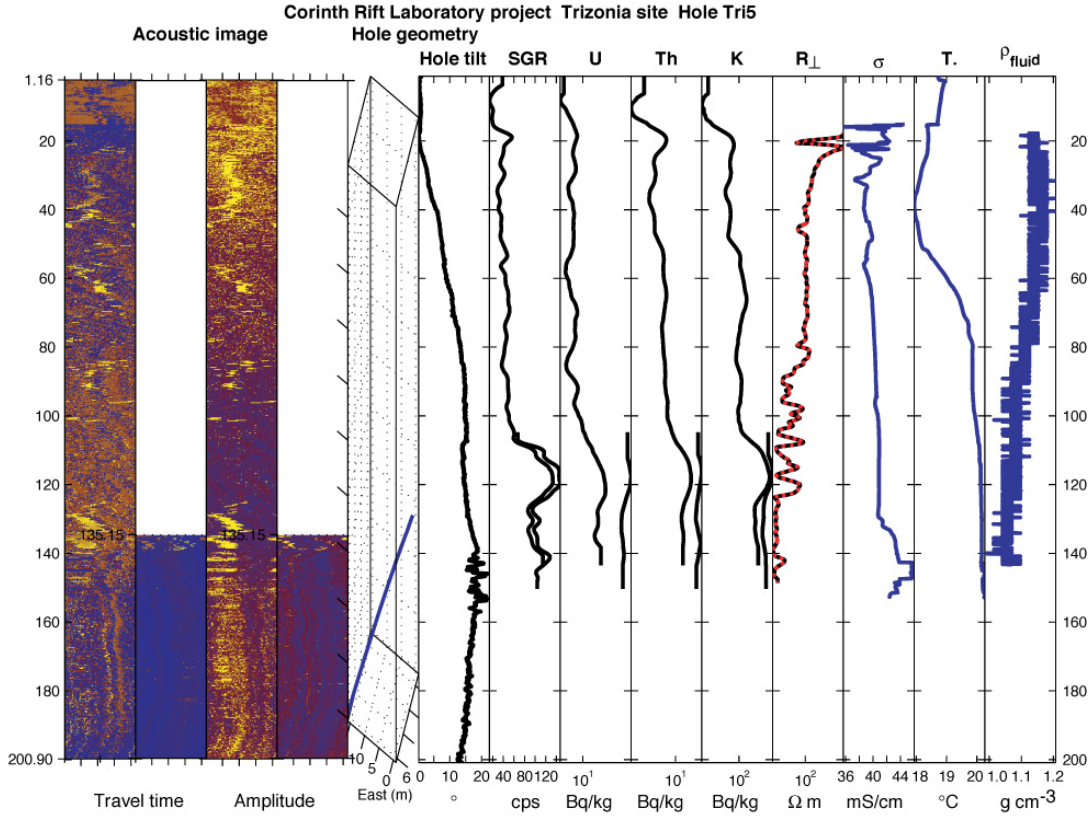

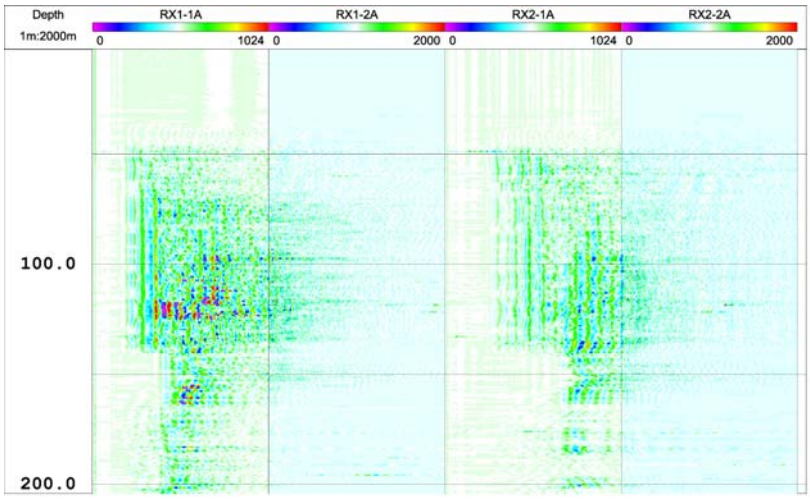

Fig. 6

3.1.3.2 Operations in Hole AIG-10 (May 31, 2003)

AIG-10 was entered on Saturday May 31st, 2003, with the IDRONAUT sonde for a single temperature log run. Zero depth was set at the top of the Blow Out Preventer. The high density mud stopped the tool descent at 71 mbbop where the log was terminated.

Table 2: Logging operations summary (May 2003)

Hole	Date	Run	Tool	Pass	Interval (mbrf)	Comments
TRI5	28-05-2003	1	GLOG	down	0-141	In casing
TRI5	28-05-2003	1	GLOG	up	0-141	In casing
TRI5	28-05-2003	2	SGR	down	0-143	In casing
TRI5	28-05-2003	2	SGR	up	0-143	In casing
TRI5	29-05-2003	1	GLOG	down	0-151	10 m in open hole
TRI5	29-05-2003	1	GLOG	up	0-151	10 m in open hole
TRI5	29-05-2003	2	SGR	down	0-151	10 m in open hole
TRI5	29-05-2003	2	SGR	up	0-151	10 m in open hole
TRI5	29-05-2003	3	FWS	down	0-206	65 m in open hole
TRI5	29-05-2003	3	FWS	up	0-206	65 m in open hole
TRI5	29-05-2003	4	FAC40	down	0-206	65 m in open hole
TRI5	29-05-2003	4	FAC40	up1	136-206	[150, 216] µs window
TRI5	29-05-2003	4	FAC40	up2	136-206	[86, 142] µs window
TRI5	29-05-2003	4	FAC40	up3	141-13	In casing, lower resolution
TRI5	29-05-2003	5	IDRONAUT	down	0-151	10 m in open hole
AIG10	31-05-2003	6	IDRONAUT	down	0-71	stopped in heavy mud

Table 3: Downhole geophysical sondes deployed by the Montpellier group in the Corinth Gulf as part of « DG-Lab Corinth » (May 2003)

Acronym	Measurement	Manufacturer
GLOG	Focused electrical log	Robertson
SGR	Spectral gamma ray	Antares
FWS	Full wave form sonic	ALT
FAC40	Acoustic televiewer	ALT
IDRONAUT	Fluid temperature, pressure	ALT

3.2 HYDRAULIC TESTING, HYDROGEOLOGY/ HYDROSTRATIGRAPHY OF THE AIGION AREA (UNIV. OF KARLSRUHE WITH GFZ-POTSDAM AND IPG-P)

Within the DGLab project for the IPG-P participation, this work was mostly supported by the German DFG for the work conducted by Univ. of Karlsruhe and GFZ-Potsdam.

As a result of a comprehensive study within a subproject headed by the GFZ Potsdam and the University of Karlsruhe the hydrostratigraphy of the sedimentary succession in the AIG10 borehole (Fig. 2) and the larger Aigion area was established (GIURGEA ET AL., 2003). From these studies, five aquifers can be delineated to a depth of 1000 m (total depth of AIG10 borehole).

The weakly consolidated, highly permeable sand and gravel sediments of the Meganitas river deposits constitute the uppermost aquifer with an approximate hydraulic conductivity of $10^{-2} – 10^{-3}$ m/s. This phreatic aquifer is separated from a second conglomeratic aquifer by a 50-m thick clay. This second aquifer is known from an adjacent borehole Γ_1 in 112 m depth, in which artesian flow was observed with flow rates up to 5 m^3/h (F. Lemeille pers. comm., 2001). That the thin clay layer at 158-160 m depth within the 250 m thick conglomerates separates two completely different aquifer systems is supported by hydrochemical analyses. The third and fourth aquifers were the subject of the pump tests performed in the AIG10 borehole. Furthermore, water-flow rate and pressure were monitored during a production test in the final open-hole interval of the well.

3.2.1. Hydraulic test in the conglomerates (1st pump test)

The pump test was made in a 9 5/8“ diameter open-hole interval in the conglomerates between 211 and 256.4 m. A “Grundfos SP60-10” pump was installed at 90-m depth in the cased borehole interval and a pressure probe (Eijkelkamp M2.11.11.50E) for the continuous registration of the drawdown was taped on the water pipe 10 m above the pump. The total duration of the step test was 67 hours. The automatic drawdown registration was made every 15 seconds. Results are published in GIURGEA ET AL. (2003) and reported here in less detail.

The hydrochemical analyses of the pumped water showed a very strong domination of the Na and Cl ions. This result, together with the calculated ion-ratios of the major elements and the minor and trace element contents (Br, Sr, Li, etc.), led to the conclusion that the water in the conglomerates in this 3rd aquifer is clearly of marine origin, though the total dissolved content (56 mS/cm) is higher than the seawater. This aquifer must be hydraulically isolated from the formations above and beneath; a hydraulic contact with the seawater in the Gulf of Corinth is very probable. Pump test interpretation shows that the tested aquifer is confined and almost artesian (water level only 1 m below preventer) but may leak through the thin, overlaying clay at 160-m depth or from deeper layers within the conglomerates.

3.2.2 . Hydraulic test (2nd pump test) in the Olonos-Pindos limestone

After cementing casing down to 708 m and coring from 708 to 744.8 m, the second pump test was performed in the 6 ¾” open hole in the Olonos-Pindos limestone (Fig. 7, 4th aquifer). The same equipment was used as in the first pump test. The natural water pressure was 5 bar and

the artesian flow rate 0.68 m^3/h. Because of the very poor permeability of the limestones it was necessary to reduce the pumping rate through curbing. After several tries it was finally possible to perform the test at a flow rate of 1.4 m^3/h. The hydrochemical analyses of the pumped water show a total mineralisation < 1 g/l (tab-water quality), a strong domination of Na ions (similar to the 1st test in the conglomerates), but a relatively high HCO_3 concentration (different compared to the 1st test). This leads to the conclusion that the water in the limestones was recharged in the hinterland of Aigion to the South, where the limestones are outcropping.

The tested aquifer is hydraulically well isolated from the aquifers above by the existence of aquicludes. Any hydraulic contact with seawater can be discarded. Pump test interpretation shows a hydraulic conductivity of the aquifer between 4×10^{-6} (in case of leakage) and 1×10^{-7} m/s (fractured aquifer).

3.2.3. Results from two production tests in the Olonos-Pindos limestone (footwall of the Aigion Fault)

After crossing the Aigion fault by drilling, a sudden increase of pressure and water flux was observed. This observation calls for conditions typical for karstic or densely fractured units, which is supported by analysis of drill core obtained at 773–786 m depth.

A production test was undertaken by IPG-P, together with Univ. of Karlsruhe, while the drill string was still in place, together with the BOP at the top of the well. The water production lasted 3 days (Sept 19- 22, 2002) and was accompanied by a very significant production of cuttings. During this production test, covering the complete openhole section of the well that extends mostly below the fault (708 – 1001 m), a practically constant flow rate of 54 m^3/h was observed. The artesian pressure before and after the test was 9 bars (measured with a manometer of the drilling company). Data point to an average hydraulic conductivity between 0.8 and 1.2×10^{-6} m/s for the 300-m interval. Analysis of the water chemistry shows that the bulk mineralization is about 1.03 g/l, so that the water practically is of tap-water quality except for the Na concentration. The difference in water pressure (4 bars) and in the hydraulic properties of the limestone in the hanging wall and in the foot wall of the Aigion fault provides evidence that two compartments (aquifers?) exist that communicate hydraulically through an extremely low-permeable zone (Aigion fault zone plus radiolarites in the foot wall).

At the end of this production test, the well was filled up with dense mud in order to stabilize the well. Results from this production tests were used to design the water evacuation system required for the installation of the permanent downhole instrumentation. A year later (September 2003), after the water evacuation system had been built, the mud was displaced and the well was left to flow freely. Again a significant production of solid particles was observed, but the flow was much larger than the initially planned 60 m3/h. It over-flooded the evacuation system and a temporary storage system was improvised. A scale was improvised which provided means to measure the rate of filling of the reservoir by measuring the water level at various time intervals. Results indicate a flow rate somewhere between 400 and 450 m3/h, i.e. about ten times larger than that measured when the drill string and the drill bit were in the well. This discrepancy comes from the fact that, during measurements in September 2002, the large flux of solid particles developed a screen around the drill bit which reduced significantly the flow rate. This phenomenon was observed at various stages during the cleaning of the well, in September 2003.

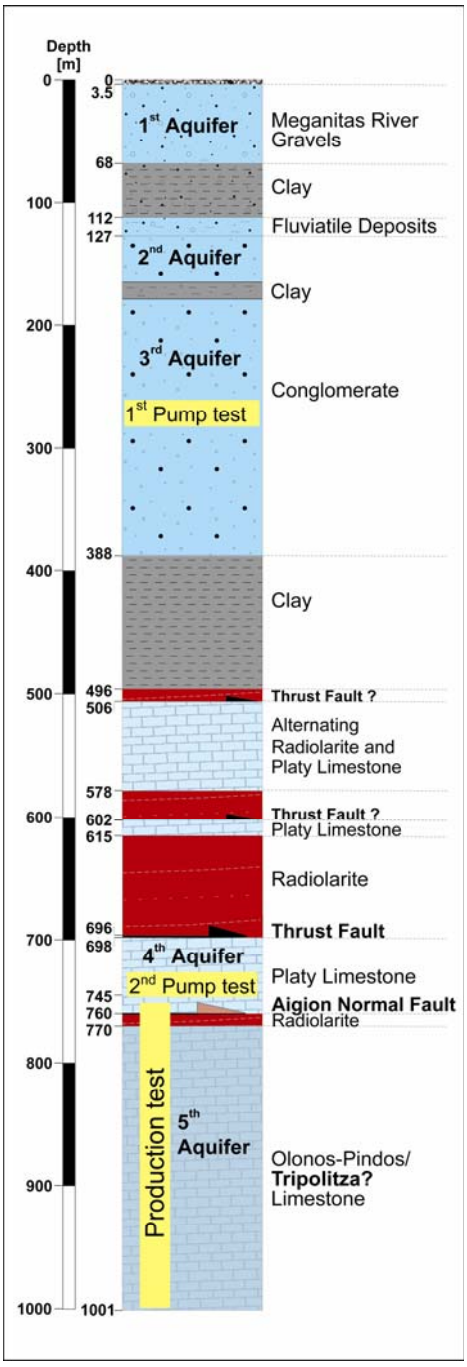

Fig.7: Schematic litho-log of the AIG10 borehole with hydrostratigraphy and location of pump tests (from GIURGEA ET AL., 2003)

3.2.4 Conceptual hydrogeological model of the Aigion area

Results of experiments in the AIG10 borehole, hydraulic tests performed earlier in the limestones of the Selinous valley, and the geological field work focused on the structural pattern at regional scale in the area south of Aigion (RETTENMAIER, 2002; UNKEL, 2003) gave rise to a preliminary conceptual hydrogeological model (Fig. 8) that will serve as a basis for a future numerical thermo-hydraulic model of the Aigion area.

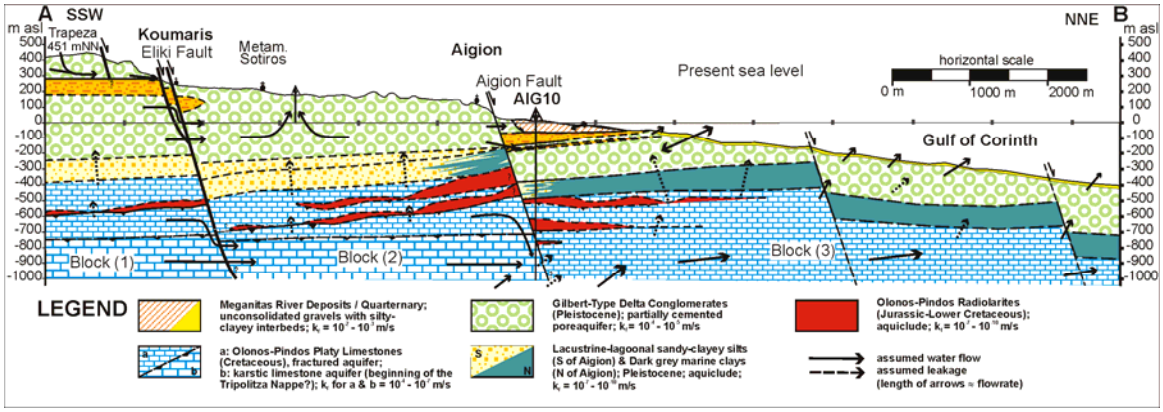

Fig.8: Preliminary conceptual hydrogeological model of the Aigion area with assumed flow paths (arrows) Length of arrows correlates with Darcy-flow rates. Hydraulic properties in legend (from GIURGEA ET AL., 2003).

This model is based on a SSW-NNE oriented, 14 km-long cross-section through the location of the AIG10 borehole, which is in the centre. The model area is subdivided into three main blocks: (1) the area south of the Eliki Fault; (2) the area between Eliki Fault and Aigion Fault and (3) the area north of the Aigion Fault. While the hydraulic conductivity of the aquifers was determined through the different hydraulic tests, the respective parameter for the aquicludes was approximated. The flow paths were defined on the basis of the water pressures encountered in the AIG10 and GAMA1 boreholes as well as in the water-supply wells of the Selinous valley.

Thus, the conceptual hydrogeological model integrates all information of the region available at this moment. Model features are:

- The phreatic water in the uppermost conglomerates of block (1) flows parallel to the clay layer and is emerging in the form of springs.
- The water pressure in the limestones is higher than in the conglomerates in all three blocks. This gives rise to assume that an upward-oriented leakage occurs not only through the thick clay sequence at the basis of the Plio-Pleistocene sediments, but also through the thin clay layers in the conglomerates.
- In the conglomerates of block (2), the S-N-oriented flow through the Eliki fault zone and upward leakage is additionally stimulated by intensive water catchments (shallow boreholes for drinking water and agricultural purposes).
- The hydrochemistry of the groundwater in the conglomerates of block (3) suggests mingling with the Gulf of Corinth water (double arrow).

- The formation water of the Olonos-Pindos Platy Limestone is recharged in the mountains, in the hinterland of Aigion (10 km or more to the south), flows rapidly, and finally is discharged in the Gulf of Corinth (indicated by submarine springs).
- Because the fault zones within the Olonos-Pindos nappe units obviously act as hydraulic barriers, the fluid flow beneath the radiolarites of the footwalls is forced to downward flow along fault planes. This flow occurs probably until higher-permeable fault zone segments are reached at depth, which allow the flow direction to become sub-horizontal again. After trespassing this higher permeable fault zone, the flow pattern will be again upward and S-N oriented. The short upward arrows at the base of the cross section indicate this. The high hydraulic resistance induced by this assumed complex flow paths is supported by the water pressure difference of 5 bar between the limestones in the footwall and those of the hanging wall of the Aigion fault.

3.3. VSP SURVEY: ACQUISITION , PREPROCESSING AND FIRST RESULTS (IFP, UPSL & IPG-P)

The AIG-10 well actually encountered the limestone formation at 696m, then intersected the Aigion fault at 760m, earlier than expected, then the well was deepened to 1000m Total Depth. After drilling and wireline logging, a 6 source position VSP survey (Fig.9) was successfully operated by a group of geophysicists from UPSL, IPGP and IFP, using the new SSR-CGG four component (4C) downhole seismic tool (4C: 3 orthogonal geophones + hydrophone), with the following initial aims:

1) illuminate the major structural features in the well vicinity: faults, dipping reflectors, etc…and obtain seismic velocity measurements in P and S modes.

2) investigate the reasons for the lack of surface seismic results in the immediate well vicinity.

3) study the additional information brought by the hydrophone measurements.

4) eventually study the S-wave anisotropy.

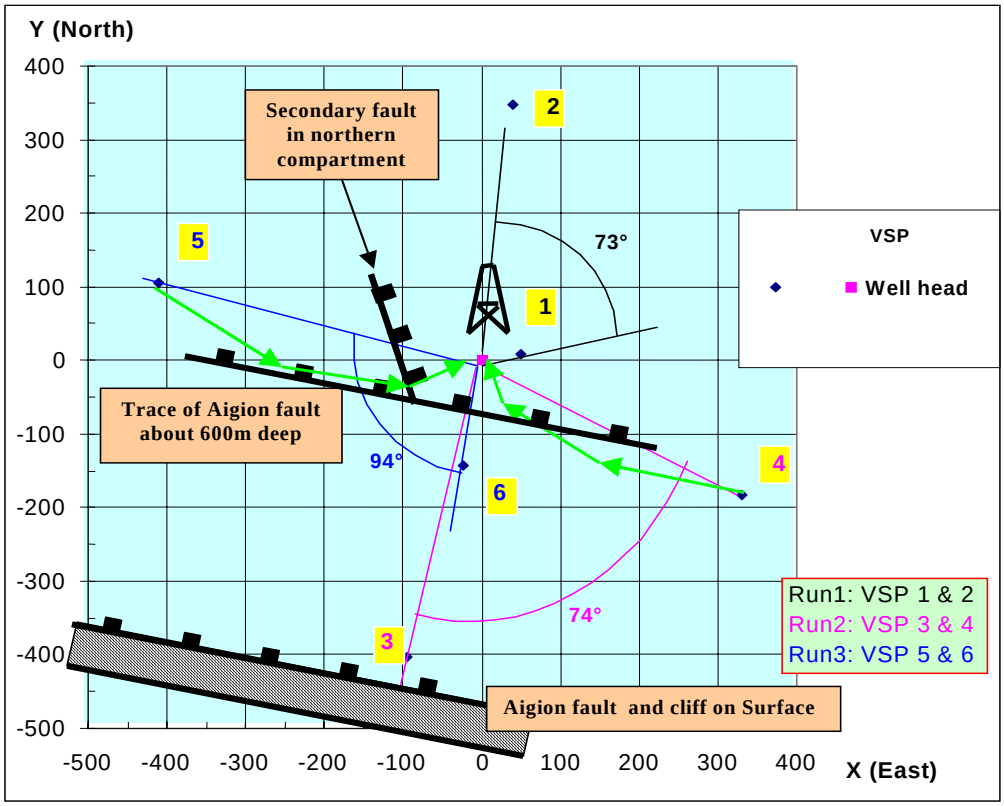

Fig.9: Plane view of wellhead and VSP source positions

VSP#3 yields the dip of the Aigion fault plane (60°), and the vertical throw of the Aigion fault (150m). Below depth 600m, VSP#5 detected a secondary accident located 100m west of the well. Conventionally, the direct arrival azimuths of all VSP's nearly follow the source to well direction. However, the direct arrival azimuths of VSP#4 and 5 are deviated below 600m due to

total refraction on the nearby Aigion fault plane (green rays), confirming the higher velocity in the southern fault compartment, as the fault plane is associated with a strong lateral velocity contrast.

The VSP survey took place after removal of the drilling machine due to operational and financial reasons. In consequence, as the VSP tool could not be lowered deeper than 755m, the borehole obstruction of the mud column at that depth could not be cleaned. The VSP acquisition is detailed in the E.U. 3F-CORINTH second year progress report (IFP report # 57348, March 2003).

3.3.1 VSP first processing results

Unexpectedly, in spite of major velocity contrasts expressed by the sonic log and by the interval velocities derived from direct arrival VSP times, the 3C-VSP processing results do not evidence clear P-P reflected events, even on the depth stations located right above the major impedance contrast levels (results not shown). Nevertheless, a few P-S converted reflected line-ups can be detected after downgoing wave train removal and call for further analysis.

In contrast, diffracted or refracted arrivals lead to constructive structural information:

On Offset VSP#3, located right on the surface trace of Aigion fault, it is clear that the direct arrival at shallow depth (right side of displays **Fig.10, 3**) is weaker than in depth, in contrast with all other 5 VSP's . Actually, in the deep part, the first arrival appears with higher energy (left half displays **Fig.10,3**), and exhibits a diffraction pattern with apex at 500-520m: this event actually corresponds to a P-P diffraction on the hard carbonate fault corner of the southern side of the Aigion fault (see the above structural sketch from surface refraction). At apex depth, the vertical component weakens, the horizontal-radial component gets stronger, and the energy on the hydrophone component remains consistent (**Fig.10**) thus the diffracted wave propagates in P-wave mode with near horizontal polarisation from the fault corner to the well sensors, at apex depth.

Last, on the deeper part of VSP#3 (leftmost traces on **Fig.10**), a weak refracted arrival appears in first arrival, 25ms earlier than the above mentioned diffraction; its energy is larger on the horizontal radial component, as its incidence measurement at the well is 70° (**Fig.13**): knowing the velocity on both fault compartments, the dip of the Aigion fault plane between 660m and 690m (see **Fig.13**) can be determined. The 60° dip value obtained corresponds precisely to the dip of a straight line joining the position of VSP#3 on surface, to the observed intersection of the well with the fault at depth 760m. The 60° dip value also correspond to the observed value of the dip of the Aigion fault suurface on the dipmeter log: therefore, the Aigion fault is characterised by a main fault plane with 60° dip.

The direct arrival polarisations from VSP#4 and 5 strongly deviate from the source-to-well-receiver radial direction below 600m, due to the close proximity of the high velocity southern compartment of the Aigion fault generating a partially refracted propagation along the fault plane, as illustrated by the green rays on **Fig.9**: therefore it was difficult to orient the horizontal components.

Hydrophone VSP data: Strong P-Tube upgoing converted arrivals appear on the hydrophone sensor, mainly generated right at the depth of a permeable fracture/fault at 744m. The hydrophone data show none of the strong S-wave events recorded by the 3C geophones. Many undesired downgoing tube wave arrivals are recorded by the hydrophone only: they would have been attenuated by aerating the mud column if the VSP operation had been carried out in presence of the drilling machine, as initially planned.

3.3.2 Present conclusions on the AIG-10 VSP study

The oriented 4 component VSP data helped refining **with confidence** the geometry of the Aigion fault, which appears as a single step extension fault dipping 60° to the N-NE, with a throw of 150m to 160m. The VSP revealed the existence of a secondary accident striking about SSE-NNW in the lowered northern compartment of the Aigion fault, located about 100m west to the well at depth 650m, with an eastward downthrow of 50m about, as illustrated on the plane view sketch **Fig.9**.

Although additional seismic results can be expected from more extensive data processing, the question raised by the lack of seismic reflection in surface and well seismic remains to be answered.

The hydrophone data yield innovative results, different and complementary to the geophone results, calling for deeper investigation and encouraging 4C VSP recording. The S-wave anisotropy will probably not be attained due to the complexity and heterogeneity of the geological medium.

VSP#3: Raw Hydrophone data **Fig.10**
Constant gain display

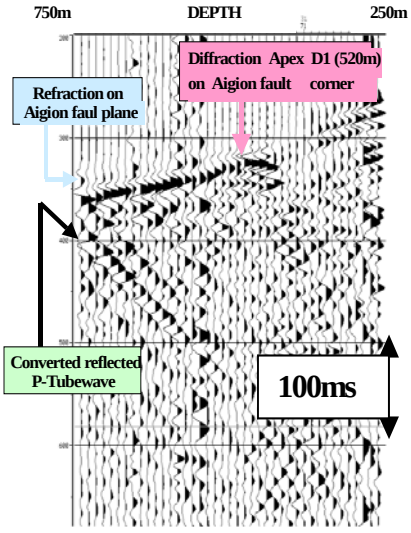

VSP#3: Z-component **Fig .11**
Constant gain display

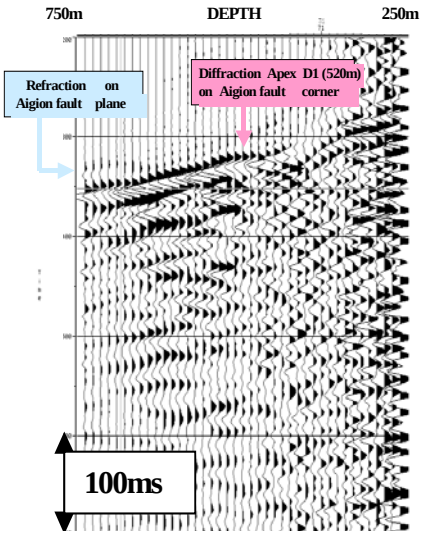

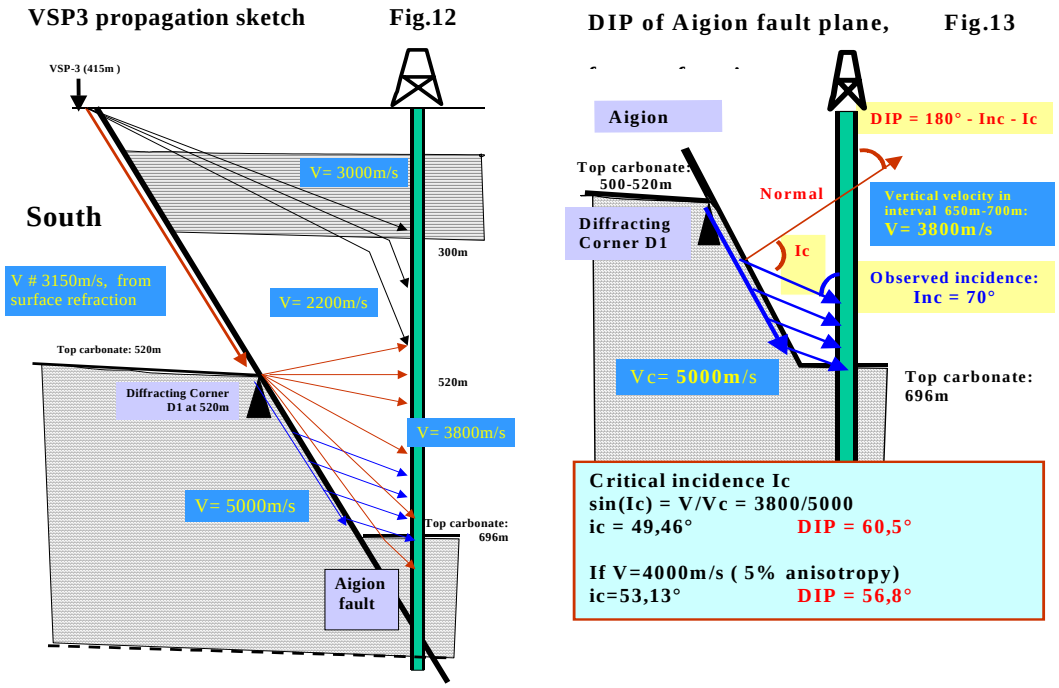

Fig.10,11,12,13: P-wave diffraction on Aigion fault corner and head wave arrrival refracted on fault plane, observed on Offset VSP 3:
Black rays: WEAK amplitude, near vertical polarisation
Red rays: STRONG amplitude, Diffraction on fault corner: at Apex depth, the diffracted propagation and polarisation are nearly horizontal: thus the observed apex depth nearly corresponds to the fault corner depth, at 500m (+/- 15m).
Blue rays: MEDIUM amplitude, Refraction on fault plane along high velocity carbonates, vertical incidence measured: 70°, leads to a 60° DIP for the Aigion fault plane (**Fig. 13**)

These results, combined with the sonic logs and the stratigraphic description provided by the cuttings and core analysis, together with the refraction data collected during the preliminary reconnaissance program, lead to the integrated cross section proposed on figure 14 The fault offset is found to be about 150 m, while the south (footwall) compartment exhibits a slight dip toward the South.

Figure 14 : cross section proposed by C. Naville for integrating, sonic logs and the VSP survey as well as the results from cuttings and cores analysis together with the preliminary reconnaissance seismic profile. Note that the limit at 520 m results from sonic observation and not from cuttings analysis; the upper 25 m of radiolarites are associated with the quaternary calcilutite (denominated clay in fig.14) because of its low velocity.

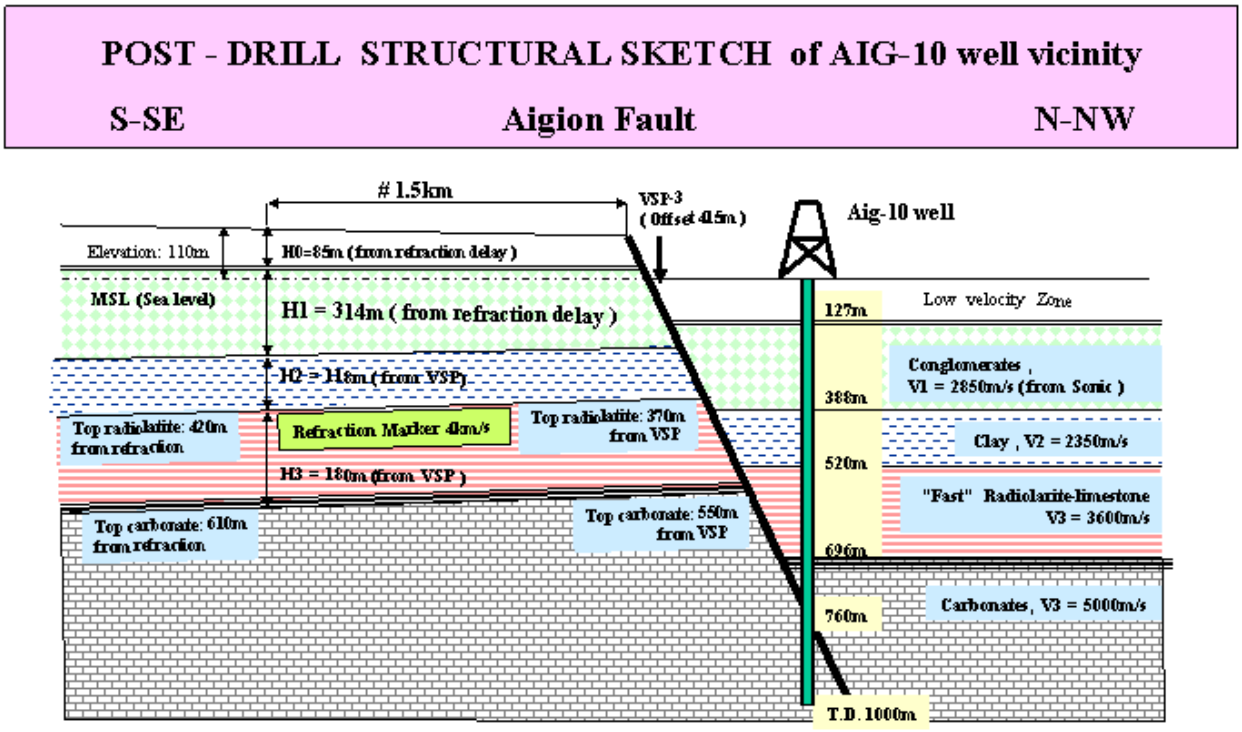

- The 4km/s refraction Marker on the South side of Aigion Fault corresponds to the top of the High velocity alternate radiolarite / limestone formation (or a bit deeper due to a possible diving propagation effect).
- The thickness and velocity of the radiolarite and clay formation on the South side of Aigion Fault are identical to the ones encountered by the Aig-10 well, since the Aigion fault is younger than these deposits.
- Therefore, the surface refraction measurements in a location about 1.5km to the South of Aigion fault yield a good estimate of the thickness of the consolidated conglomerates (314m).

4. WORK PACKAGE 4 – CORE ANALYSIS (IFP)

The coring operations in Aig10 well have been very successful above the Aigion fault, which resulted in a unique database for studying the structural impact of a normal fault on limestone tectonic fabric and its influence on fluid flow (Fig WP4-1). Below the fault, the core recovery was low due to karstic conditions. IFP scientists have been present on the well sites from early July 2003 up to Oct 2003 to follow the field work in progress. The IFP geologists also participated in the cutting descriptions. The cores have been described and completely pictured (Fig WP4-2). The transport and storage has been organised. Some rock samples have been mailed to the various partners and the main part is stored in the NCMR in Athens. The cores have latter been oriented by IFP thanks to the borehole images.

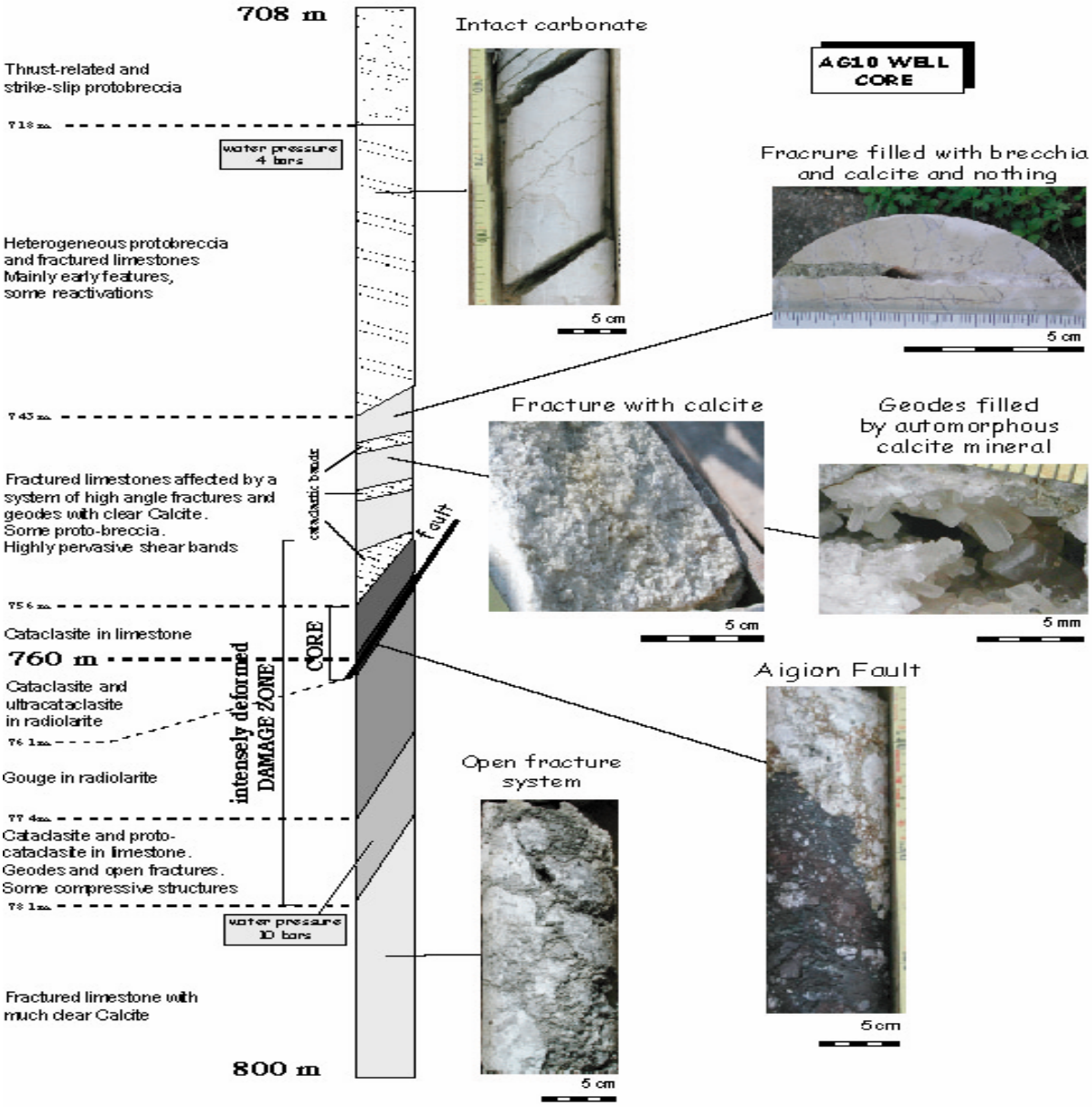

Fig WP4-1 : synthesis on the type of samples, rock matrix/fractures core in AIG-10.

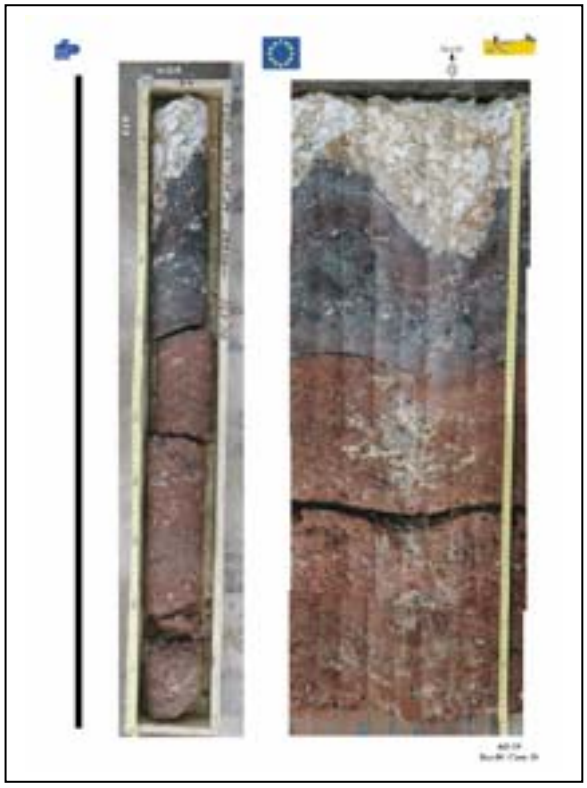

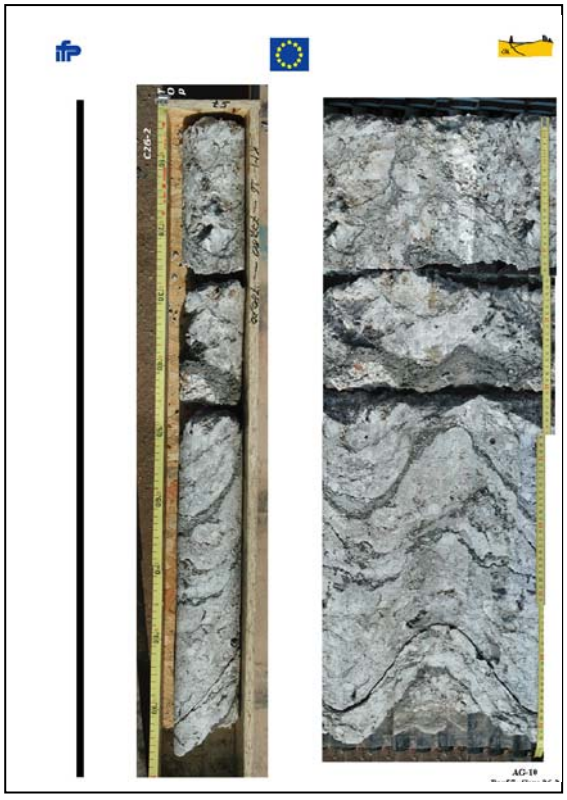

Fig WP4-2 :

Samples of the plates of the report on the well cores showing the facies above (box 27), on, and below (box 57) the fault plane. The report contain 65 plates like these 3 ones and a CD with the full digital information as well as a description of the lithology fabrics and structures.

A thorough record of the all sampling achieved by the different partners has been compiled and a database will be build with a copy of all the thin sections. The laboratories that have now samples of the AIG-10 wells are: Un of Kahruhl, Un of Edinburg, Ecole de Ponts et Chaussée, IFP (all partners of the EEC projects) and Un. of Grenoble, Un. of Montpellier, IPG-Strasbourg, Un. of Orsay (linked to DG-Lab and 3F-Corinth by national research projects).

As shown in the previous figures, the core of the fault plane is rather shally and the cataclastic zone full of void. It was therefore very difficult to cut theses samples and we din't wan to take any risk. It has been decided to inject the resin within the brittle pieces of core before to saw it. Machines able to inject the resin and previously to make void in large samples (up to 20 cm long) are rather rare. It has been done in Strasbourg (IPG-S) but the full set of thin section of the wells is not yet achieved. A long process of complete description of the core has taken place before.

Fig WP4 – 3: for each sample, after orientation and description, at least 3 thin sections are under realisation, on horizontal and 2 vertical, each one is done twice in order to main one copy of each on the data base.

Samples of the calcite veins have been extracted first and the isotope values (δC13 and δ18O SNOW) are now available. The data show that at least two fluids have participated to the veins growth, meteoric water and seawater.

We have to note that a large part of this work has been done with no-EEC fund since the budget was over before having the samples. Nevertheless the study of this extraordinary material will continue, the team is organised and studies are on progress: on the core macro-description, on the thin section analyses, on the stables isotopes of veins, on veins deposit analyse under SIMS, on the fluid inclusions, on the dates of veins (by U / Th approach), on the modelling of the veins growth (in collaboration with INGV that made the chemical description of the water).

The structures find on the Aigion fault will be compared to the ones already described on the Helike and Pirgaki faults (Fig WP4-3 and 4). On the Pirgaki fault, the analyse of the shale traps in the fault core have shown the mark of relatively high temperatures that could be interpreted in term of formal burial (more than 3 km) of local circulation of hot fluid. Up to now, it seems that the Aigion samples show the same phenomena (on the isotope values), which in this second case may be only interpreted as a circulation of hot fluid. The work is in progress, a part will be avalaible for the final report of 3F-Corinth but I think that 2 more years will be necessary to complete the core analyse.

Fig WP4-3 Helike fault core in limestones. (a) Cemented cataclasite displaying a closely-spaced system of veins, cutting all the other microstructures (cut sample, survey site H3). Sketch shows the orientation of the main microstructures compared to the fault plane. (b) Blocks of older, highly cemented cataclasite involved within the more recent core (cut sample; survey site H3). (c) Contact between an older cataclasite block and the more recent cataclasite. Newly formed cataclasite displays a system of preferentially oriented veins, totally

or partially filled by subhedral calcite (plain light microphotographs; blue is the impregnation of the epoxy resin in pores). (d) Fine crush breccia and highly fractured limestone (cut sample, survey site H4), affected by a system of sub-vertical microfractures (see the sketch in the top). (e) Extensional microfractures are empty or partially filled by calcite and cut all other structures (plain light microphotographs; blue: impregnation of the epoxy resin in pores). (f) Micro synthetic shear zone affecting the limestone in the pervasively fractured damage zone close to the Helike fault plane (survey site H5; plain light microphotographs; blue: impregnation of the epoxy resin in pores).

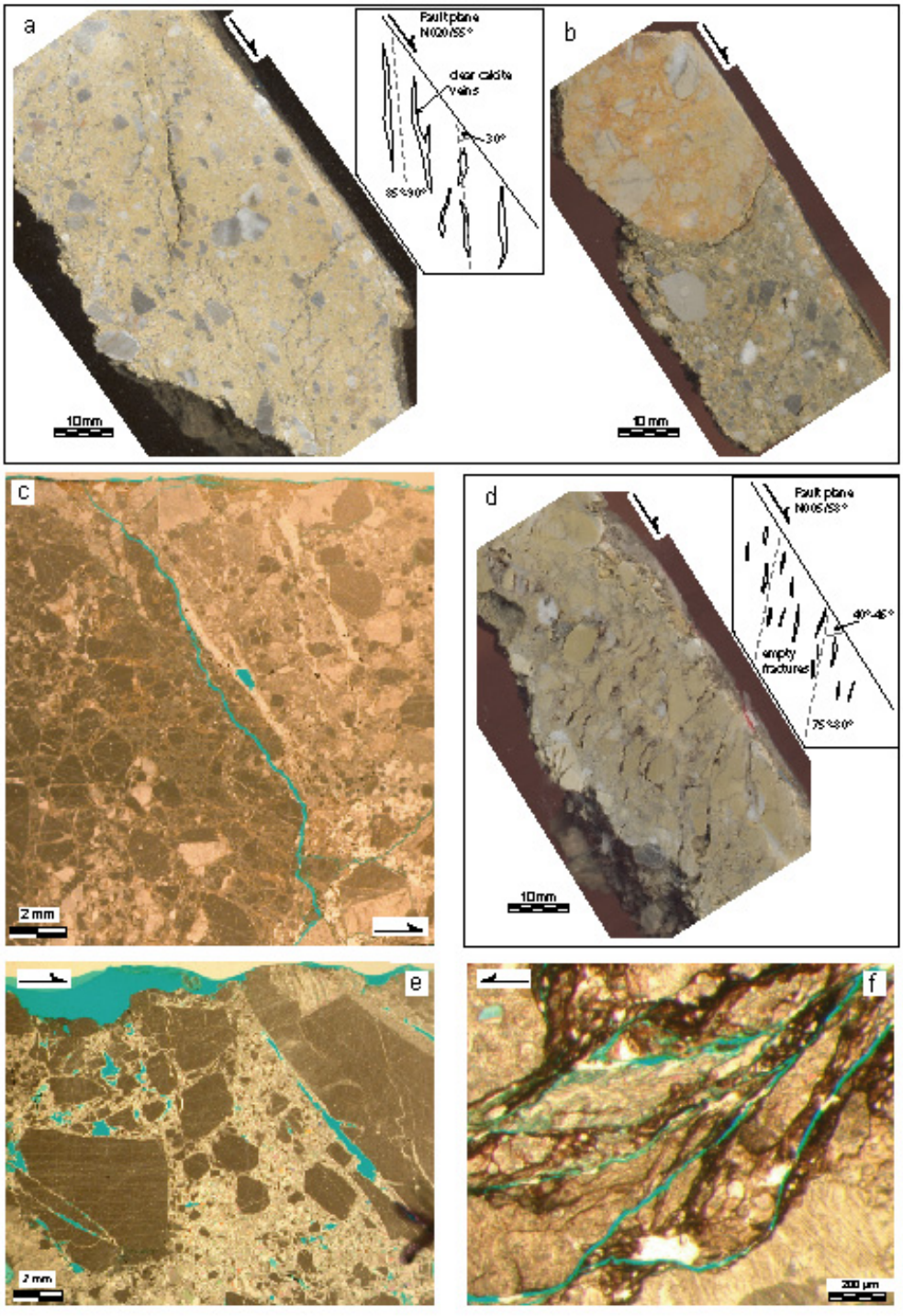

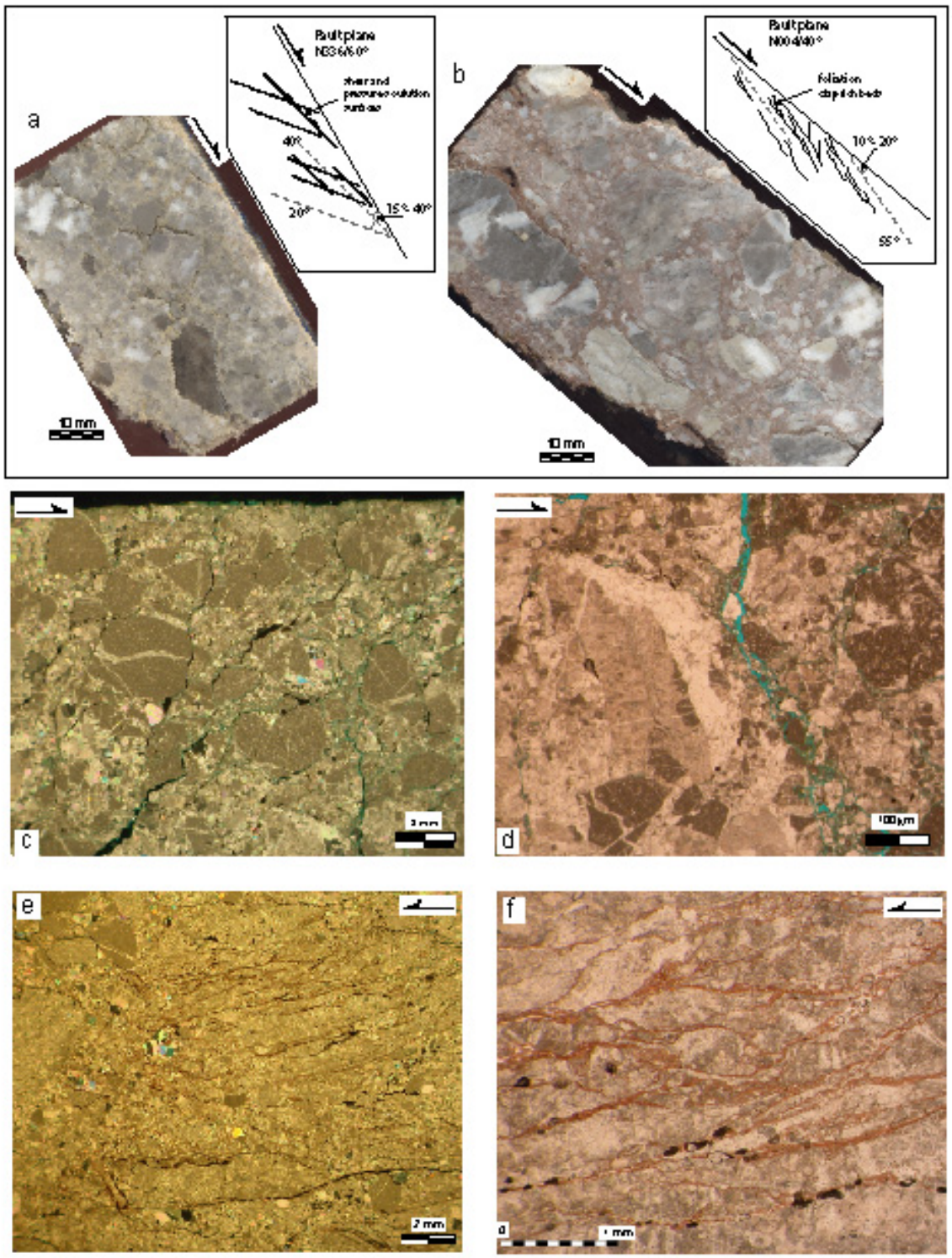

Fig. WP–5: Pirgaki Fault core. (a) Highly cemented protocataclasite and cataclasite displaying random fabric (cut sample; survey site P1). Sketch shows the orientation of the shear and pressure-solution surfaces compared to the fault plane. (b) Cataclasites and ultracataclasites displaying foliated fabric (cur sample; survey site P2). Sketch shows the orientation of the main microstructures compared to the fault plane. (c) Random fabric cataclasite (crossed polarized microphotograph; survey site P1), with random or preferentially

oriented shear and pressure-solution fractures. (d) Random fabric cataclasite: open fractures within the fault rock (plain light microphotographs; blue: impregnation of the epoxy resin in pores; survey site P1). The few calcite extensional veins are all within blocks of re-involved older cataclasite. (e) Foliated cataclasite-ultracataclasite (crossed polarized microphotograph; survey site P2). The foliation is defined by a dense system of clay-rich and oxide-rich beds. (f) Foliated ultracataclasite: elongated aggregates and preferentially oriented alignments of fine-grained mineral grains sub-parallel to the sense of shear (plain light microphotographs; blue: impregnation of the epoxy resin in pores; survey site P2).

Bibliography:

Moretti I, Micarelli, L., Daniel, JM, Eyssautier, E., Frima C., 2003. The core of AG10. IFP report n° 57240. 70 pp (including a CD with the digital data).

S. Eyssautier-Chuine, L. Micarelli, 2003**,** Cataclastic microfabrics and diagenesis in active fault zones : the Pirgaki and Helike faults (Gulf of Corinth), in prep.

5. WORKPACKAGE 5 – LABORATORY MECHANICAL AND HYDRAULIC CHARACTERIZATION (UNIV. EDINBURGH & CERMES)

5.1 HYDRAULIC AND MECHANICAL CHARACTERIZATION (UNIV. OF EDINBURGH)

5.1.1 Introduction

The objective of studies carried out by the University of Edinburgh under Work Package 5 has been laboratory mechanical and hydraulic characterisation of gouges and limestone within the Aigion fault zone, and the relation of these properties to regional hydraulic flow and rock rupture patterns. This work has encompassed two themes, detailed below. The first was the development of new permeametry techniques capable of better laboratory measurement of the hydrological properties of bulk rock samples from the Aigion region, the second was laboratory measurement of rock properties of both bulk rock samples from the region, and borehole materials. These measurements were undertaken on commonly used 38mm core samples, and also on 70mm and 100mm samples in the specialist 'BigRig' compression testing machine at Edinburgh. Despite some problems from the delivery schedule of core materials, all the original deliverables have been produced, and additional work on hydraulic properties of fine-grained calcitic powders has been undertaken to better understand the peculiarities of AIG10 fault gouge materials, at no extra cost to the Project.

Our laboratory data has given important insights into both the hydrological and mechanical environment of the Aigion fault zone. It predicts that bulk water flow in the basal limestones is fracture flow, that there is a sealing unit between the upper conglomerates and lower limestones, that within the borehole itself the old and new gouges and breccias are hydraulic seals, and explains the borehole overpressure encountered below the fault. It also gives insights into the deformation response of the bulk limestones of the region, and of the old and new gouge and breccia within the current active zone.

Two papers arising from these studies have been submitted, one on the permeameter design (to Journal of Geophysical Research) and one on the unconsolidated materials (to Comptes Rendus at the invitation of the overall Project Leader). The work has been presented orally to the American Geophysical Union and the European Geophysical Society meetings, as well as to an internal project meeting in Aigion.

Background

Reliable measurements of the strength and hydraulic flow parameters of rocks are essential for the modelling of many geologic processes, for the prediction of seismic sensitivity, and for the design of extraction, aquitard and flush systems for the sustainable use of groundwater supplies. Thus accurate laboratory techniques are especially important for areas such as the Gulf of Corinth, which is a region of restricted water supply, and of active seismic disturbance. For earthquake studies, it is critical to note that, in conjunction with the physical properties of reservoir rocks, the hydraulic characteristics of the fluid trapped within the pore space influence the

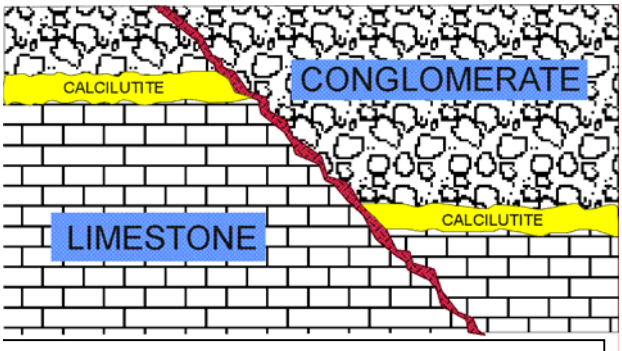

Fig 1 Schematic of Aigion sequences

elastic response (Biot, 1941; Rice and Cleary, 1976; Detournay and Cheng, 1988), the inelastic behaviour (Wong and Biegel, 1985; Fournier, 1996; Simpson, 2001; Simpson et al., 2001), and the time-dependent reactions of rocks. (Johnson et al., 1973; Mortensen et al., 1977; Roeloffs et al., 1989)

The geology of the study area consists mainly of a thick formation of tight, highly fractured micritic limestone as a bedrock, covered by Late Pleistocene marine terrace deposits, composed mainly of conglomerate. As illustrated in Figure 1, separating the two sequences is commonly a laminated calcitic mud (properly, 'calcilutite') up to several metres in thickness providing an unconformable ductile top cap for the limestones. The calcilutite is important because it can control the hydraulic connectivity between limestone and conglomerate, and because it is an excellent analogue for fine-grained cataclasite expected to be found on major regional faulting through the limestone sequence. Hence its properties are important for understanding the hydro-mechanical response of the Aigion fault zone. Within the Aigion (AIG10) borehole itself the active fault transects the radiolarian sequence, so that comparison of material properties of calcilutite and recovered siliceous fault gouge provides insight into both local and regional hydromechanical coupling in the Aigion fault in the AIG10 borehole area.

In the sections below, we detail our development of new laboratory techniques suited to the Aigion area, and our laboratory mechanical and hydraulic tests and results.

5.1.2 Laboratory Technical Development

5.1.2.1 Introduction

As part of the Edinburgh contribution to studies of the Aigion fault zone and its geological setting and responses, we have developed a new laboratory method of determining the hydrological permeability and storativity of rock samples. The particular advantage of this new method is its speed, and its applicability across a surprisingly wide sample permeability range.

The nature of fluids in rocks can be characterised in terms of quantity (concentration) and mobility of the fluid. The specific storage S_s deals with the capacity of a rock in storing a fluid as a function of fluid pressure, whilst the permeability k measures the ability of the rock to transmit a fluid through its interconnected passages and voids. Because saturated rock is a mixture of three phases, fluid, pore space and solid matrix, the compressive storage of fluid in the rock can be obtained from the compressibility of each separate part and the connected porosity of the rock sample (Brace et al., 1968).

At its simplest, according to Darcy's law, rock permeability can be determined by measurement of the steady-state pressure drop along a sample under constant flow conditions. However, for extremely low permeability rocks long periods of time are required to establish a steady state (Hsieh et al., 1981; Olsen et al., 1985; Zeynaly-Andabily and Rahman, 1995; Esaki, 1996). If a fluid is pumped into a cylindrical rock specimen at one end at a constant flow rate, the pressure in the pump (or upstream reservoir) increases with time and eventually stabilises to a steady state where the downstream flow rate equals the injection flow rate, and the Darcy permeability of the sample is calculated. Morin and Olsen (1987) presented an analytic method for determining values of the specific storage and permeability from the

initial transient response during the early testing time. Esaki et al. (1996) improved this method by taking into account the compressive storage of the flow pump system. However this method also requires a tedious curve matching routine.

For faster results, non-steady state methods such as the transient flow method were suggested by Brace et al. (1968) as a pragmatic approximation in low permeability rocks. As a consequence, these methods have long been adopted to measure the permeability of tight rocks, with slight modifications (e.g., Zoback and Byerlee, 1975; Trimmer et al., 1980; Neuzil, 1981; Lin, 1982; Lin et al., 1986; Zeynaly-Andabily and Rahman, 1995; Liang et al, 2001; Kwon et al., 2001). The experimental configuration consists of a cylindrical specimen between two fluid reservoirs. A sudden pulse in the fluid pressure in the upstream reservoir induces fluid flow across the specimen due to the pressure difference between the two reservoirs. The decay rate of the pressure difference between the reservoirs is related to the permeability of the sample. However it is still necessary to measure the specific storage of the sample independently.

5.1.2.2 Theoretical Analysis

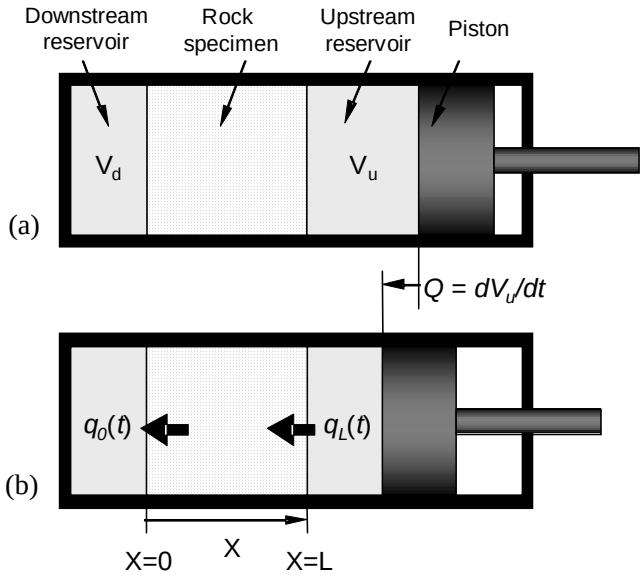

Fig. 2. Conceptual model of permeameter.

The new technique for simultaneously measuring permeability and specific storage of a single core sample is based on theoretical analysis of one-dimensional fluid flow induced by constant-rate pumping into a specimen placed between two reservoirs (Fig 2). In the conceptual model, the downstream reservoir is sealed, the sample is held at a fixed position between $x = 0$ and $x = L$, and fluid from the upstream reservoir is forced through the rock at a constant rate by a piston. Our analytic solution of the general diffusion equation with this new boundary condition provides a new method of simultaneously determining the permeability and the specific storage of a rock sample in a straightforward, reliable and relatively rapid way. We have validated the method by applying it to three well-known rock types, Westerly granite, Berea sandstone and Indiana limestone, and then applied the method to determine the properties of Olonos-Pindos limestone.

5.1.2.3 Governing Equation and Initial-Boundary Conditions

For the test geometry shown in Fig. 2, the actual flow rate entering the specimen at a certain time t equals the difference between the total pumping rate generated by the movement of piston and the extra volume induced by the compliance of pump system and the compressibility of the fluid per unit time interval. Thus the actual flow rate $q_L(t)$ at $x = L$ can be written as (Esaki et al., 1996):

$$q_L(t) = Q - S_u \frac{dp_u}{dt}, \tag{1}$$

where Q, S_u and p_u are the constant pumping rate, the compressive storage of the upstream reservoir and the upstream pressure, respectively.

The inlet fluid, compressed due to the stroke of the piston, migrates through the interconnected voids in the rock to the other side of the specimen (Fig 2b). The downstream reservoir is closed, so the inflow of the fluid into the limited space results in a fluid pressure increase. The relationship between the flow rate $q_0(t)$ at $x = 0$ and the rate of change of the pressure dp_d/dt is expressed as

$$q_0(t) = S_d \frac{dp_d}{dt}, \tag{2}$$

where S_d and p_d are the compressive storage and the fluid pressure of the downstream reservoir, respectively.

Both S_u and S_d are controllable in laboratory tests by changing the volumes of the upstream and downstream reservoirs V_u and V_d, respectively. For example, if the downstream reservoir V_d is zero, S_d becomes negligible because there is no flow into this reservoir, *i.e.* $q_0(t) = 0$. The upstream reservoir volume V_u can be easily controlled by changing the position of the piston (Fig 2a).

The fluid pressure p as a function of time t and distance x within a finite specimen when a flow pump injects fluid into the specimen at one end can be described by the general diffusion equation with appropriate boundary conditions as discussed above. The governing equation is then

$$\frac{\partial^2 p(x,t)}{\partial x^2} - \frac{1}{\alpha}\frac{\partial p(x,t)}{\partial t} = 0, \tag{3}$$

where α is the hydraulic diffusivity expressed as $k/\mu S_s$, with μ the dynamic viscosity of the fluid. The basic system variables are:

$$K = \frac{k}{\mu}$$

$p(x, t)$: fluid pressure in the sample as a function of x and t
p_d: fluid pressure at the downstream reservoir
p_u: fluid pressure at the upstream reservoir
x: distance from the downstream boundary along the sample
t: time from the start of pumping
A: cross-sectional area of the sample
L: length of the sample
k: permeability of the sample

S_s: specific storage of the sample
S_u: upstream compressive storage
S_d: downstream compressive storage

5.1.2.4 Analytic solution

The solution to the partial differential equation (3) with appropriate boundary conditions for constant pump input rate in terms of fluid pressure p as a function of position x and time t is

$$p(x,t) = \frac{F}{\beta}\left(t + \frac{x^2}{2\alpha} + \lambda_d x - \frac{L^3}{6\alpha^2\beta} - \frac{\lambda_u + \lambda_d}{2\alpha\beta}L^2 - \frac{\lambda_u\lambda_d}{\beta}L \right) - 2F\sum_{m=1}^{\infty} \frac{\exp(-\alpha\phi_m{}^2 t)(\cos\phi_m x - \alpha\lambda_d\phi_m \sin\phi_m x)}{\phi_m a \sin\phi_m L + \phi_m{}^2 b\cos\phi_m L}, \quad (4)$$

$$\text{where } \lambda_u = \frac{S_u}{KA},\ \lambda_d = \frac{S_d}{KA},\ F = \frac{Q}{KA},\ \beta = \frac{L}{\alpha} + \frac{S_u}{KA} + \frac{S_d}{KA},$$

$$a = 3 - 5\lambda_u\lambda_d\alpha^2\phi_m{}^2 - \alpha L(\lambda_u + \lambda_d)\phi_m{}^2,\ b = L + 4\alpha(\lambda_u + \lambda_d) - \lambda_u\lambda_d\alpha^2 L\phi_m{}^2.$$

The eigenvalues ϕ_m are the roots ϕ of

$$\tan\phi L = \frac{\alpha\phi(\lambda_u + \lambda_d)}{\lambda_u\lambda_d\alpha^2\phi^2 - 1}. \quad (5)$$

The analytic solution consists of a dominant part (asymptotic solution) and a transient part (series solution). At the beginning of pumping, the transient dominates, but then decays with time because of the negative exponential term in (4) and eventually becomes negligible. In a realistic test, we can only measure the upstream and downstream fluid pressures. These pressures at the upstream and downstream reservoirs as a function of time can be found by setting $x = 0$ and $x = L$ in equation (4), giving

$$p_u(t) = \frac{F}{\beta}\left(t - \frac{L^3}{6\alpha^2\beta} - \frac{\lambda_u + \lambda_d - \beta}{2\alpha\beta}L^2 - \frac{\lambda_u\lambda_d - \beta\lambda_d}{\beta}L \right) - 2F\sum_{m=1}^{\infty} \frac{\exp(-\alpha\phi_m{}^2 t)(\cos\phi_m L - \alpha\lambda_d\phi_m \sin\phi_m L)}{\phi_m a \sin\phi_m L + \phi_m{}^2 b\cos\phi_m L} \quad (6)$$

and

$$p_d(t) = \frac{F}{\beta}\left(t - \frac{L^3}{6\alpha^2\beta} - \frac{\lambda_u + \lambda_d}{2\alpha\beta}L^2 - \frac{\lambda_u\lambda_d}{\beta}L \right) - 2F\sum_{m=1}^{\infty} \frac{\exp(-\alpha\phi_m{}^2 t)}{\phi_m a \sin\phi_m L + \phi_m{}^2 b\cos\phi_m L}. \quad (7)$$

The full analytical solution and detailed methodology is further discussed in Song et al, (2003b)

5.1.2.5 Experimental Configuration

Tests were conducted using the experimental pressure cell shown in Fig. 3. In this cell, a 38mm diameter core sample 40-60mm long, with a 3mm porous stainless steel distribution disc at each end, is confined between two fixed pistons, while a static confining pressure is applied hydraulically via the cylindrical rubber jacket. Three well-characterised rock types; Berea sandstone, Indiana limestone and Westerly granite were used as standards to validate the new technique, before the hydraulic properties of Olono-Pindos limestone were determined. The basic physical parameters of each rock type are listed in Table 1.

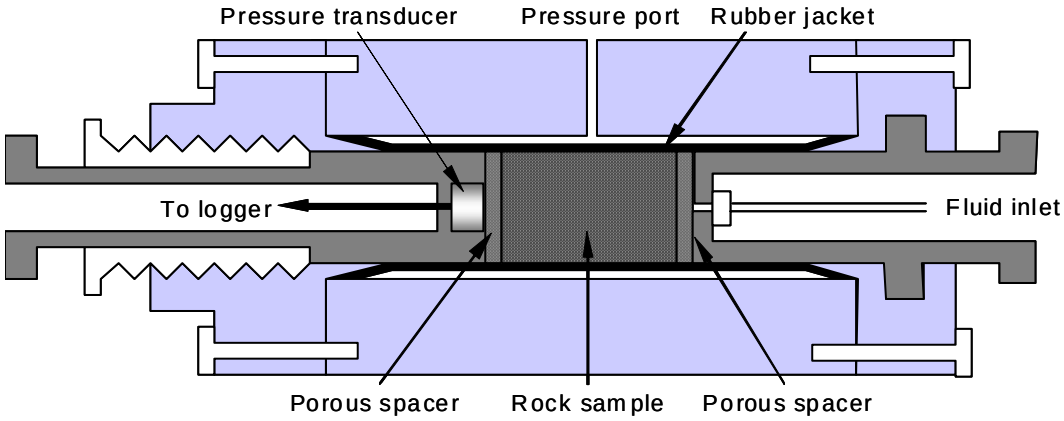

Fig. 3. Schematic section of permeameter cell for 38mm diameter core.

During preparation, the sedimentary rocks were cored perpendicular to the bedding plane, and all specimen ends were machined to smooth parallel faces. Samples were vacuum saturated with degassed-deionised-distilled water for 24 hours at room temperature. During testing, the confining pressure was kept constant throughout each test cycle at 5 MPa for

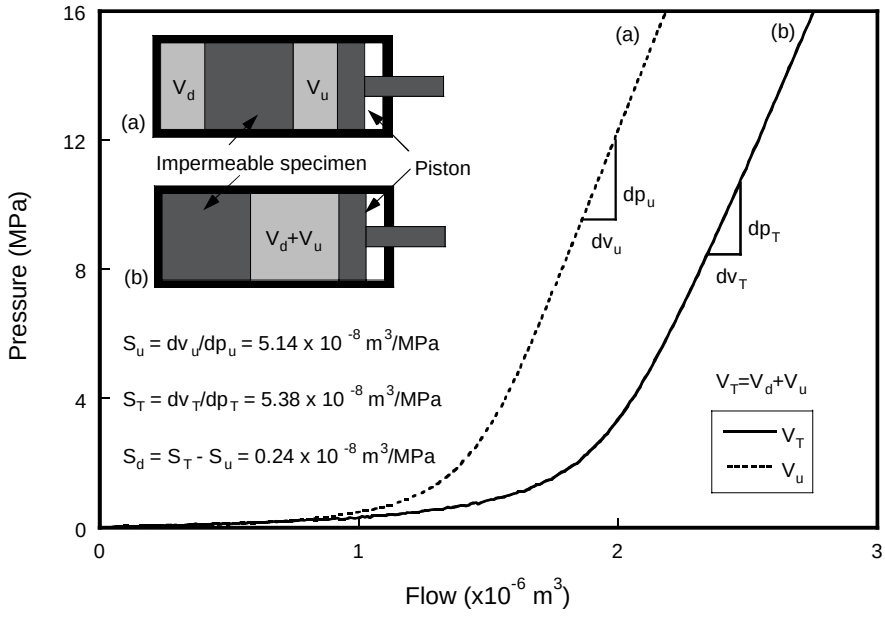

Fig. 4. Graphical analysis to determine apparatus compliance

Indiana limestone

and Berea sandstone, and at 35 MPa for Westerly granite. A pressure transducer endplug was used at the downstream side, while the upstream end was connected to a stepper-drive piston pump, with a pressure gauge between pump and rock specimen. The upstream and the downstream fluid pressures induced by constant-rate flow pumping through each sample were computer logged.

Before any rock tests, the system compliance was calibrated in terms of the compressive storages of the upstream and downstream reservoirs as required for equations (1) and (2). The calibration geometry was the same as for the rock tests except that an impermeable steel specimen was used instead of rock, as in Fig. 4 above. Notably, the upstream compressive storage S_u is a function of the volume of reservoir; *i.e.* it is dependent upon the position of the pump piston. The starting position of the piston was kept consistent in the calibration and in every test to minimise any difference in the system compliance between the calibration and the test. Also, by changing the starting position of the piston, it was possible to test a sample to validate the consistency of rock properties under different system compliances.

5.1.2.6 Results

Typical examples of the time-based record of fluid pressure variation at the upstream and downstream reservoirs arising from constant-rate flow injection are given in Fig 5 for the three different rock types.

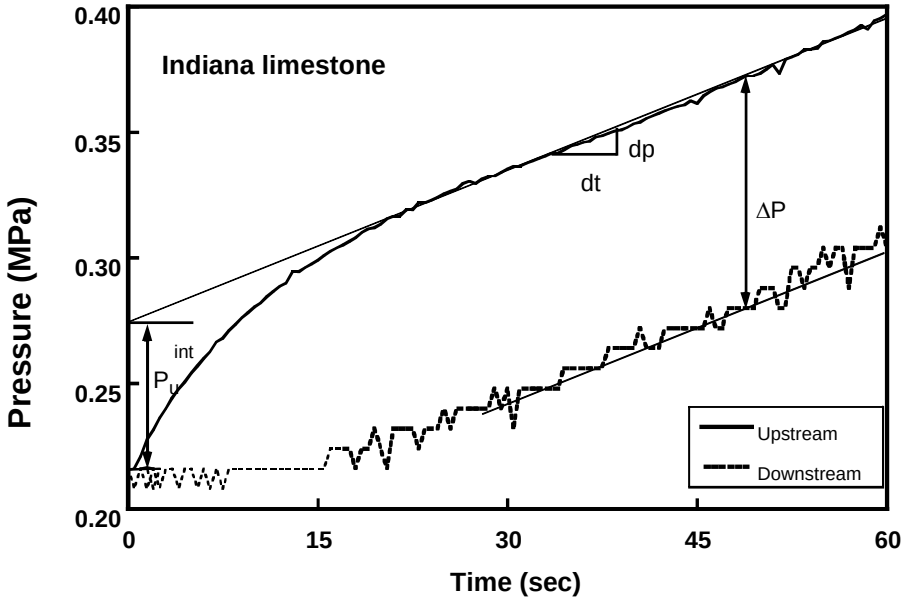

Fig. 5a. Hydraulic response across Indiana limestone

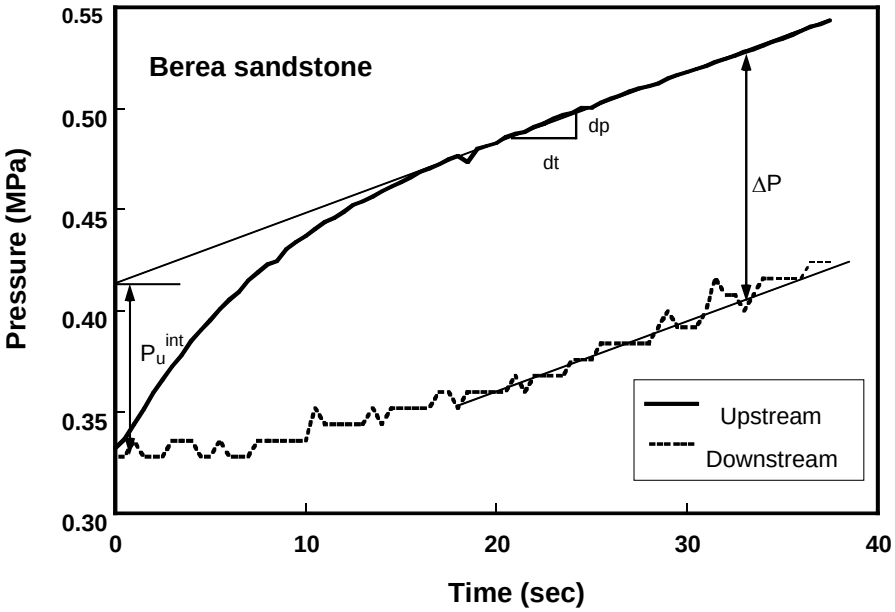

Fig. 5b. Hydraulic response across Berea sandstone

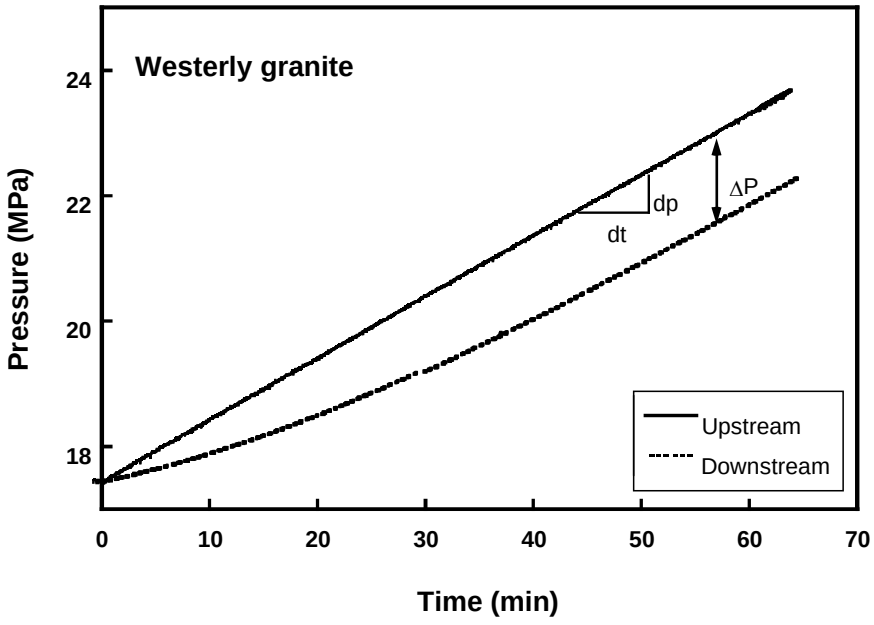

Fig. 5c. Hydraulic response across Westerly granite

At the beginning of each test, the pressures in both reservoirs were in equilibrium, and the upstream pump was started. In agreement with the theoretical analysis mentioned above, the upstream pressure increased immediately at the start of pumping, and rose at a decreasing rate during the transient phase, whilst the downstream pressure reacted after some delay, and then at a monotonically increasing rate. Eventually both rates of pressure increase became identical and maintained a constant value, so that both curves become linear and parallel as predicted by theory. In the highly porous Indiana limestone and Berea sandstone, the

transient curve for the upstream pressure is clearly convex upward (Figures 5 a and b). In the tighter Westerly granite, however, the transient for the upstream pressure is less clearly curved (Fig. 5c). This distinct behaviour results from the difference in specific storage. Note that the noise on the downstream pressure records for Indiana limestone and Berea sandstone is a digitisation effect in the pressure transducer installed at the endcap. This noise becomes insignificant in the test record of Westerly granite.

From each test record, the slope (*dp/dt*) was determined using a linear regression method and the differential pressure (ΔP) of the stabilised curves was measured, as shown in Fig. 5c. From these data and the analytic solution it was possible to calculate the specific storage S_s and the permeability k of each specimen. Because the downstream reservoir was closed, tests could be run at several different pore pressure values for the same sample. The soft rocks, Indiana limestone and Berea sandstone, were tested at low pore pressure levels, whilst the granite was tested at high pore pressures, as detailed above.

In order to examine the reliability of the new technique, the permeability of the calibration samples was measured using the conventional steady-state method. The average value of the permeability for each sample was found to be essentially the same as that obtained from our new technique. The steady-state method could not be used for Westerly granite because a steady state condition could not be reached within the pressure capacity of our pump, even at the lowest flow rate allowed by the pump. In this case, we compared our result with those from previous references. As shown in Figure 6, our data are consistent with those obtained from the pulse transient method (Brace et al., 1968; Lin, 1982).

A particular advantage of the new method was the relatively short time taken to conduct a complete test cycle. For example, it took less than a minute for Berea sandstone and Indiana limestone (Figure 5a and b), and about an hour for Westerly granite (Figure 5c) in our

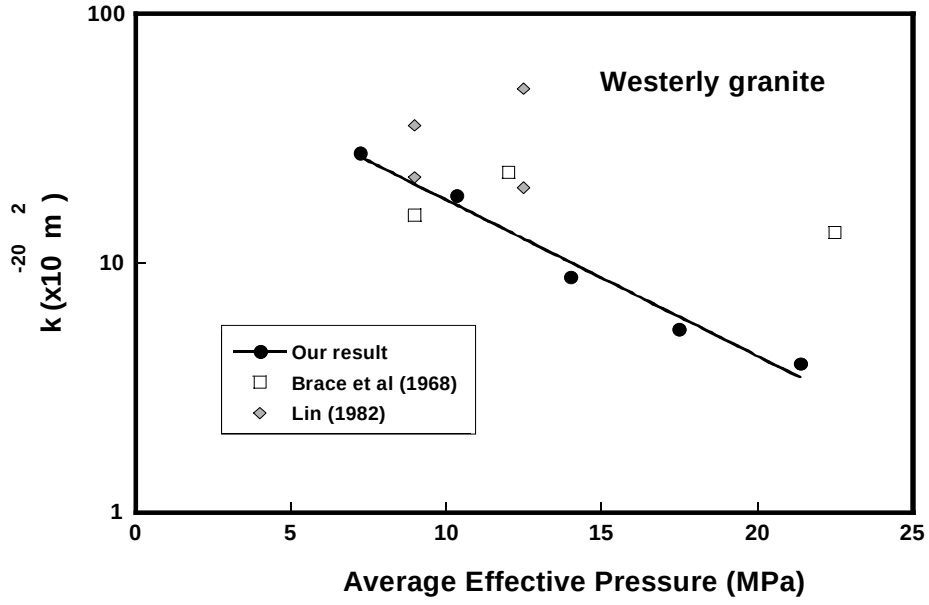

Fig. 6. Calibration of new method with literature.

test system. The differential pressure ΔP can be controlled with the speed of piston (the pumping rate Q) and the test system compliance S_u and S_d. A good control of ΔP is important because the permeability is a function of the pore pressure for a given confining pressure or

effective stress (Wu and Pruess, 2000; Liang et al., 2001). With a large ΔP, it is hard to examine the variation of the permeability as a function of the effective stress because the effective stress varies along the specimen. By decreasing Q and increasing S_u and S_d, it is possible to test at different pore pressure levels for a given confining pressure.

Another advantage is the flexibility in varying the system parameters. For example, S_u can be easily controlled by changing the position of the piston. This allows several tests for one specimen with different system parameters without changing the test set-up.

In order to assess the robustness of the new methodology in terms of experimental parameters, a series of hydraulic tests were conducted on two Westerly granite samples, under various conditions in terms of the compressive storage S_u and the pumping rate Q. The data for the repeated measurement series is listed in Table 1 below, where it can be seen that even at 350 nanoDarcy the consistency of the calculated hydraulic properties for different test conditions demonstrates that the new method is robust for laboratory measurements.

Table 1. Data for repeated measures of permeability of Westerly granite.

Test	S_u	S_d	Q	dp/dt	ΔP	S_s	k
	m^3/MPa	m^3/MPa	m^3/sec	MPa/sec	MPa	MPa^{-1}	m^2
WG1F07	1.7×10^{-8}	2×10^{-11}	6.82×10^{-10}	0.0293	10.6	1.5×10^{-4}	3.4×10^{-19}
WG1R07	4.1×10^{-8}	2×10^{-11}	6.82×10^{-10}	0.0148	4.09	1.3×10^{-4}	3.7×10^{-19}
WG1F10	1.0×10^{-8}	2×10^{-11}	9.74×10^{-10}	0.0380	13.4	1.6×10^{-4}	3.7×10^{-19}
WG1R10	3.7×10^{-8}	2×10^{-11}	9.74×10^{-10}	0.0221	9.45	1.8×10^{-4}	3.3×10^{-19}
Average						1.6×10^{-4}	3.5×10^{-19}
St. dev.						2.0×10^{-5}	2.1×10^{-20}
WG2R07	4.3×10^{-8}	2×10^{-11}	6.82×10^{-10}	0.0147	3.26	9.5×10^{-5}	3.5×10^{-19}
WG2R10	4.3×10^{-8}	2×10^{-11}	9.74×10^{-10}	0.0212	3.98	8.4×10^{-5}	3.6×10^{-19}
WG2F10	1.9×10^{-8}	2×10^{-11}	9.74×10^{-10}	0.0430	8.16	8.9×10^{-5}	3.8×10^{-19}
Average						8.9×10^{-5}	3.6×10^{-19}
St.dev.						5.4×10^{-6}	1.7×10^{-20}

5.1.2.7 Summary

As part of our contribution to the Gulf of Corinth project we have developed a new permeability and storativity test for one-dimensional fluid flow along a cored rock sample induced by constant-rate flow pumping. Based on analysis of the analytic solution for these specific boundary conditions we have developed an experimental technique and used it to test well-characterised rock types; Berea sandstone, Indiana limestone and Westerly granite. Computed values of specific storage and permeability of each specimen have proven consistent with data from conventional methods. We have used the method to measure the permeability and storativity of Olonos-Pindos limestone, with the data given below.

In addition to the simplicity, we also found many other merits of our method to evaluate the hydraulic properties of rocks, such as reliability, economy of time and flexibility of system parameters for testing in different conditions.

5.1.3 Laboratory Experimental Results

5.1.3.1.Properties of fine-grained materials

Mechanical Properties

As part of the present study, we have investigated the hydraulic properties of the active siliceous fault gouge from the 760m level of the AIG10 borehole, and compared them with the properties of a calcilutite sample from surface outcrop.

As noted in the introduction, and illustrated in Figure 1, this unit separates the Late

Fig. 7. Calcilutite outcrop, vertical 2 m section

Pleistocene marine terrace deposits, composed mainly of conglomerate, from the underlying massive formation of tight, highly fractured micritic limestone. This unit, up to several metres in thickness, provides an unconformable ductile top cap for the limestones. The calcilutite is therefore important because it can control the hydraulic connectivity between limestone and conglomerate, and because it is an excellent analogue for fine-grained cataclasite expected to be found on major regional faulting through the limestone sequence. Hence its properties are important for understanding the hydro-mechanical response of the Aigion fault zone.

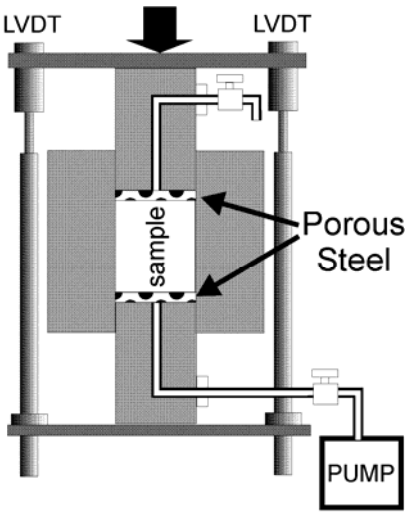

Fig. 8. Oedometer schematic

Within the Aigion (AIG10) borehole itself the active fault transects the radiolarian sequence, so that comparison of material properties of calcilutite and recovered siliceous fault gouge provides insight into both local and regional hydromechanical coupling in the Aigion fault in the AIG10 borehole area.

The compaction and permeability measurements were undertaken on 38mm diameter samples in a specially designed oedometric cell shown in Fig 8. The full data is presented in Song et al (2003b), and will only be summarised for this report

Calcilutite samples were from an outcrop, shown in Fig. 7, above the Selinoutas River adjacent to the Helike fault 4km southwest of Aigion. The fault gauge was from the 760m level in borehole AIG10. Fig 9. shows the original 100m core of this latter material. This red siliceous gouge, derived from radiolarite, was tested in the form of a reconstituted sample kindly provided by J. Sulem et al, which had all material >2mm diameter removed.

Fig. 9. 100mm diameter core of radiolarite-derived fault gouge (760m AIG10)

The experimental protocol used is illustrated in Fig 10, and consisted of 24-36 hour compaction steps at increasing fixed applied load, followed by cross-flow permeability measurement. The difference in compaction behaviour between siliceous fault gouge and

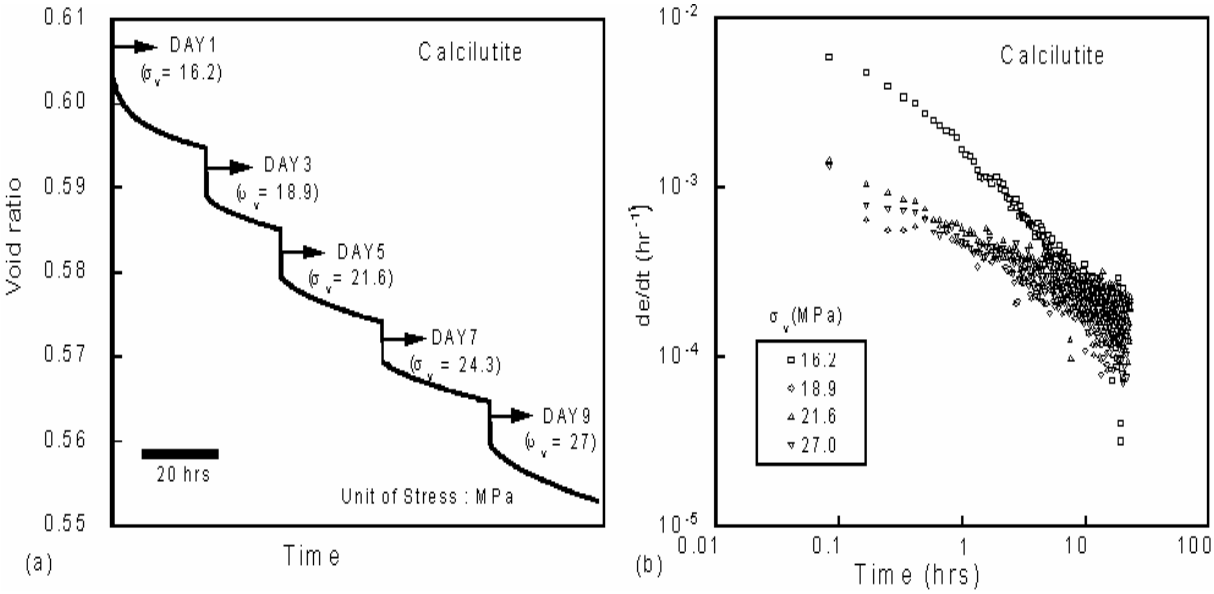

Fig.10. (a) Compaction as void ratio reduction (e) vs. time at increasing vertical stress (b) Reduction of void ratio vs. time showing bi-linear behaviour

calcilutite is shown in Fig 11. A notable feature of the compaction data is minor discontinuities, arrowed in Figure 11b, in the fault gouge compaction curves, missing in the calcilutite curves. These are traceable to minor changes in applied load arising from slight temperature sensitivity of the load frame gas pressure buffers. This direct causal relationship between subtle change (less than 1.5%) of vertical stress and the sudden change in consolidation curve (about 10%) show that transient compaction is extremely stress-sensitive in the siliceous fault gouge. This implies that stress transmission through the gouge is

extremely inhomogeneous, with distinct volumes always lying close to a critical collapse strength.

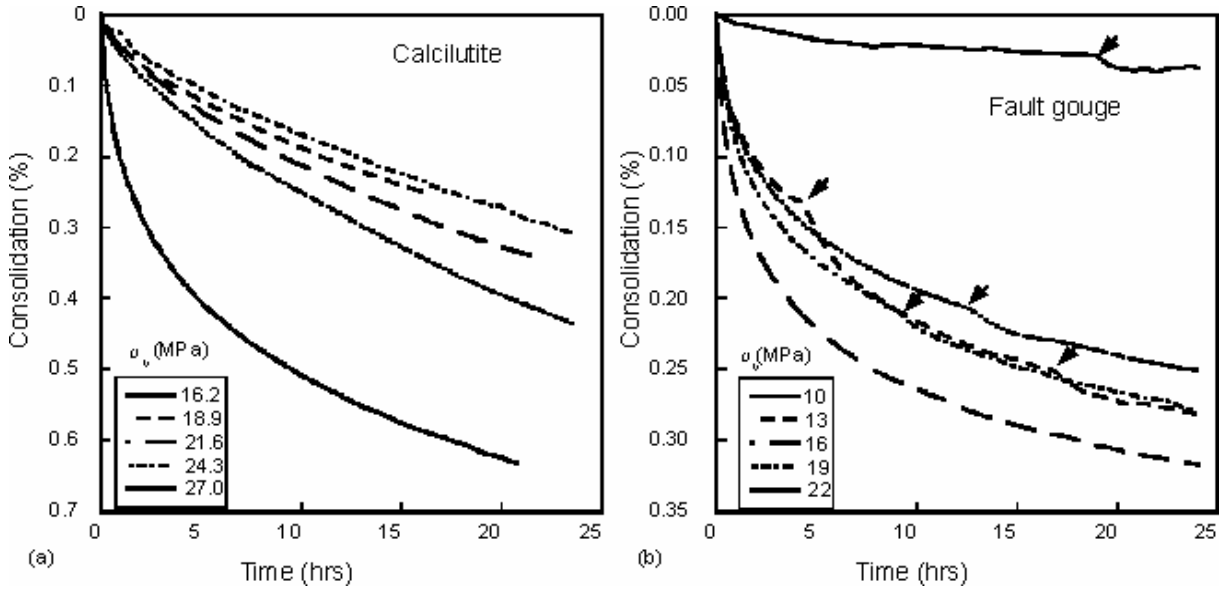

Fig. 11. Consolidation curves for calcilutite and fault gouge.

Hydraulic Properties

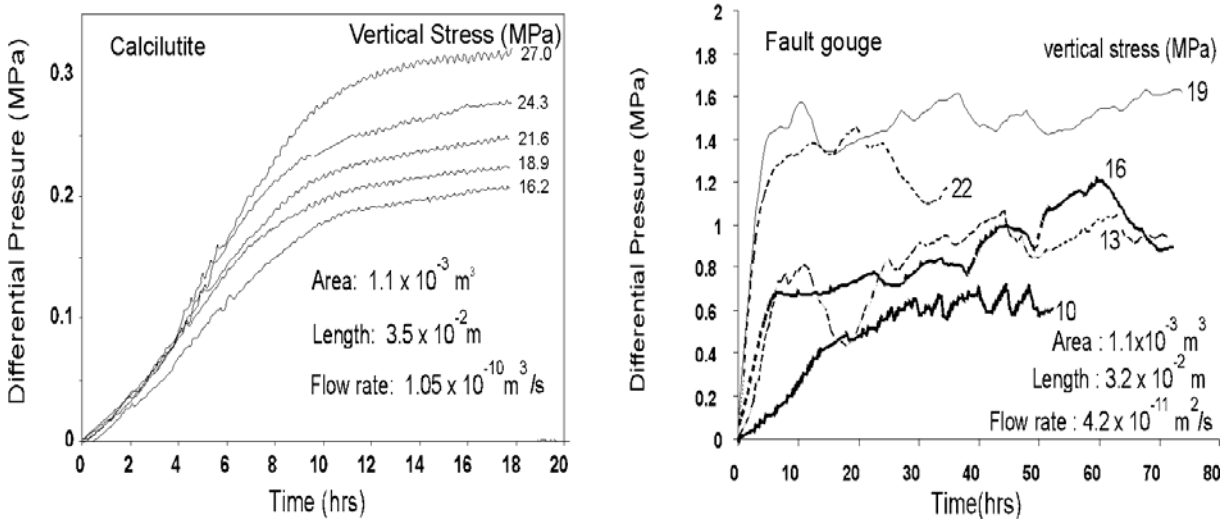

Fig. 12. Pressure build-up across calcilutite and fault gouge samples under constant flow conditions

Cross-flow sample permeability was determined by pumping degassed-deionised water into the sample at constant flow-rate (1.05×10^{-10} m^3/sec for calcilutite and 4.2×10^{-11} m^3/sec for fault gouge) following the initial 24 hour consolidation at each vertical stress value (see Fig. 8 for test configuration). The time-based records of differential pressure along the sample are shown in Fig 12.

There are clear differences in the hydraulic response of the calcilutite and siliceous fault gouge. At constant applied flow rate the differential fluid pressure across the calcilutite rises steadily, and trends asymptotically to a steady-state value related to the applied load,

with the stabilised level of the differential pressure systematically higher as the vertical stress is raised. However, for the siliceous fault gouge, the flow pattern is very different, with an initial very rapid differential fluid pressure rise, indicating that the intrinsic permeability of this material is very low. At some load-related value an unsteady fluid flow pattern is established, whose average hydraulic gradient is related to applied load. From the particular behaviour of calcilutite versus fault gouge, we can conclude that the pattern in calcilutite is classic homogeneous plug flow, whereas in the gouge it is packet flow, which correlates with the extreme load sensitivity of the compaction behaviour noted under the section on mechanical testing above.

5.1.3.2 Summary of Results for Fault Gouge / Calcilutite

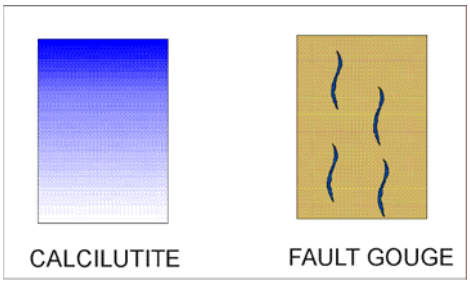

Fig. 13. Bulk vs. packet flow

Two fine-grained samples from the Aigion fault zone, located on the southern shore of the Gulf of Corinth, Greece, have been characterised in terms of hydraulic and mechanical behaviours. One is calcilutite from an outcrop 4 km south of the Aigion fault, and the other is fault gouge from the fault originally positioned at 760m depth. Both hydraulic and mechanical behaviours are clearly different between the two samples. For the mechanical deformation, both samples show a clear transient behaviour for a sudden change of external loading. However, calcilutite is more time-dependent, and fault gouge is more pressure-dependent. For hydraulic characteristics, the permeability measured at each stress level is negatively and linearly correlated to the porosity, and ranges from 9 ~ 15 x 10^{-18} m^2 for the calcilutite to 0.9 ~ 2.0 x $10^{-18}m^2$ for the fault gouge. The difference of hydro-mechanical behaviours comes from the clear difference in particle chemistry and distribution between the two samples.

Both the calcilutite and siliceous fault gouge are flow sealing compared to the heavily-fractured limestone bedrock in the area. However, values for the calcilutite are shear-insensitive global values, whereas those for the siliceous gouge are local limits under cross-flow, and must be shear rate sensitive. In other words, the permeability of the calcilutite, and by implication, calcitic fault gouges derived from local micritic limestones, is a function of unit thickness, with flow occurring homogeneously through the unit. The permeability characteristics of the radiolarite-derived siliceous gouge, on the other hand, is controlled by "packet" flow of water through the material, and hence is essentially independent of the thickness of the unit. The schematic of Fig 13 illustrates these differences. The oedometer data indicates that the breakthrough differential pressure for the gouge at the bottom of AIG10 should be approximately 10bar (1Mpa), which is indeed the differential pressure encountered across the fault zone at 760m. Based on our result, we also conclude that the transient response to sudden changes in effective stress may play a crucial role in the time-dependent triggering of fault movement in the Aigion region.

5.1.3.3 Properties of Aigion Limestone and Breccia

Fig. 14. Typical platey Olonos-Pindos limestone

Hydraulic properties

The new permeability test method developed for the current project has been applied to samples of the Olonos-Pindos limestones, and as the table below shows, demonstrates that the platey limestones of the Aigion region are extremely tight, with bulk sample

Table 2. Hydraulic test results for Olonos-Pindos Limestone

Sample	dH/dt	ΔH	H_{int}	S_s	$k^{\Delta H}$	k^{Hint}
	m/s	m	m	m^{-1}	m/s	m/s
LSD3	0.158	686	18.5	2.30×10^{-06}	3.20×10^{-21}	3.24×10^{-21}
LSE2	0.158	236	9.4	8.97×10^{-07}	2.04×10^{-20}	1.85×10^{-20}
LSA5	0.155	179	20.8	9.81×10^{-07}	3.09×10^{-20}	1.21×10^{-20}
LSD2	0.156	141	14.1	2.54×10^{-06}	2.32×10^{-20}	1.01×10^{-20}
Average				1.68×10^{-06}	1.94×10^{-20}	1.10×10^{-20}
St. dev.				8.61×10^{-07}	1.17×10^{-21}	6.27×10^{-21}

$k^{\Delta H}$: permeability based on differential head (ΔH)
k^{Hint}: permeability based on intercept (H_{int})

permeabilities in the tens to hundreds of nanoDarcy range. The result is that all flow through these materials must be fracture flow, and the hydrogeology dominated by spatially-restricted flow zones separating pockets of trapped water.

Mechanical Properties

Mechanical test samples have been collected from both the AIG10 borehole material and from an outcrop of Olonos-Pindos platy limestone on the south side of the Selinoutas

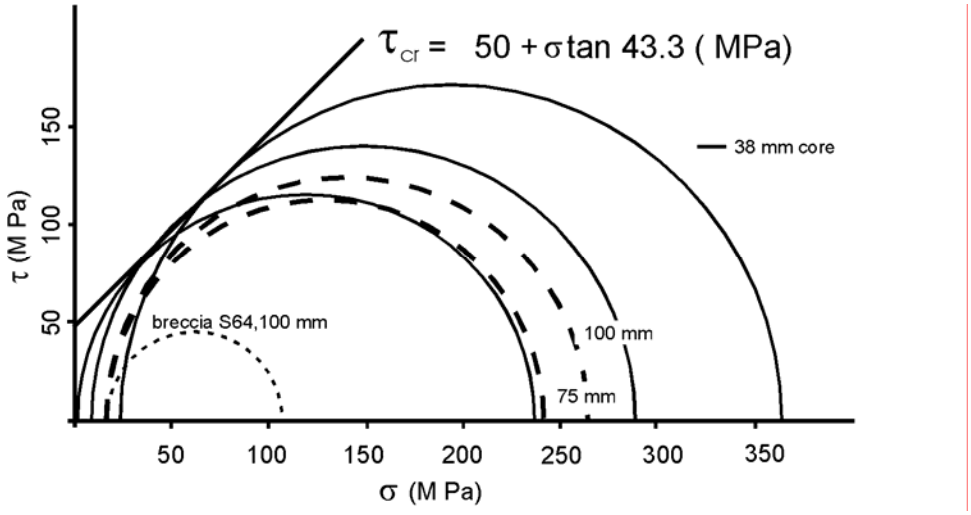

Fig. 15. Mohr-Coulomb criteria for Olonos-Pindos

River west of the Helike fault 8 km south of the Aigion fault. The outcrop limestone was chosen to provide massive samples of materials retrieved in more fragmentary form from the borehole. Mechanical failure testing has been conducted on 38mm samples in a specially-constructed Hoek-type cell, and on 75mm and 100mm samples in the Edinburgh 'Big Rig' facility. During this report period we developed the instrumentation on the 38mm compression tester to include high-definition strain gauge measurement. Considerable laboratory time was also spent on developing a jacketing system for the 'Big Rig' facility to allow compression testing of core from AIG10 which had very porous and irregular surfaces. A polyurethane casting system was developed to vacuum prejacket the samples so that testing was feasible at high confining pressures, without damaging sample chemical constitution.

The Mohr diagram for 38mm diameter tests on Olonos-Pindos limestone is shown in Fig 15. together with data for the 100mm and 75mm samples of limestone deformed in the 'BigRig' compression tester. The stress-strain curves and summary data for the 38mm samples is given in Fig 16. All these tests were undertaken at 16MPa confining pressure, to examine the effect of sample size and centimetric sample fracturing and veining at confining pressures found at the major fault surface in AIG10.

Data in Fig 15 demonstrate that larger bulk samples of Olonos-Pindos limestone are notably weaker than the 38mm samples generally used for rock testing. Examination of the retrieved samples after compression failure showed that shear failure follows existing veining and fractures where these were parallel or sub-parallel to the plane of maximum stress in the samples. Thus the 38mm sample data measures the intrinsic bulk properties of the homogeneous Olonos-Pindos limestone, whereas the large sample data indicates the bulk unit properties because it allows for the weakness introduced by previous calcite-sealed fracturing and veining. Fig 15 demonstrates that these flaws weaken the bulk limestone by 20-30%.

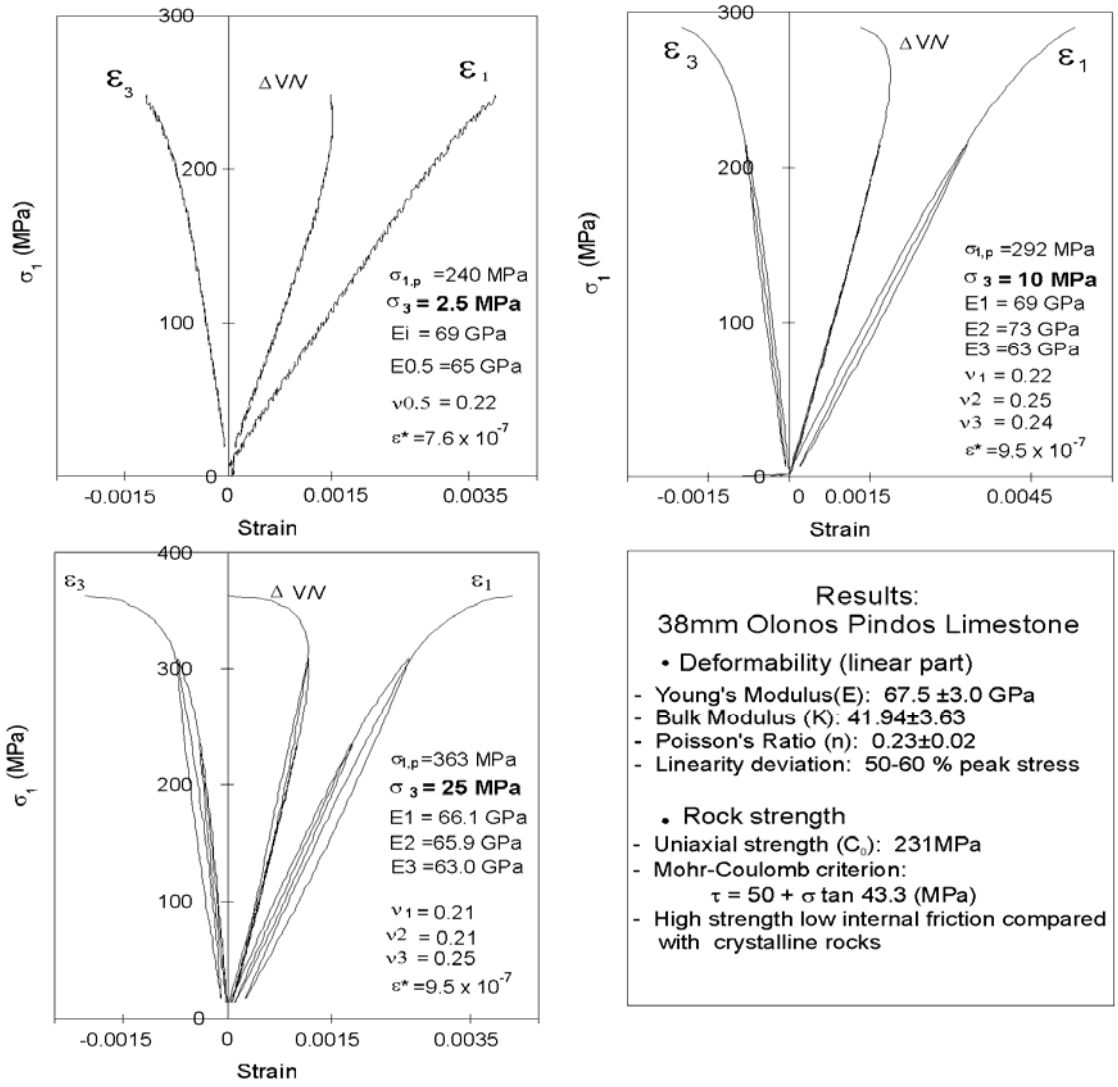

Fig. 16. Axial strain (ε1), radial strain (ε3), and volumetric strain (ΔV/V) for 38mm Olonos-Pindos limestone

Also plotted in Fig 15 is the failure envelope for limestone breccia Sample 64 from the 780m level in AIG10. This breccia is considerably weaker than the limestone from which it is derived, with a failure strength of 107MPa at 16MPa confining pressure.

The load response for a 100mm 'BigRig' test of this breccia is shown in Fig 17, demonstrating that for this sample failure occurs by bulk plastic deformation. The reload/redeform cycle undertaken after an initial 1.1% strain also shows that there is little frictional stress locking in this breccia

During the second load cycle, an attempt was made to measure the permeability of this 100mm sample by pressurising one end with 8MPa applied water load. No water flow was detected across the sample for the entire second load/slide cycle, demonstrating that this calcitic breccia is essentially impermeable even during bulk plastic deformation.

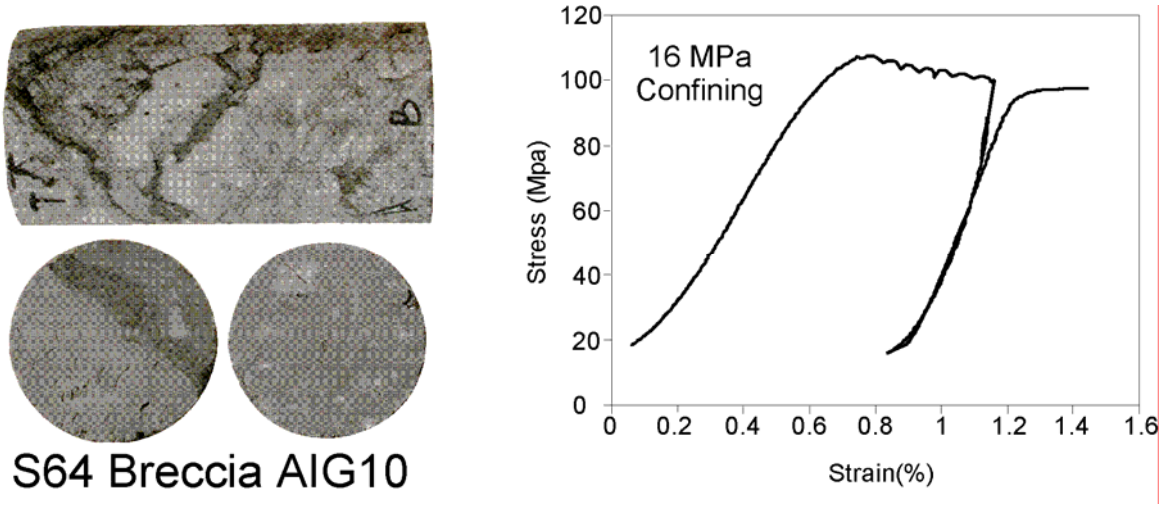

Fig. 17. Stress-strain response of S64 breccia from 780m depth in AIG10

5.1.3.4 Summary

Hydraulic testing of the massive limestones and related breccias show that both are effectively impermeable, and that regional hydrological flow patterns will be determined by cross-cutting open fracture patterns, and the properties of clay materials along bedding, solution, and parting planes. Surprisingly, even the calcitic breccias appear impermeable unless connected water packets are entrained during deformation. Mechanically, the limestones are extremely strong at high strain rates, although standard rock tests overestimate their bulk properties. However, once comminution has occurred through shearing, the resulting breccias will continue to be planes of local weakness until recemented through local chemical reactions.

5.1.4. Summary of Geological Results for Work Package 5

The mechanical and hydraulic test of outcrop and borehole materials enables important conclusions to be drawn about the geology of the Aigion fault region.

- The massive limestones of the region have high intrinsic strength and can undergo brittle failure with little yield near peak strength. However, small sample mechanical tests overestimate bulk rock strength by at least 20-30%.
- The bulk limestone is essentially impermeable, and fluid flow is through fracture or solution networks. Thus fluid flow will be highly channelled.
- The calcilutite and related fine-grained deposits which form a basal unit to the massive conglomerates, separating conglomerates from basal limestones, forms a hydraulic seal between the two units wherever it occurs in any substantial thickness.
- Similarly, the fine-grained siliceous gouge encountered in the AIG10 borehole, and the calcitic equivalents up and down strike in the fault zone, is of low permeability compared with fracture flow in the surrounding units, and will act as a fluid seal.
- However, the raw calcitic gouges will have permeabilities proportional to their thickness, whereas the siliceous gouges derived from radiolarite will have permeabilities independent of thickness, but dependent on overburden load.

- At the AIG10 site, the 1 MPa differential water pressure developed across the active fault zone is a function of inhomogeneous packet flow through the siliceous gouge, and thus further calculation will enable limits to be placed on maximum water flow rates both across and along the fault.
- Older limestone fault breccias near the current active fault plane continue to be zones of low strength, and also of low permeability, further channelling water flow parallel to the fault plane.

5.1.5.Recommendations

The Gulf of Corinth Project has yielded important insights into the geomechanics of active rift zones, and represents an important advance in the rationalisation and integration of research within the context of the European Union.

Important scientific questions remain to be answered. Why is the rupture geometry so different between limestone and overlying conglomerate? In the limestone, fault rupture occurs across relatively wide crush zones, whereas in the conglomerate it is expressed on outcrop mainly as knife-sharp slickenslided planes of rupture. Are these depth-related differences, or a reflection of the manner in which earthquake shock waves are propagated by the two media? Further laboratory work on the strain-rate dependence of limestone strength is urgently needed. These experiments must also consider the effect of trapped pore water on final failure strength.

At greater depths, how does the regional geology express itself in terms of relative deformation rates and strain propagation? Geophysical measurement, especially seismics, necessarily blurs these important structural controls, because they operate on an intermediate size level not readily resolvable by acoustic techniques. The next logical step after AIG10, to answer some of these critical questions, is the sinking of a fully-instrumented deep borehole to investigate brittle-ductile coupling and earthquake triggering as a function of depth and geology. Such a borehole will provide critical scientific data in its own right, but will also act as a focus for pan-European instrumentation and data collection development.

In the immediate future, effort needs to be maintained to further integrate the data collected during the current phase of work, and maintain the network of collaborating institutions which has proven so fruitful during the current project. Further, the Gulf of Corinth is a superb training resource which should be better utilised now that basic data sets are developed.

In summary, the Gulf of Corinth Project is an example of pan-European collaboration by a large number of relatively small scientific units. To date the EU has proven that it can successfully encourage the collaboration of large scientific groups, but the future scientific health of the Union may well depend more critically on successful linkages between smaller research units, with better continuity than the current Framework mechanisms can provide.

5.2 MECHANICAL CHARACTERIZATION (CERMES)

5.2.1 Introduction

Within the frame of the European projects DG-Lab Corinth, the task of CERMES-ENPC consists in the experimental characterisation and constitutive modelling of fault-rock material. The AG-10 well has been drilled vertically trough the Aigion fault from July to September 2002. Fault zone cores have been collected continuously from depths between 708 m to 782 m. At depth 760m the Aigion fault was intercepted, dipping at an angle of about 60°. The heart of the fault is a zone of clay-rich material on a length of about 1m. This zone is surrounded by a damage zone of highly fractured rock (breccia). The fault material is embedded between limestone cataclasite on top with a thickness of about 3m and radiolarite cataclasite below with a thickness of about 9m and is characterized as gouge clayey matrix and radiolarite fragments (Fig.1) (Moretti et al, 2002)

Fig.1. Box 49 containing the core at depth 759.70m, characterised as "Aigion fault" core (Moretti et al, 2003)

In this report we present results from rock-mechanical laboratory analyses on specimens taken from the Aigion fault core. Triaxial compression tests have been performed on samples from the different zones : fractured limestone, breccia, clayey core. Direct shear tests along the interface between the limestone and the cataclastic bands as encountered at depth 744m have been performed in the Laboratoire 3S, Grenoble by Prof. M. Boulon and the results are also presented in this report.

Special attention is paid on temperature effects on the behaviour of the clayey core of the lower part of Aigion fault drilling core. This zone corresponds to the weakest gouge clayey matrix and radiolarite fragments material encountered in this sequence and is recognisable from its red-brown coloration. The observations from the active fault drilling operation of the Geological Survey of Japan at Nojima Hirabayashi after the 1995 Hyogoken-nanbu (Kobe) Earthquake and the following analysis by Otsuki et al. (2003) renewed the interest of the geophysics community on the role of temperature and fluids in active faulting (e.g. Lachenbruch, 1980, Mase and Smith, 1985). Shear heating tends to increase pore pressure and to decrease the effective compressive stress and the resistance to slip. On the other hand dilatancy tends to decrease pore pressure. Such coupling has been studied in the recent paper of Garagash and Rudnicki (2003).

Fault zones are often characterized by large amounts of clay minerals, which form well-defined structures within the fault zone. The total concentration of the clay minerals in the fault zone is usually larger than in the host rock. These clay minerals inside the fault gouge are widely believed to affect significantly the mechanical behavior of faults as normally consolidated clays tend to contract when heated.

Based on the above mentioned literature and the recent experimental work by Sultan et al. (2000), Vardoulakis has demonstrated (2002a,b) the importance of thermally collapsible and thermally softening clay on the overall dynamic thermo-poro-mechanical behavior of clay-rich gouges. Accordingly, conditions for possible softening behavior of the clay under thermal loading are investigated. The sensitive parameter for the description of the thermo-poro-mechanical coupling is the thermal expansion coefficient of the material. Possible collapse of the clay under thermal loading may activate fluid pressurization inside the fault and lead to substantial reduction of the apparent friction.

5.2.2. Thermo-poro-mechanical properties of the red Aigion Fault clay

5.2.2.1. Samples preparation and in situ stress

In geotechnical engineering special techniques exist to obtain high-quality undisturbed soil samples and try to prevent alteration of soil structure. It is however very difficult to obtain undisturbed samples from great depths. Unfortunately within the frame of DG-Lab project no resources could be made available to use these techniques and the cores have been disturbed to some degree during sampling and transportation. However this is not so detrimental for the type of gouge material that was recovered as it can be with cemented sands or with soft clays. As the first reports from the drilling site confirm, the clayey gouge which was extracted from Aegion fault was a remarkably soft material, Fig.1. Most probably this because this material was continuously stressed due to the aseismic and seismic movements of the fault. Thus it is expected that the effect of remoulding is of lesser importance, as long as the density and the water content of the samples are preserved for testing.

The in situ density of the material is reasonably retrieved by applying the in situ stresses onto the sample. Notice that it is programmed within the DGLab project to perform direct stress measurements inside the borehole. The data are not available at present. Thus the in-situ state of stress has to be estimated. Assuming that the density of the overburden is about 2.5 gr/cm^3 we estimate a total vertical stress of about 19 MPa, which in turn is corresponding to an effective vertical stress of 11.4 MPa.

Once the Aegion fault core was taken from the borehole, it was stored for few days on site and then it was transported to the Soil Mechanics Laboratory of Ecole Nationale de Ponts et Chaussées, where it was stored in a room with controlled temperature and humidity. Obviously it was not possible to avoid partial drying of the core during extraction, storage and transportation but then it was regularly wetted as soon as it was stored in good conditions. As it was not possible to use in the experiments the same saturation fluid as in situ, we have used demineralised water in which a certain amount of particles from the sample have been placed during 24 hours. The mixture has been then filtered and the resulting fluid has been used for the saturation of the tested samples. This technique is commonly used in soil testing to avoid any chemical influence of the saturation fluid on the mechanical properties of the tested material.

5.2.2.2.Particle size characteristics, Atterberg limits and mineralogy of the material

We distinguish in the clayey core two zones: the first one in contact with the breccia has a gray coloration and will be called in the following the ‘gray clayey gouge’, the second one has a red coloration and will be called the ‘red clayey gouge’.

Fig. 2 shows the grain-size distribution curve for the red and the gray Aigion fault clay materials. The coarse fraction for the red material corresponds to radiolarite fragments. For the red clayey gouge, the percentage of fines (fraction smaller than 80 μm sieve size) is 32% and the percentage of clay particles (mass fraction smaller than 2 μm) is about 15%. For the gery clayey gouge, the percentage of fines is 49% and the percentage of clay particles is about 25%.

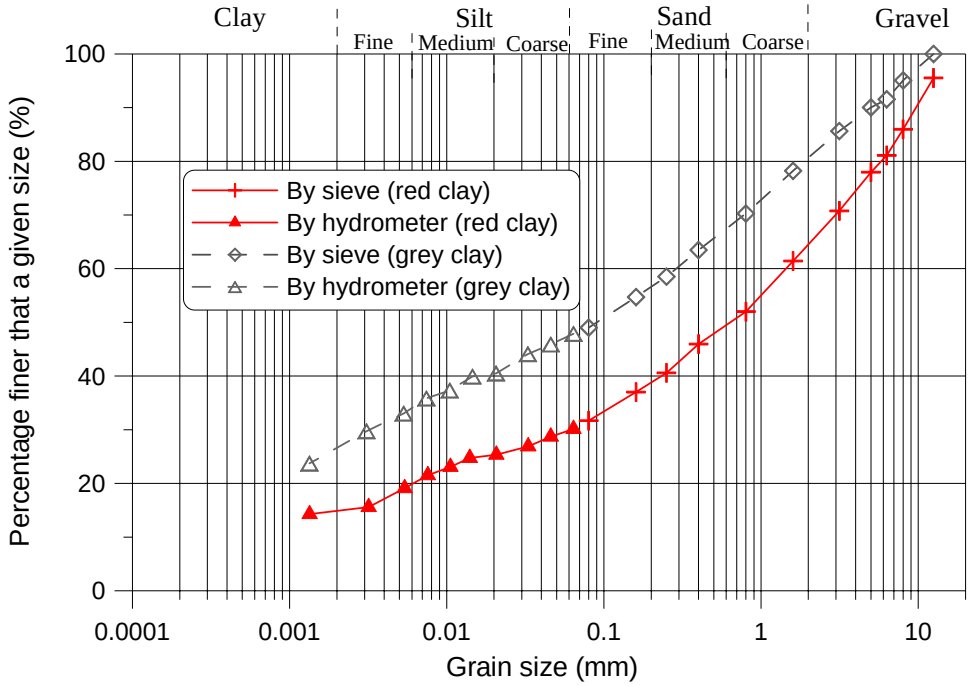

Fig. 2 : **Grain size distribution of the red and the gray Aigion fault clayey gouge**

The corresponding Atterberg limits are:

For the red clayey gouge

Liquid Limit w_L = 29%, Plastic Limit w_P = 15% which corresponds to a relatively low Plasticity Index (PI = 14%). According to the USC system, the material is classified as a "clayey sand".

For the gray clayey gouge

Liquid Limit w_L = 46%, Plastic Limit w_P = 30% which corresponds to a relatively low Plasticity Index (PI = 16%). According to the USC system, the material is classified as a "clayey silt".

The mineralogical analysis of the samples was carried out by X-ray diffraction techniques at the Technical University of Crete by Prof. Perdikatsis. The fragments as well as the clay matrix have been studied. The results are shown on Tables 1a & b.

Sample	Quartz (%)	Chlorite (%)	Illite (%)	Albite (%)	Hematite (%)
Clay particles <80μm	74	3	10	9	3
Clay matrix <400μm	66	2	15	13	3.5
Fragments and gravels	73	2	9	8	2.5

Table 1a : **Mineral composition of red fault clayey gouge (after Perdikatsis, 2003)**

Sample	Quartz (%)	Chlorite (%)	Calcite (%)	Albite (%)
Clay particles <80μm	49	47.4	2.5	1
Clay matrix <400μm	56	34	6.5	2.5
Fragments and gravels	61	24	12	2

Table 1b : **Mineral composition of red fault clayey gouge (after Perdikatsis, 2003)**

On this tables the mineral composition is normalized to 100%. The amorphous content is about 20% for the red material and 40% for the gray one. We notice that the red gouge contain illite and hematite (responsible for the red coloration) but no calcite and no chlorite which are present in the gray material.

5.2.2.3 Oedometric compression test

The oedometer test is commonly used in Soil Mechanics practice to measure compressibility. Here for completeness we outline the basic concepts of this test: A fluid-saturated cylindrical specimen is confined latterly by a stiff metal ring and the specimen is stressed along vertical axis. Due to the lateral rigid confinement of the specimen the strains in horizontal directions are suppressed. Porous stones are employed on the top and bottom of the specimen in order to permit the free drainage of the pore-fluid in or out of the specimen. During the test the vertical load is applied in small increments. For each load increment the vertical deformation of the specimen is monitored using displacement gauges. Assuming that the grains of the solid constituent are incompressible all volume changes are attributed to changes in the voids ratio of the specimen and are directly linked with the extrusion of the pore-fluid from the pore-space. Thus we relate the change in the void ratio of the specimen Δe with the volumetric strain ε_v:

$$\varepsilon_v = \frac{\Delta e}{1+e_0} \tag{1}$$

where e_0 is the initial void ratio.

The commonly observed non-linear stress-strain response of a soft geomaterial in oedometric compression makes it more convenient to plot the void ratio versus the effective vertical stress σ'_v in a logarithmic scale because. As was first observed by Terzaghi (1943), at large stresses the corresponding curve becomes a straight line, so that a unique parameter, the so-called compression index

$$C_c = -\frac{\Delta e}{\Delta(\log \sigma'_v)} \tag{2}$$

is sufficient to characterise the compressibility of the material over a wide range of stresses. Similarly one is defining upon unloading the so-called swelling index C_s .

A special high-pressure oedometer has been designed in CERMES (Marcial et al 2002). A system of double cantilever beam allows a maximum vertical load of 12t corresponding to a maximum stress of about 31 MPa on a cylindrical sample with a diameter of 70 mm (Fig. 3).

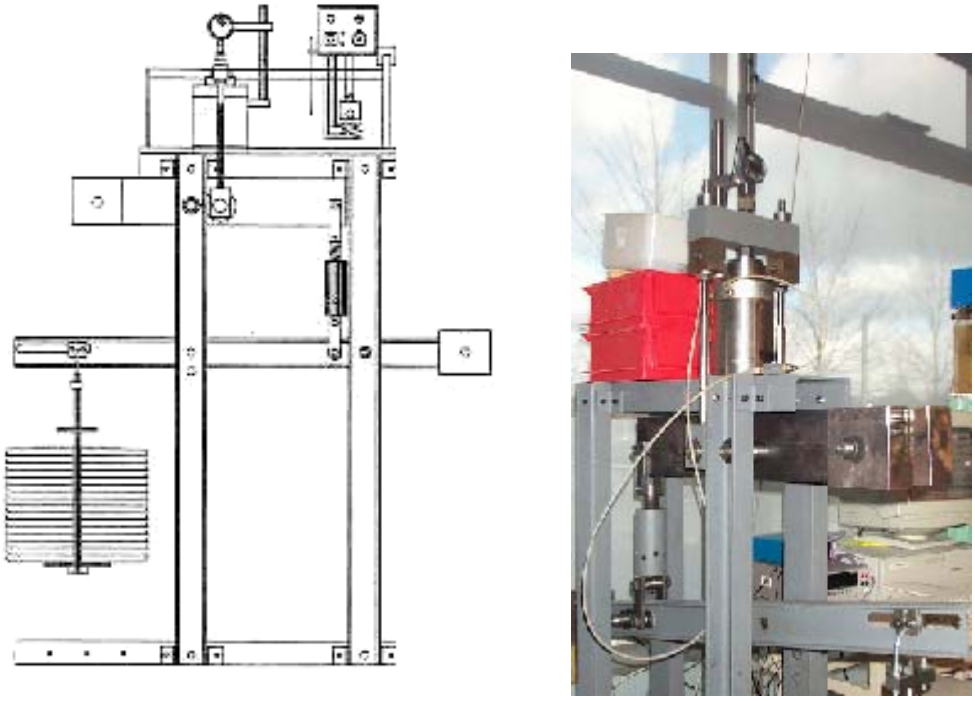

Fig.3 Double cantilever high pressure oedometer

In Fig. 4 we see the results from two oedometric compression tests performed on a saturated samples of the red and the grey gouge using the high-pressure oedometer. The curve can be divided in two parts: the first part, starting at the beginning of the curve represent the recompression phase; at the end of the recompression, the curve presents a significant curvature and then enters in a more-or-less straight line corresponding to the consolidation line of a normally consolidated sample.

The vertical stress σ'_{vp} at the point where the sample starts to present large irreversible deformation when loaded is the so-called pre-consolidation stress. The small value of the pre-consolidation stress obtained here shows that the material has been remoulded during the coring process and has lost the memory of the loading history.

The evolution in time of the compression of a fluid-saturated, fluid-permeable porous material is described by Terzaghi's (1925) consolidation theory. According to this theory, the compaction of the material is associated with the extrusion of the pore-fluid through the permeable boundaries of the specimen. In the considered one-dimensional setting of a specimen compressed vertically in an oedometer, this theory results into the following equation for the dissipation of excess pore pressure

$$\frac{\partial u}{\partial t} = c_v \frac{\partial^2 u}{\partial z^2} \qquad (3)$$

where u is the excess pore pressure, z is the coordinate in vertical direction, t is the time and c_v is the consolidation coefficient,

$$c_v = \frac{k_f (1+e)}{\gamma_f a_v} \qquad (4)$$

In this equation k_f is the hydraulic conductivity of the material with respect to a given fluid, and

$$a_v = -\frac{\Delta e}{\Delta \sigma'_v} \approx 0.434 \frac{C_c}{\sigma'_v} \qquad (5)$$

is the compression modulus of the material; e is the actual voids ratio and γ_f is the unit weight of the pore-fluid.

By using the Casagrande method[1] it is possible to estimate the consolidation coefficient c_v directly from oedometer test results and thus, from equation (4), to evaluate the hydraulic conductivity of the gouge as a function of the applied oedometric pressure (Fig. 5). Notice that the physical or Muskat permeability k of the material, with dimension of square length, is related to the hydraulic conductivity k_f by

$$k = \frac{\eta_f}{\gamma_f} k_f \qquad (6)$$

where η_f is the viscosity of the pore fluid.

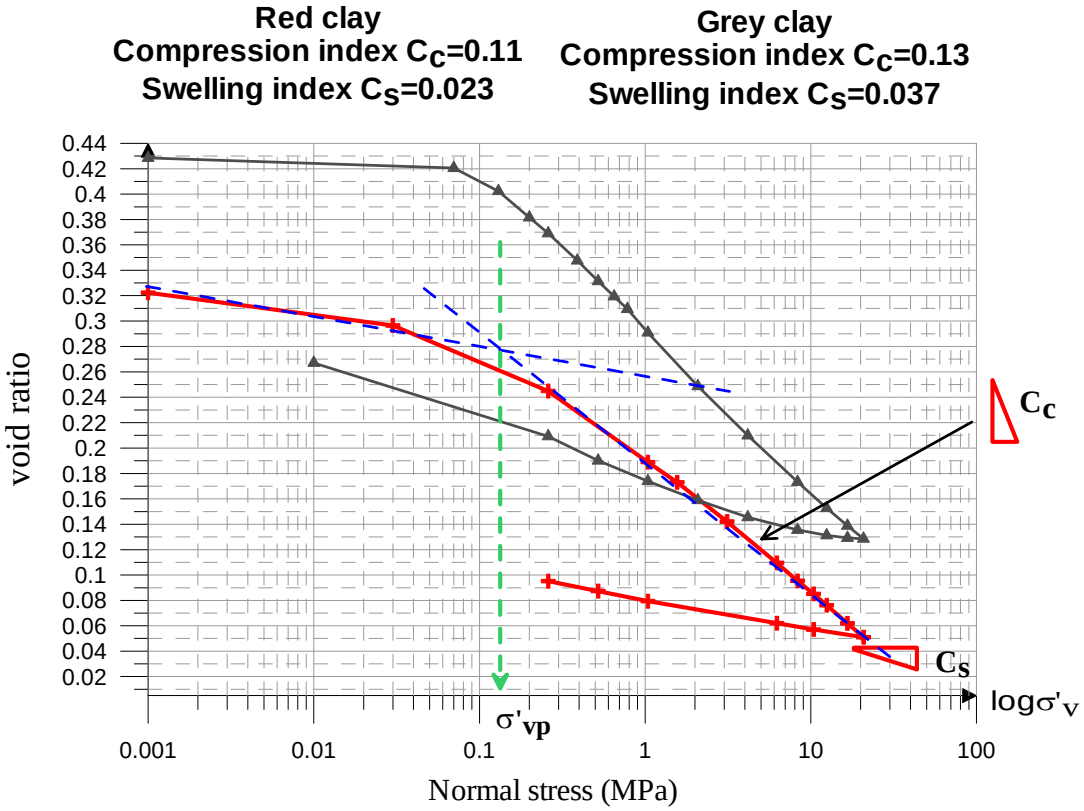

Fig. 4 : Oedometric compression curves

[1] cf. D.W. Taylor. Founamentals of Soil Mechanics. Wiley, 1948.

After the last stage of the loading process at 21 MPa, the sample was unloaded and the corresponding swelling index is measured. The specimen was then removed from the oedometric cell, weighted and then dried in an oven at 105°C for 24 hours. The evolution of the porosity with axial stress was back calculated from the axial strain measurements, as shown on Fig. 5.

Fig. 5 shows that the permeability of the clayey gouge is of the order of 10^{-19} to $10^{-20}m^2$ and that consequently the clayey core of the fault acts as a barrier for fluid transport. This result is consistent the result obtain from direct permeability tests by the University of Edinburg (Elphick et al 2003) and with the pump tests performed on site.

For the red clayey gouge, the initial porosity of the material is about 19.7% and the porosity of the sample loaded at 16.6MPa in oedometric compression was 5.8%.

The oedometric test allows the determination of the isothermal compressibility coefficient

$$c = \frac{1}{1+e}\frac{\overline{C}_c}{|\sigma'_v|}, \overline{C}_c = \frac{\overline{C}_c}{\ln(10)} \qquad (7)$$

Thus for loading at 16 MPa, the isothermal, compressibility coefficient is estimated as $c \approx 0.0028\ \mathrm{MPa}^{-1}$.

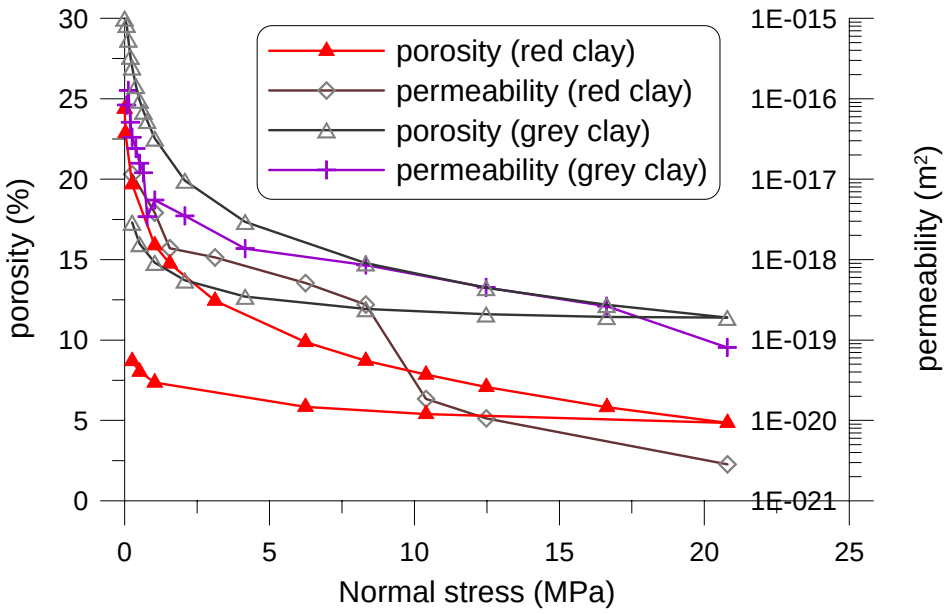

Fig. 5 : Porosity and permeability evolution during oedometric compression

5.2.2.4 Strength parameters from drained triaxial compression tests

The experimental equipment used for compression and thermal tests is shown on Fig. 6.

Due to the small amount of material available for experimental studies only two specimens could be used. The 1st specimen was tested at room temperature ($\theta = 22^{\circ}C$) and

the 2nd at an elevated temperature ($\theta = 70^{o}\,C$). For the same reason "stepped" triaxial testing programmes were imposed, following the stress paths shown in Fig. 7.

The 1st specimen was sheared sequentially at confining pressures $\sigma_c = 8\,MPa$, $\sigma_c = 16\,MPa$ and $\sigma_c = 18\,MPa$. At the end of each shearing phase at constant confining pressure, the specimen was unloaded axially and the confining pressure was augmented to reach the next prescribed level. For the 2nd specimen the axial load was kept constant during the augmentation of the confining pressure from $\sigma_c = 16\,MPa$ to $\sigma_c = 18\,MPa$. As we are interested here in the response of the material during the shearing phase and considering that the volumetric strains are not significant during the unloading phases (the material is practically rigid upon unloading), the stress paths followed in the triaxial tests of the 1st and the 2nd specimen do not differ significantly.

The corresponding stress-strain curves are shown in Figs. 8 and 9, respectively. Axial and volumetric strains are measured with respect to an initial state, corresponding to the beginning of the first deviatoric phase of the test.

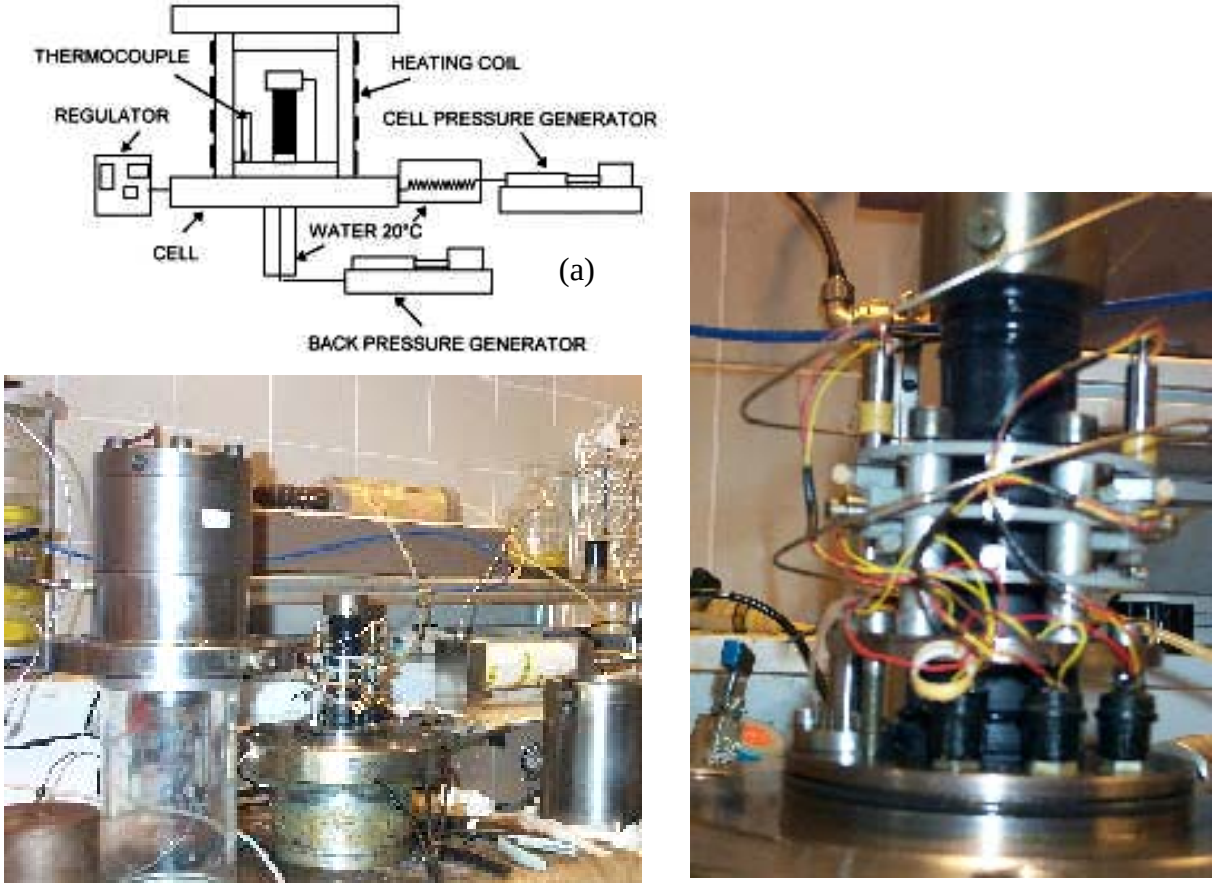

Fig. 6: Experimental equipment: (a) Principle, (b) General view, (c) Instrumented sample

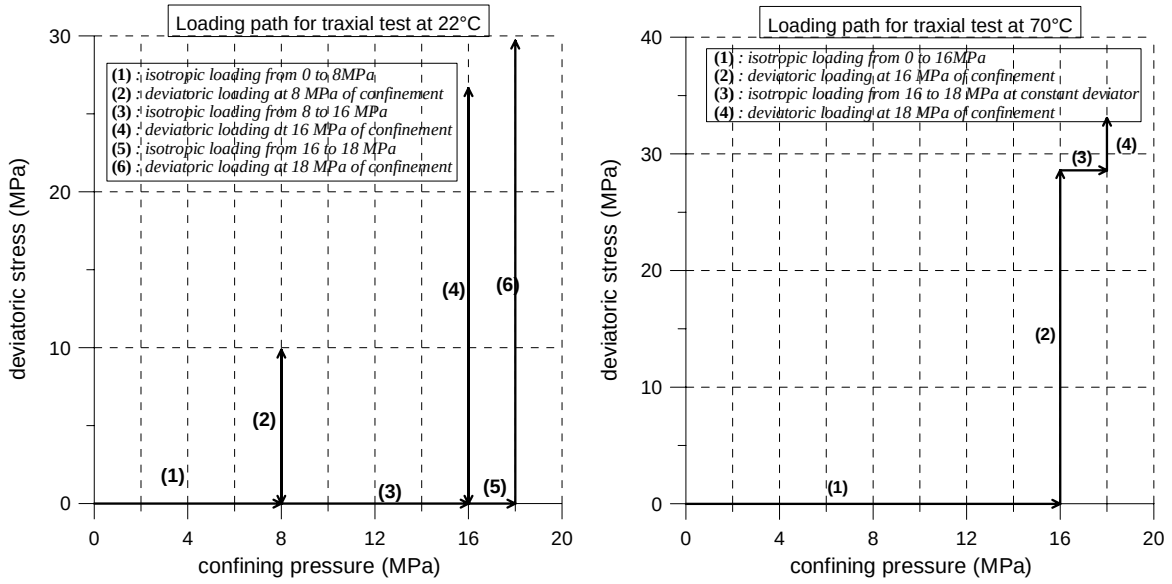

Fig.7 : Stress paths followed for triaxial compression tests

For the 1st specimen, tested at $\theta = 22^{o}\,\mathrm{C}$ and $\sigma_c = 8\,\mathrm{MPa}$, the loading phase was interrupted at an axial strain, $\varepsilon_a = 7.2\%$ corresponding to a deviatoric stress $q = \sigma_a - \sigma_c = 9.9\,\mathrm{MPa}$. Since this value of the deviatoric stress is actually smaller than the value, q_f, at which failure occurs, the specimen remained homogeneous. This justifies the loading strategy applied here, according to which the same specimen could be used for a different higher pressure. Using a hyperbolic fitting of the data we could estimate that, at $\sigma_c = 8\,\mathrm{MPa}$, $q_f \approx 14\,\mathrm{MPa}$. For the shearing phases at $\sigma_c = 16\,\mathrm{MPa}$ and at $\sigma_c = 18\,\mathrm{MPa}$ the material was compacting and it reached the critical state of maximum compaction at a mobilized friction angle of $\varphi_{cs} = 27.9^{o}$. For both tested specimens the critical state was reached for large strains. For the 1st specimen the maximum volumetric strain (resp. axial strain) was $\varepsilon_{v,max} \approx 3.3\%$ (resp. $\varepsilon_{a,max} \approx 17.8\%$). The corresponding values for the 2nd specimen are $\varepsilon_{v,max} \approx 1.3\%$ ($\varepsilon_{a,max} \approx 14.5\%$). We notice that the dilatant behaviour, which is observed at the end of the test is attributed to the occurrence of shear-banding in the sample.

The frictional resistance of the material at critical state increases slightly with the temperature and with the strain rate. The influence of temperature on the friction angle can judged by comparing the value of maximum friction angle $\varphi_{cs} \approx 29^{o}$, for 2nd specimen and for a strain rate, $\dot{\varepsilon}_a = 10^{-6}\,\mathrm{s}^{-1}$, with the aforementioned value $\varphi_{cs} = 27.9^{o}$, holding for the 1st specimen, tested at the same strain rate. Thus a temperature difference of $\Delta\theta = 48^{o}\,\mathrm{C}$ results into an increase of maximum friction angle of $\Delta\varphi_{cs} \approx 1^{o}$.

As is shown in Fig. 6 changes in the strain rate during the test indicate also some rate sensitivity. Here we evaluate the rate sensitivity of the tested material in terms of the mobilized-friction coefficient f

$$f = \frac{2\sqrt{3}\sin\varphi_m}{3-\sin\varphi_m} \tag{8}$$

where φ_m is of the corresponding mobilized friction angle. Thus assuming an exponential law of the form[2]

$$f = f_{ref}\ \exp\left(S_f\ \frac{\dot{\varepsilon}_a}{\dot{\varepsilon}_{a,ref}}\right) \tag{9}$$

the frictional rate-sensitivity is estimated from the test data by using the following formula,

$$S_f = \frac{\Delta f / \left((f^+ + f^-)/2\right)}{\ln\left(\frac{\dot{\varepsilon}_a^+}{\dot{\varepsilon}_a^-}\right)} \tag{10}$$

For the of the tested red clay we found that $S_f \approx 0.01$.

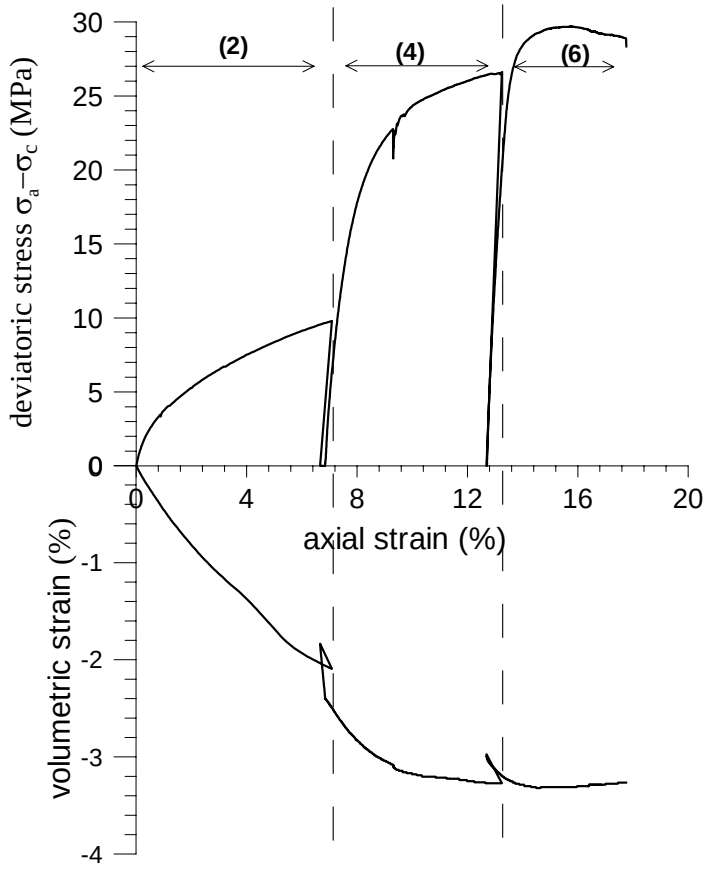

Fig.8 : Drained triaxial tests at room temperature (numbers indicate the loading phases according to Fig. 7)

[2] cf. Prandtl, L. (1928). Ein Gedankenmodell zur kinetischen Theorie der festen Körper. Z. Angew. Math. Mech., 8, 85-106.

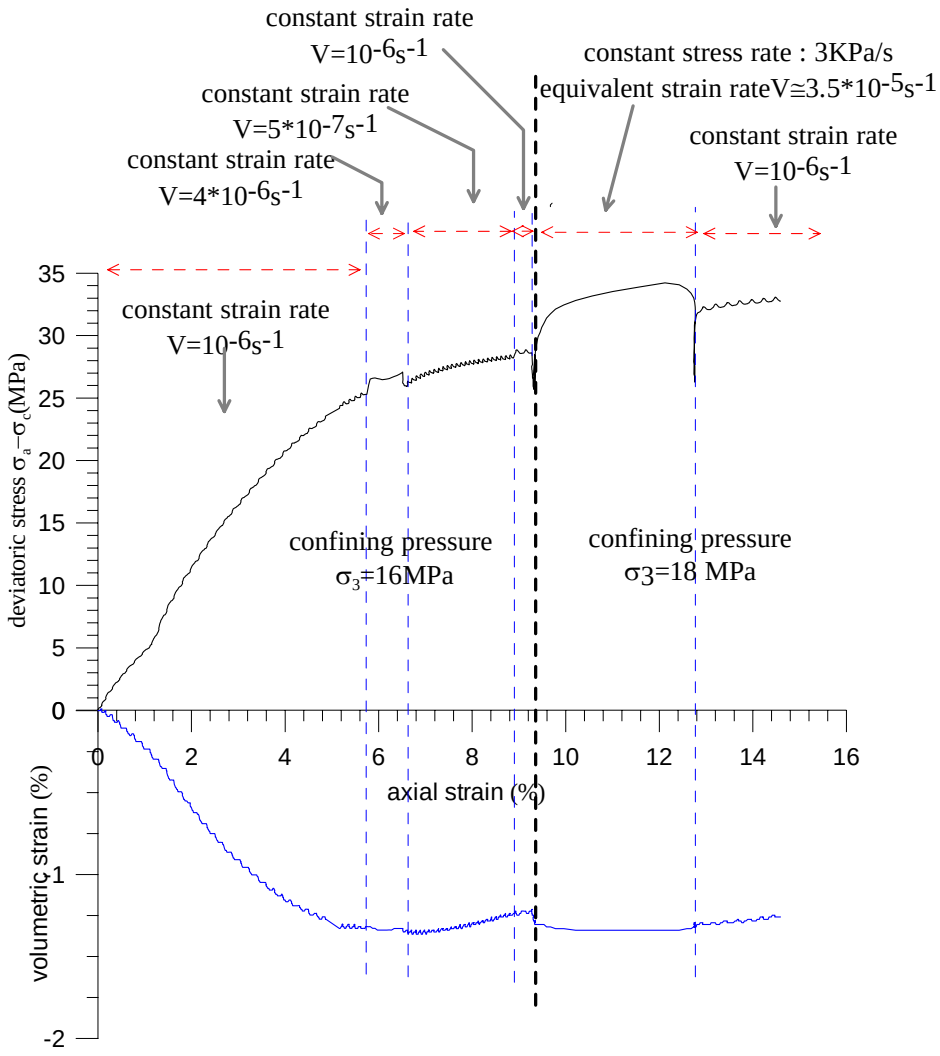

Fig. 9 : Drained triaxial tests at 70°C

From the constitutive point of view, the above results justify a plasticity model for the clayey gouge with two yield surfaces (cap model), one describing the frictional character and the other the compacting character of the material. For simplicity in numerical applications, these two surfaces can be interpolated with a single mathematical function of the form (Fig. 10):

$$F(T,p',\varepsilon_v^p) = T + fp'\left(1-\frac{p'}{p_c(\varepsilon_v^p)}\right)^{1/n} = 0 \qquad (11)$$

where T is the second invariant of the deviatoric stress tensor, p' is the effective mean stress and p_c is a function of the accumulated plastic volumetric strain ε_v^p calibrated on the experimental data

$$p_c(\varepsilon_v^p) = a_1 + a_2\varepsilon_v^p + a_3\sqrt{1+a_4\varepsilon_v^p + a_5\left(\varepsilon_v^p\right)^2} \qquad (12)$$

with

$$a_1 = -99.03\text{MPa} \; ; \; a_2 = 2389\text{MPa} \; ; \; a_3 = 101.08\text{MPa} \; ; \; a_4 = -43.18 \; ; \; a_5 = 466.56 \qquad (13)$$

f=0.6 is the friction parameter at peak strength, and n=8.

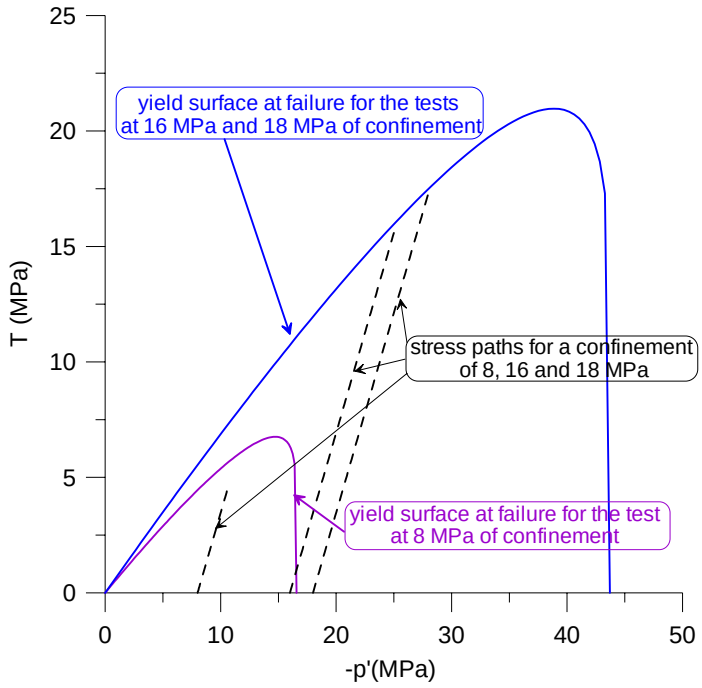

Fig. 10: Yield surface for the red clayey gouge

Drained thermal loading of the clayey gouge

In order to study the effect of temperature on the volumetric behaviour of the material, two tests of drained heating have been performed in isotropic stress conditions. The first test was run with an isotropic stress of 16 MPa and the second test with an isotropic stress of 12 MPa. For each test, the sample was first loaded isotropically to its final stress in drained conditions and at constant room temperature. Then by keeping the isotropic stress constant, the sample was heated in drained conditions at a rate of 0.02°C/min. The experimental results are shown in Fig. 11. The two tests show a good reproducibility and show also that the final state of isotropic stress is not influencing the response.

The important result from these experiments is that the clay-rich material is contracting, when heated. This phenomenon represents a thermo-plastic or structural collapse. The corresponding elasto-plastic contraction coefficient is negative

$$\alpha_c^{ep} = -2.4\text{x}10^{-4} \, / \, °\text{C} \qquad (14)$$

During the cooling phase thermo-elastic contraction is occurring with a rate of

$$\alpha_c^{e} = 1.4\text{x}10^{-4} \, / \, °\text{C} \qquad (15)$$

Thus the resulting isobaric thermo-plastic contraction coefficient is

$$\alpha_c^{p} = \alpha_c^{ep} - \alpha_c^{e} = -3.8\text{x}10^{-4} \, / \, °\text{C} \qquad (16)$$

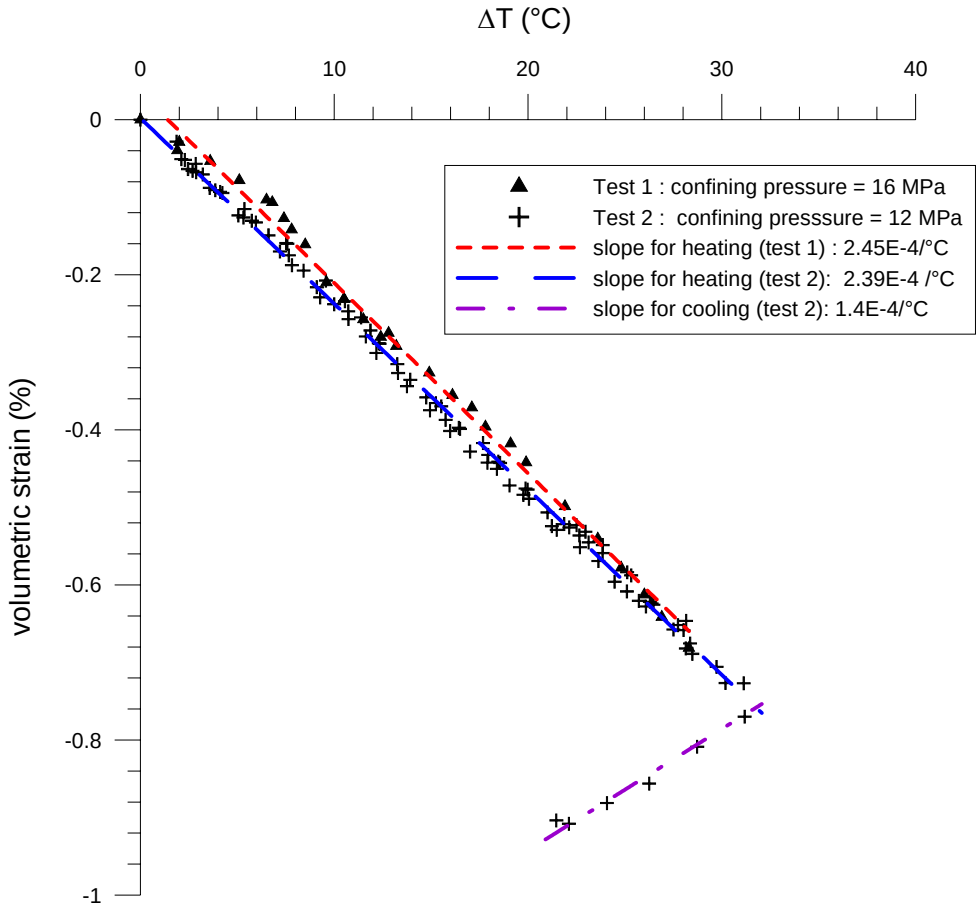

Fig. 11 : Drained heating tests under isotropic state of stress

Following Vardoulakis (2000b) the coefficient of thermal pressurization λ can be estimated from the above results

$$\lambda = \frac{-\alpha_c^p}{c} \tag{17}$$

where the compressibility coefficient is given by equation (5). The thermal pressurization coefficient is estimated to 136 kPa/°C.

5.2.2.5 Summary

The Aigion fault gouge is a clay-rock mixture. The above results have shown that although the clay fraction is relatively small, it has a significant influence on the thermo-mechanical properties of the material.

The thermo-poro-mechanical constants of the water saturated red clayey gouge at a nominal stress of 16 MPa are summarized on Table 2.

Permeability k	$7x10^{-21}$ m^2
Compression index C_c	0.11
Swelling index C_s	0.023
Consolidation coefficient c_v	$2.42x10^{-9}$ m^2/s
Compressibility coefficient c	0.0028 MPa^{-1}
Thermal pressurization coefficient λ	136 kPa/°C
Friction angle ϕ	28° ÷ 29°

Table 2 : Thermo-poro-mechanical constants of the water saturated red clayey gouge at a nominal stress of 16 MPa

5.2.3 MECHANICAL PROPERTIES OF THE JOINT BETWEEN THE FRACTURED LIMESTONE AND THE BRECCHIA ZONE

(a) (b)

Fig. 12: Interface between the fractured limestone and a cataclastic band (Box 33 – Core 13-2) at depth 744m : (a) Core sample ; (b) unfolded picture of the core surface

It is of interest to study the behaviour of the interface between fractured limestone and cataclastic bands as found above the clayey core of the faults (Fig. 12).

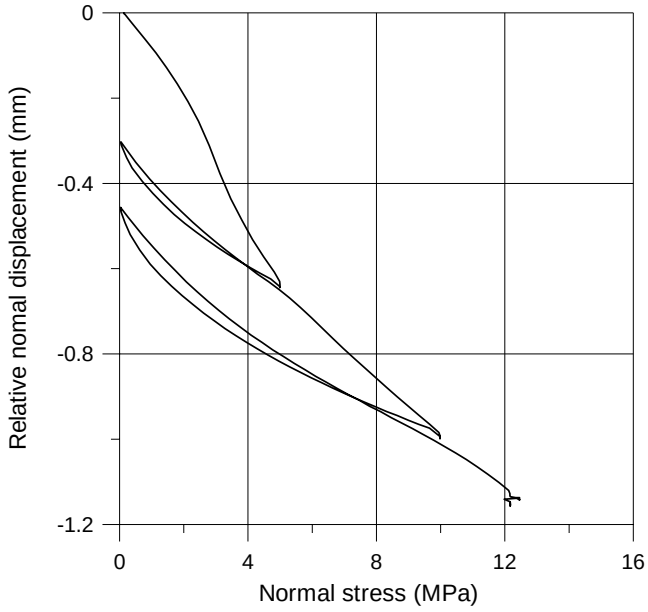

Fig. 13 : Cyclic normal loading

One sample has been tested in the direct shear box of Laboratory 3S (Soils, Solids, Structures) in Grenoble, France. The orientation of the joint with respect to the axis of the core is 112°. On the side of the vein wall of the fault, the material is a fissured limestone with open fractures often filled with calcite. On the side of the breccia, it is a crushed, relatively porous material with recent cementing. Voids of several millimeters of diameter and geodes with calcite filling are visible inside the calcite where the crystallization is uncompleted.
During the direct shear experiments, the displacement was applied on the joint in a direction which corresponds to the relative movement observed in the Corinth Gulf, i.e. from south to north. The stress path chosen is as follows:

- First an increasing normal stress was applied with two unloading and reloading cycles at 5 MPa and 10 MPa.
- Then at a nominal normal stress of 12.20 MPa, a shear displacement was applied up to relative tangential displacement $\Delta u_t = 40\text{mm}$.
- Then the tangential displacement was reversed to zero relative tangential displacement.

The tangential stiffness of the joint is estimated as $k_t = 13.9\,\text{MPa/mm}$. The response to normal loading is shown in Fig. 13. Notice that under constant normal force, the normal stress was increasing with increasing tangential relative displacement (due to cross-section reduction) and reached a value $\sigma \approx 15\,\text{MPa}$ (Fig. 14a). The normal stiffness of the joint was increasing with normal stress from about $k_n = 10.8\,\text{MPa/mm}$ at low normal stress, to $k_n = 17.7\,\text{MPa/mm}$ at normal stress $\sigma = 12\,\text{MPa}$.
The friction coefficient, defined as the ratio between shear stress and normal stress

$$\tan\phi = \frac{\tau}{\sigma} \tag{18}$$

is plotted in Fig. 14b versus the relative tangential displacement. It shows a sharp peak, which corresponds to the rupture of the contact between the limestone and the breccia. The peak corresponds to a friction angle of $\phi_p = 44^\circ$, which is close to the internal friction angle of the intact limestone. The residual friction angle of the joint is almost the same in loading and

unloading and is $\phi_r \approx 32^\circ$. It is observed that the peak is not so sharp when the direction of the shear is inverted, which reflects the rapid wear of the contact surface of the joint.

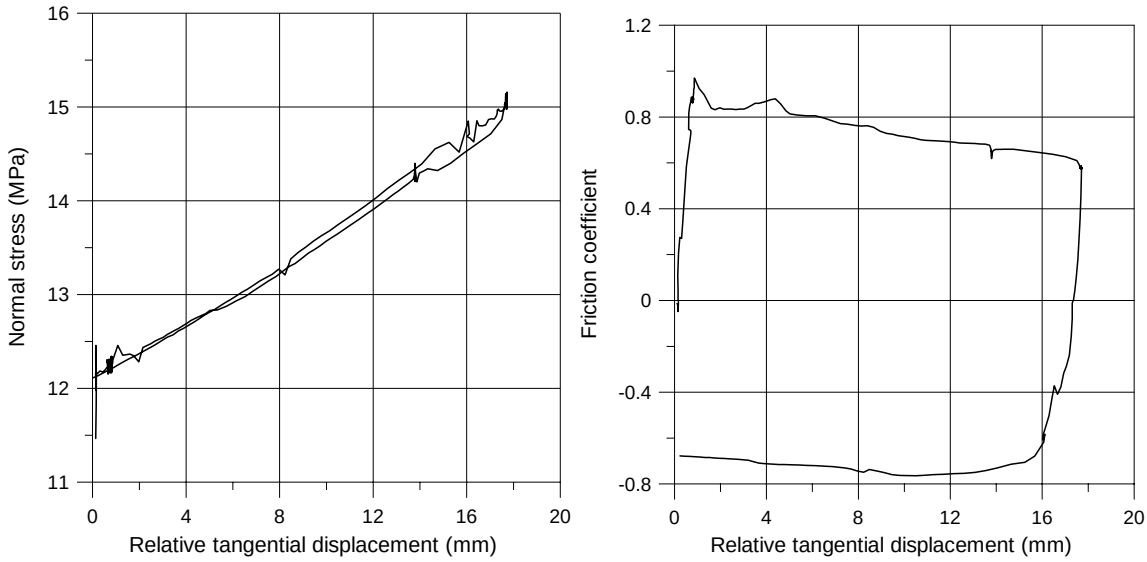

Fig. 14 : Direct shear experiment under constant normal force: (a) evolution of normal stress; (b) friction coefficient.

Important porosity reduction is observed for the first cycle. Notice that pore closure is frequently observed in uniaxial testing of highly porous rocks. The contractant character of the interface, when sheared is shown in Fig. 15. The corresponding dilatancy angle is negative, $\psi = -7^\circ$, during the loading phase and positive, $\psi = 5^\circ$, during the unloading phase.

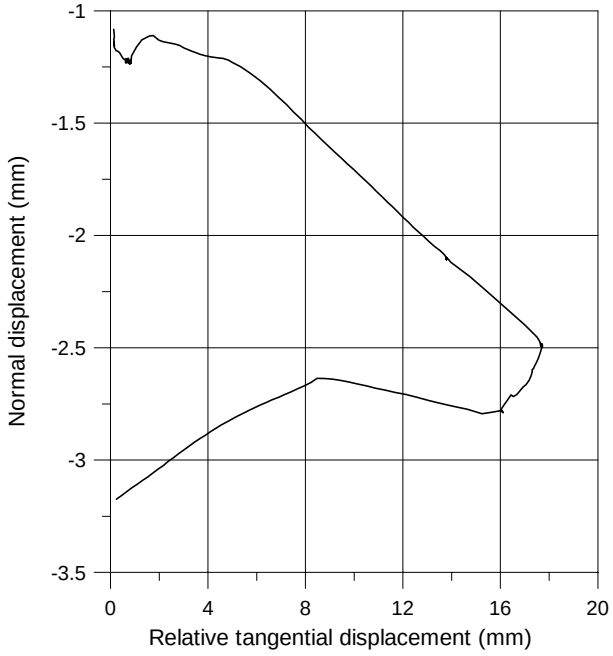

Fig. 15 : Direct shear experiment under constant normal force: Contractancy of the joint during shear

Fig. 16 : The contact zone between the limestone and the breccia tested in direct shear

The mineralogical composition of the crushed material exactly at the contact between the limestone and the breccia (Fig. 16) after the shear test has been analysed using X-ray diffraction and was found as follows:

Calcite :	77%	Chlorite :	1.5 %	Quartz :	7 %
Illite :	4.5 %	Albite :	1.5 %	Amorphous:	8.5 %

The presence of quartz can be related to the close formation of radiolarites. The presence of clay minerals such as illite and chlorite is quite common in fault zones.

5.2.4 MECHANICAL CHARACTERISATION OF LIMESTONE AND BRECCIA SAMPLES

Samples tested

Triaxial compression tests have been performed on dry rock samples from the various zones of the formation (see Fig. 17 and Table 3)

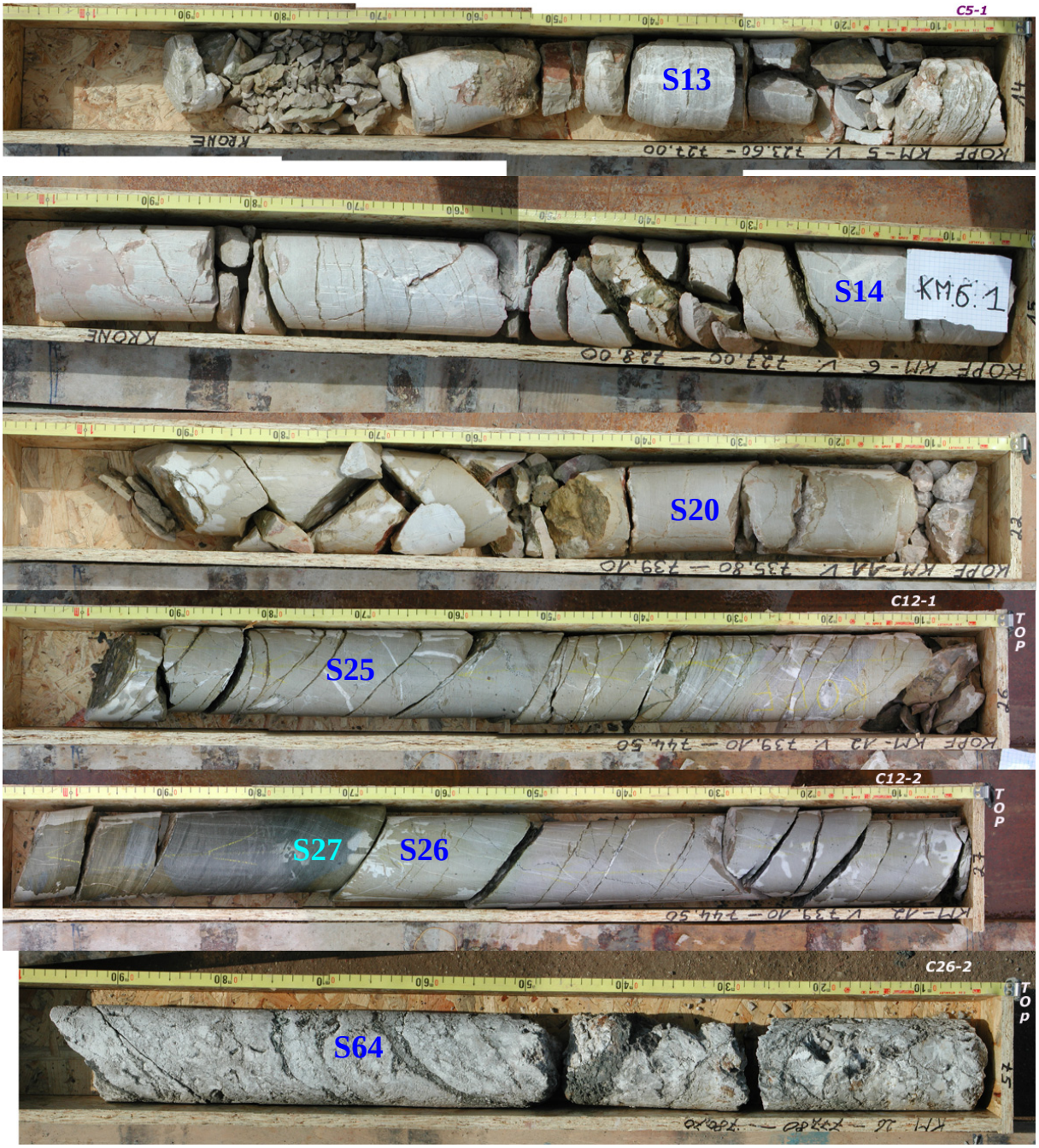

Fig. 17: Core samples tested

Sample	Core number	Depth (m)	Formation	Confining pressure (MPa)
S13-2	C05-1	724	limestone	0
S14-1	C06-1	727.20	limestone	16
S14-2	C06-1	727.20	limestone	8
S14-3	C06-1	727.20	limestone	26
S20	C11-1	736.20	limestone	0
S25-1	C12-1	739.70	limestone	25
S25-2	C12-1	739.70	limestone	8
S26-1	C12-2	740.70	limestone	16
S26-2	C12-2	740.70	sandstone	16
S27	C12-2	740.90	breccia	16
S64	C26-2	779.60		16

Table 3: Core samples tested

The limestone samples show an existing network of fractures filled with calcite. The pre-existing fractures have been mapped in order to distinguish them from the one formed during the compression test. The breccia samples are very fragile. Only one could be tested. Sample S27 is a fine-grained detritic sandstone.

Experimental setting and instrumentation

A large triaxial cell built by the company Geodesign with internal diameter of 140 mm is used (Fig. 18). This cell can sustain a confining pressure up to 60 MPa. This cell contents a system of hydraulic self-compensated piston. The loading piston is then equilibrated during the confining pressure builds up and directly applies the deviatoric stress. This deviatoric stress is applied by a servo-controlled press built by the company Metro-Mesures. The testing machine capacity is 50t (Fig. 18).

Fig. 18 : Triaxial cell and loading frame

The axial and radial strains are measured directly on the sample inside the cell with two axial transducers and four radial ones of LVDT type (see section AA on Fig. 19 and Fig. 20). These internal devices allow to avoid the main errors of strain measurements of devices external to the cell such as the compliance of the loading device, the tilting of the specimen,

the bedding errors at the ends of the specimen. This device is also more adequate that strain gages which are currently used for strain measurements on rocks. Strain gages can perturb the porous specimen because of glue penetration inside the sample and are useless beyond the onset of strain localisation.

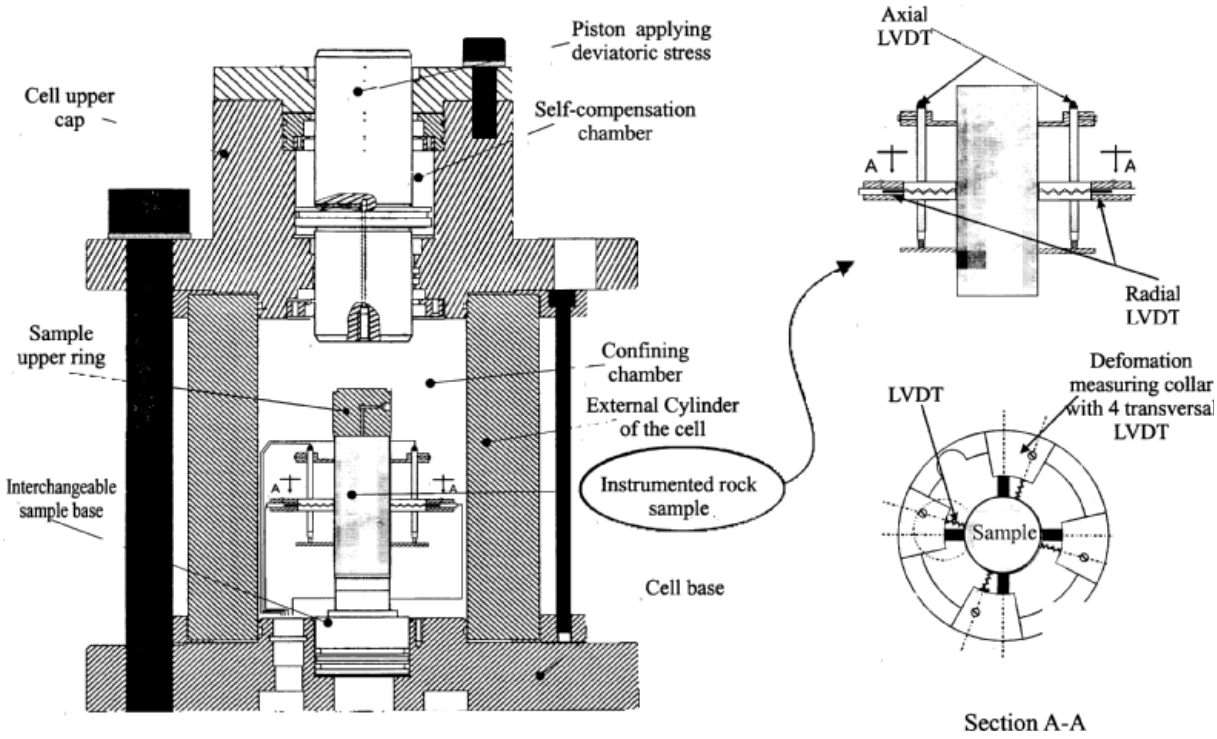

Fig.19 Testing device

Fig. 20: Instrumentation of the sample inside the cell

In due course of the test the temperature of the confining oil may fluctuate due to pumping of the confining fluid and shearing of the sample. It is guarantied by the constructor that the response of the LVDT is not influenced by temperature changes in the range of 0 to 120°. A correction for the radial deformation of the membrane during the test has been calibrated.

The lower base of the cell is equipped with a pore pressure transducer. Pore pressure measurements during test is then performed very close to the sample base.

Fig. 21 : Pressure generator TITAN

The confining pressure is applied by a servo controlled high pressure generator TITAN also built by the company Geodesign which consists of a piston moving in a pressure chamber (Fig. 21). The pressure generator is guided by an electronic regulator receiving an analogical signal from an external transducer. The regulators are programmed by a PC computer.

Elastic properties

The elastic parameters are determined from the unloading-reloading cycles performed during the test at various levels of the axial stress (Fig. 22). Two cycles have been performed for each test at about 25% and 50% of the maximum axial stress.

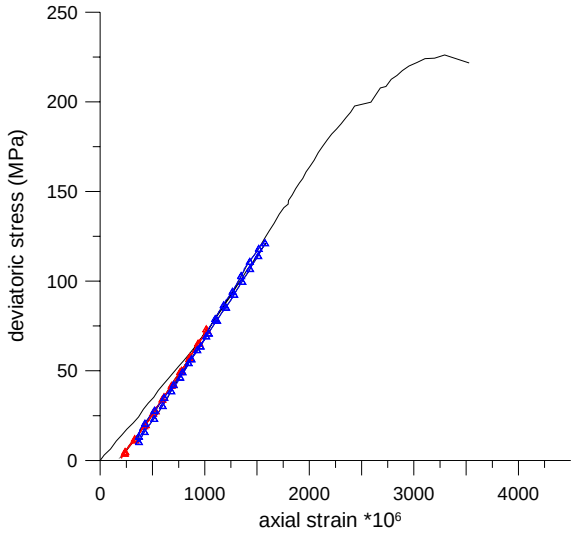

Fig. 22: Evaluation of the elastic moduli on the unloading-reloading cycles

The data of the unloading reloading cycles are approximated with a linear fit. The following strain and stress invariants are considered:

volumetric strain : $\varepsilon_{vol} = 2\varepsilon_{rad} + \varepsilon_{ax}$ (19)

shear strain intensity: $g = \frac{2(\varepsilon_{rad} - \varepsilon_{ax})}{\sqrt{3}}$ (20)

mean stress: $p = \frac{(\sigma_z + 2\sigma_r)}{3}$ (21)

shear stress intensity: $T = \frac{|\sigma_z - \sigma_r|}{\sqrt{3}}$ (22)

where
ε_{rad} is the mean value of the four measurements of the radial LVDT,
ε_{ax} is the mean value of the two measurements of the axial LVDT,
$\sigma_z=\sigma_1=\sigma_{ax}$ is the axial stress,
$\sigma_r=\sigma_3=\sigma_{conf}$ is the axial (confinement) stress.
The elastic secant moduli are defined by

Young modulus: $E = \frac{\Delta(\sigma_{ax} - \sigma_{rad})}{\Delta\varepsilon_{ax}}$ (23)

Poisson's ratio $\nu = -\frac{\Delta\varepsilon_{rad}}{\Delta\varepsilon_{ax}}$ (24)

Elastic shear modulus $G = \frac{\Delta T}{\Delta g}$ (25)

Elastic bulk modulus $K = \frac{\Delta p}{\Delta\varepsilon_{vol}}$ (26)

The following relationships hold between the elastic moduli

$$G = \frac{E}{2(1+\nu)} \quad (27)$$

$$K = \frac{E}{3(1-2\nu)} \quad (28)$$

$$\nu = \frac{3K - 2G}{6K + 2G} \quad (29)$$

$$E = \frac{9KG}{3K + G} \quad (30)$$

The results are presented on Table 4.

Sample	Confi-ment (MPa)	cycles	Shear modulus (MPa)	Bulk modulus (MPa)	Young modulus (MPa)	Poisson's ratio	Shear stress T (MPa)	Mean stress p (MPa)
S14-1	16	1	36748	46080	87092	0.18	42.4	40.5
		2	34903	75624	90749	0.33	70.15	56.5
S14-2	8	1	23559	61438	62667	0.33	31.9	25.7
S25-1	25	1	40008	58107	97620	0.22	37.6	46.7
		2	38340	70932	97461	0.27	54.3	56.4
S26-1	16	1	31084	81064	82686	0.33	42.6	40.6
		2	29855	139325	83595	0.4	65.1	53.6
S26-2	16	1	31206	57438	79264	0.27	42.9	40.7
		2	28680	86040	77436	0.35	70.6	56.7
S27-2	16	1	48028	98344	123914	0.29	37.2	37.5
		2	33906	158227	94936	0.4	54.1	47.2
S64-1	16	1	29463	76835	78372	0.33	46.8	37.6

Table 4 : Elastic parameters of the drilled samples

We observe that the elastic secant shear modulus is decreasing with increasing deviatoric stress which reflects that the sample is damaged during loading. This tendency is more pronounced for the sandstone sample S27.

These results can be compared with those obtained on outcrops on the survey sites H4 and H5 along Selinoutas river (Sulem et al, 2002) (Table 5). These blocks have been extracted from the limestone deposit. We consider here Block 172 (site H4) which is representative of the limestone close to Helike fault. Rock porosity is between 0.5 to 1.The analysis of the rock matrix shows that it is composed mostly of calcite (80%).

Confinement (MPa)	cycles	Shear modulus (MPa)	Bulk modulus (MPa)	Young modulus (MPa)	Poisson's ratio	Shear stress T (MPa)	Mean stress p (MPa)
2.5	1	28850	80260	77289	0.34	19.9	14.1
	2	27246	94632	74580	0.37	38.9	24.9
	3	27460	102860	75648	0.38	49.3	30.9
10	1	28416	85345	76732	0.35	26.8	25.4
	2	27015	113852	75105	0.39	49.8	38.7
	2	26417	130965	74258	0.40	72.7	52
25	1	36330	67811	92475	0.27	48.9	53.2
	2	34540	78747	90402	0.31	87.3	75.4
	3	33668	86649	89422	0.33	107	86.7

Table 5 : Elastic parameters of the outcrop limestone

These results show that the elastic properties of the fractured limestone of the extracted cores (samples S14, S25, S26) are comparable with those of the limestone deposit at the surface. The average Young modulus for the drilled limestone cores (respectively the limestone outcrops) is 84300 MPa (respectively 80600 MPa). The average Poisson's ratio for the drilled limestone cores (respectively the limestone outcrops) is 0.3 (respectively 0.35).

Strength

The strain-stress curves for the various samples at a confinement of 16 MPa are presented on Fig. 23. It is observed that the breccia zone exhibits weaker material properties and a more ductile behaviour than the limestone. The sandstone sample S27 is also weaker.
Table 6 summarises the maximum axial stress for the various samples tested. Due to the limited amount of material, some samples have a small size and could not be fully instrumented in the triaxial cell. They were thus tested in conventional uniaxial conditions.

They failed in an early stage of loading. This can be attributed to the pre-existing fractures which develop and propagate in an unstable manner in unconfined conditions.

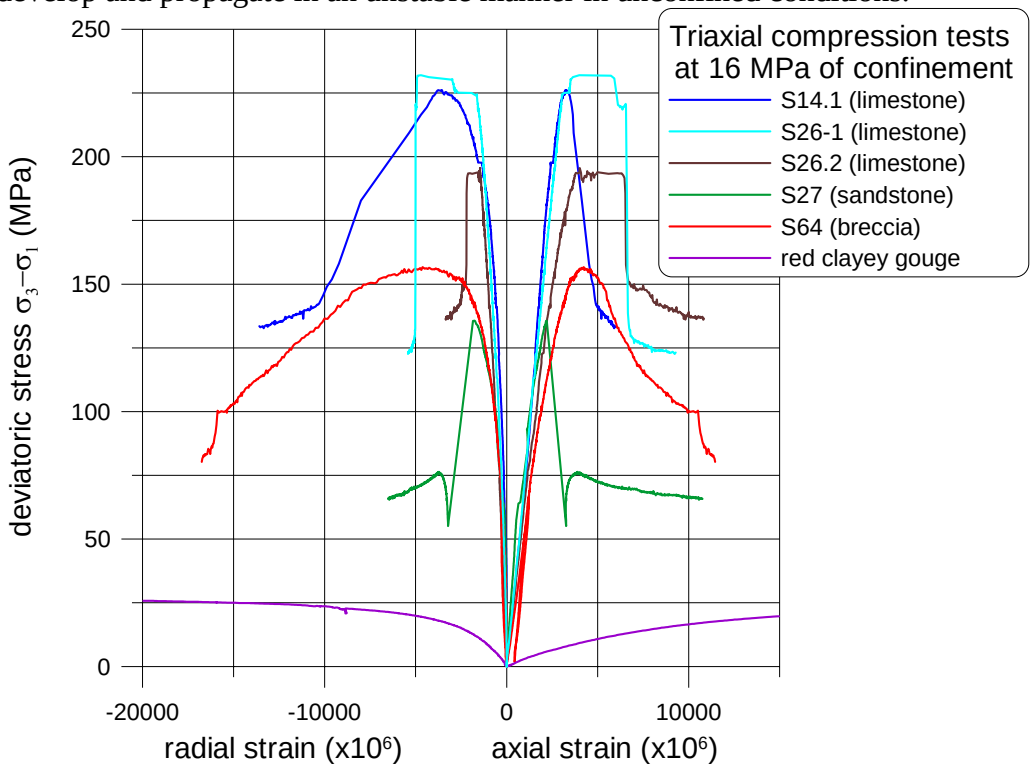

Fig. 23: Triaxial compression tests at 16 MPa of confinement

The maximum deviator profile at 16 MPa of confinement is plotted on Fig. 24 as a function of the depth of the drilled sample. This diagram shows clearly that the weakest material is the red clayey gouge.

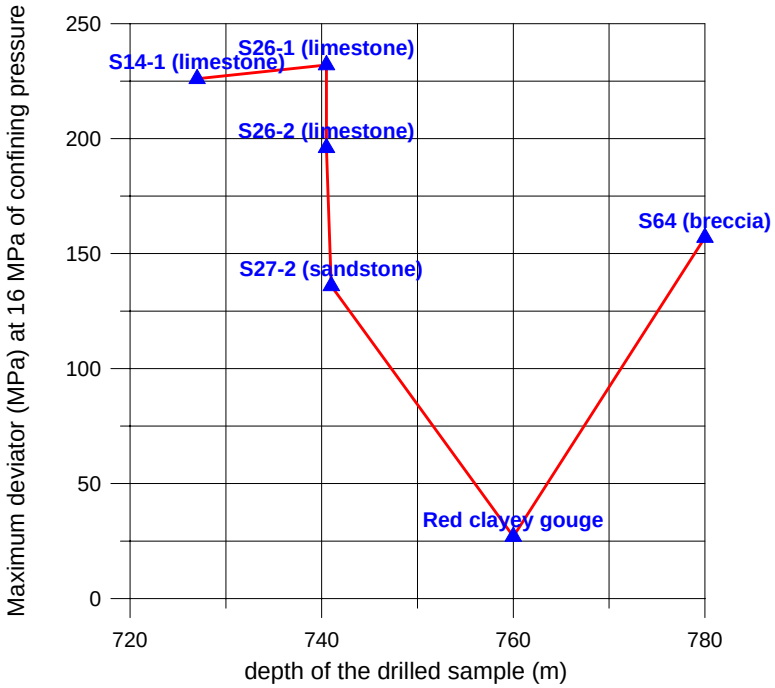

Fig. 24: Maximum deviator profile at 16 MPa of confinement

Sample	Height (mm)	Diameter (mm)	Confinement (MPa)	Axial stress at peak (MPa)
S13-2	40	36.4	0	21.76
S14-1	75.5	36.3	16	242.15
S14-2	59.2	36.3	8	80.91
S14-3	51.5	36.3	26	238.44
S20	39	36.2	0	58.17
S25-1	75	36.15	25	353.8
S25-2	65.5	36.2	8	115.44
S26-1	75.5	36.2	16	248
S26-2	72	36.15	16	211.56
S26-3	75.5	30	0	116.58
S26-4	46.1	29.9	0	122.26
S27-2	75.5	36.15	16	151.67
S27-3	58	36.2	4	91.99
S64-1	60.7	36.2	16	172.7

Table 6: Strength of the drilled rock samples

The Mohr circles at failure are shown on Fig. 25 for the limestone samples. A unique linear failure envelope can be interpolated for both the outcrops and the cores. The corresponding friction angle is 44.7° and the cohesion is 39.3 MPa. These data correspond to a uniaxial strength of 188 MPa.

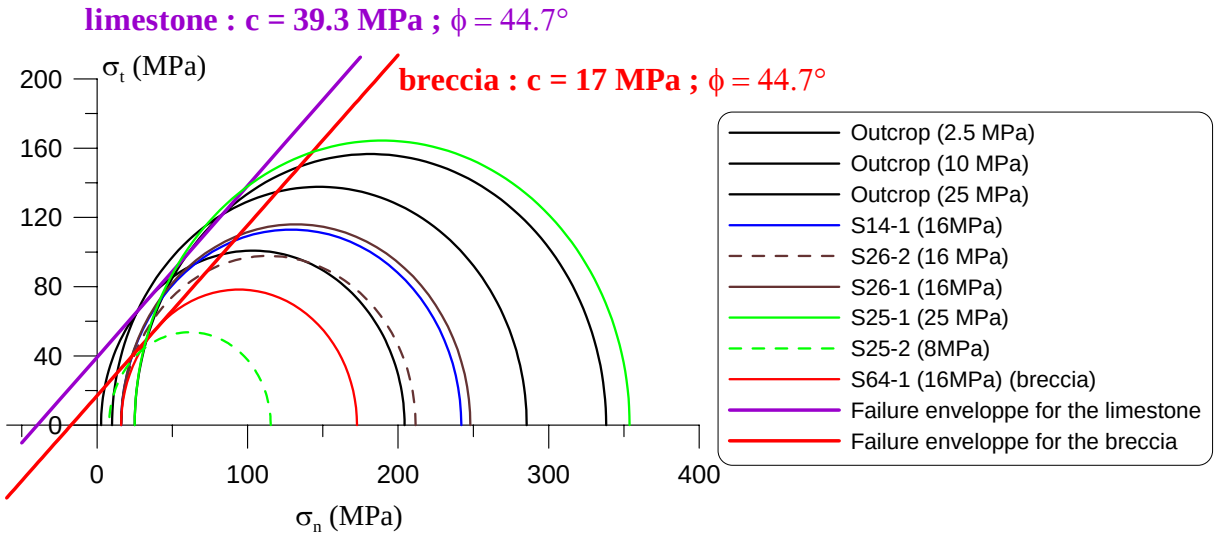

Fig. 25 Mohr circles and failure criterion for the limestone

As we have only one test for the breccia, we can assume the same friction angle as the limestone and obtain thus a residual cohesion of 17 MPa corresponding to a uniaxial strength of 81MPa. Under the same confining pressure but with a bigger sample with a diameter of 100mm carried a triaxial test carried by the University of Edinburg gave a weaker axial stress at failure of 107 MPa (Elphick et al 2003). This discrepancy is due to the fact that the breccia samples are very heterogeneous (Fig. 26).

Fig. 26: Sample S64 in the limestone breccia

The Mohr circles at failure and the Mohr-Coulomb criterion for sample 27 corresponding to the fine-grained detritic sandstone zone of core C12-2 are shown on Fig. 27. A friction angle 41.7° and a cohesion 16.2 MPa are obtained corresponding to a uniaxial compression strength of 72 MPa. These characteristics are thus smaller than those of the limestone deposit.

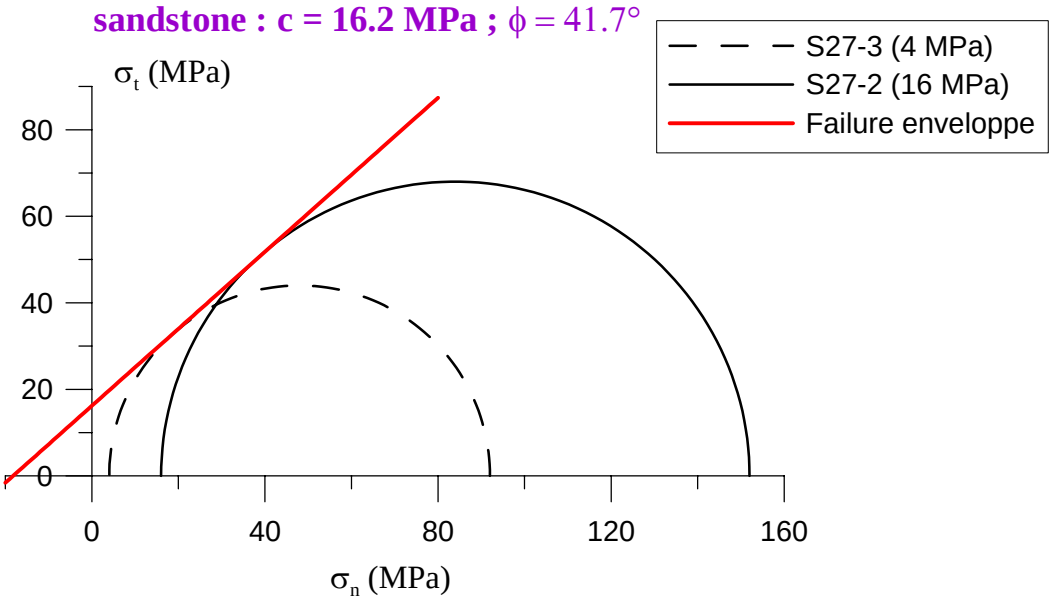

Fig. 27 Mohr circles and failure criterion for the sandstone

Fig. 28 shows a photograph of the shear zone formed in the sample 27-2. The zone of localised failure is clearly identified due to the white coloration of the band visible to the naked eye. This colour change is due to the crushing of grains and allows for a precise evaluation of the thickness (here 2mm). It does not follow any pre-existing fracture but is formed during the triaxial test. Microscopic observation of the shear zone shows that the zone consists in a series of shear bands (Fig. 29).

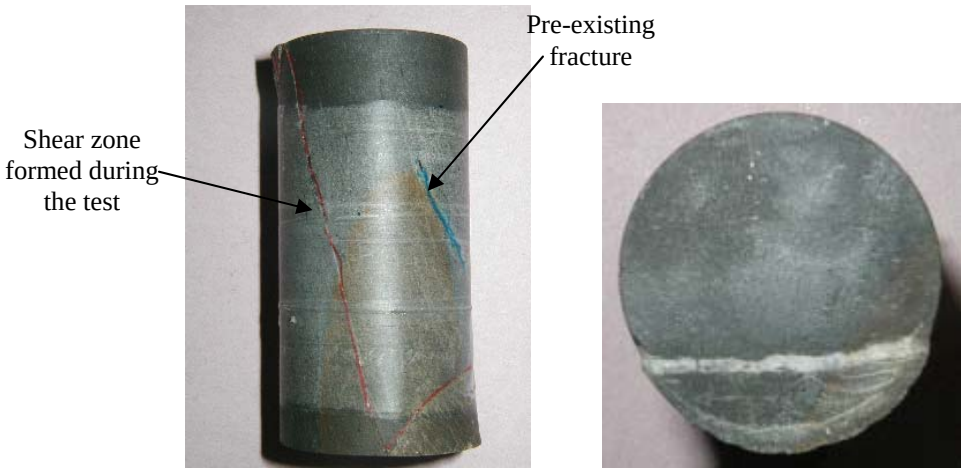

Fig.28: Shear zone observed in sample 27-2

Fig. 29 : Microscopic observation of the shear zone of sample S27

5.2.5 CONCLUSIONS

In rapid fault shearing of clay-rich faults the effects of pore-water heating and consequent pore-pressure rise cannot be disregarded. Thermal run-away instabilities are possible to occur as soon as the particular clay shows frictional strain-rate hardening and thermal softening (e.g. Vardoulakis, 2002b).
The experimental characterisation program performed on fault zone cores from Aigion fault has showed that:

- The Aigion fault gouge is a clay-rock mixture. Although the clay fraction is relatively small, it has a significant influence on the thermo-mechanical properties of the material. The clayey core of the fault has a very low fluid permeability and exhibits contractant volumetric behaviour when heated. Thus rapid shear deformation may lead to fluid pressurisation inside the fault.
- The material is contracting when sheared at constant temperature. However at large shear strains critical state is reached with no further volumetric deformation.
- The frictional resistance of the material increases slightly with temperature and strain rate.
- The joint between the carbonate zone and the cataclastic bands shows a brittle and contractant behaviour with a residual friction angle of about 32°, which is higher by 3° than the friction angle at critical state of the clay core.
- The limestone samples from the drilled hole exhibit similar elastic properties and strength as the samples from the deposit at the surface.
- The breccia zone has a more ductile and a much weaker behaviour than the limestone zone.

6. WORKPACKAGE 6 – PERMANENT SITE INSTRUMENTATION (IPG-P & NKUATHENS)

The objective of the Corinth Rift Laboratory is to monitor continuously, and simultaneously, ground deformation, fluid motion, and water geochemistry, within the perimeter of interest (30 km x 30 km). This monitoring covers all frequency ranges, from the kilohertz to the continuous signal. The contribution of DGLab to this scheme concerns the participation to the short period seismic network and the instrumentation of the well AIG10.

6.1 CONTRIBUTION TO THE CRL SHORT PERIOD SEISMIC NETWORK- - (NKUA.DGG.SL)

The detailed recording of local seismicity is crucial for understanding the fluid fault interactions. For that purpose, the local CRL surface seismological network was installed. The main role of the University of Athens was to participate in the installation and maintenance of the CRL network, as well as in the data acquisition, in collaboration with IPGP.

The Corinth Rift Laboratory (CRL) seismological network currently consists of 12 Titan stations installed both on the southern (Aigion area) and the northern (Eratini area) coast of the Gulf of Corinth. The 7 southern stations are equipped with three components borehole seismometers (2 Hz Mark Products), in depths ranging from 50m to 130m, while the 5 northern ones involve surface seismometers. In addition, 5 Reftek seismological stations equipped with BB surface seismometers were provided by the University of Athens and were installed in the study area, 4 on the southern and 1 on the northern coast of the Gulf. 3 of them were installed just above the borehole seismometers of the CRL network. Currently, seismic data are recorded and stored on local hard discs. Once a month a visit was performed in every station in order to maintain them and to collect the data. Following, two copies of the data were saved on CD's, one for the University of Athens, while the second was sent to IPGP.

After the construction of the database, data analysis was performed partly automatically, partly by hand. All the stored data are checked by seismologists in order to perform time corrections and to minimize the P and S residuals. The first task was the location of the recorded events. Following, focal mechanisms were constrained for selected events. These data are currently available to all the participants of the project.

The installation of the CRL seismological network began on April 2000. A very large number of earthquakes were recorded until now. Due to the high amount of data, the analysis is already performed for the years 2000 and 2001. For that period more than 6000 earthquakes were located within the study area and its vicinity. An important number of these events was located with very small residuals. This was achieved due to the geometry of the network. During the period of operation of the CRL seismological network several seismic crises occurred. The most important one began on March 2001 and its largest event occurred on 8 April with magnitude 4.2.

The selected seismic activity is presented in Figure 1 and is mainly concentrated within the Gulf of Corinth. The spatial distribution of the events covers approximately the whole study area. The analysis of the data revealed that the seismicity is mainly clustered. The most evident cluster is located southern of the city of Aigion. Seismic activity is mainly concentrated between 4 and 12 km. The magnitude of the majority of the located earthquakes is less than 3R.

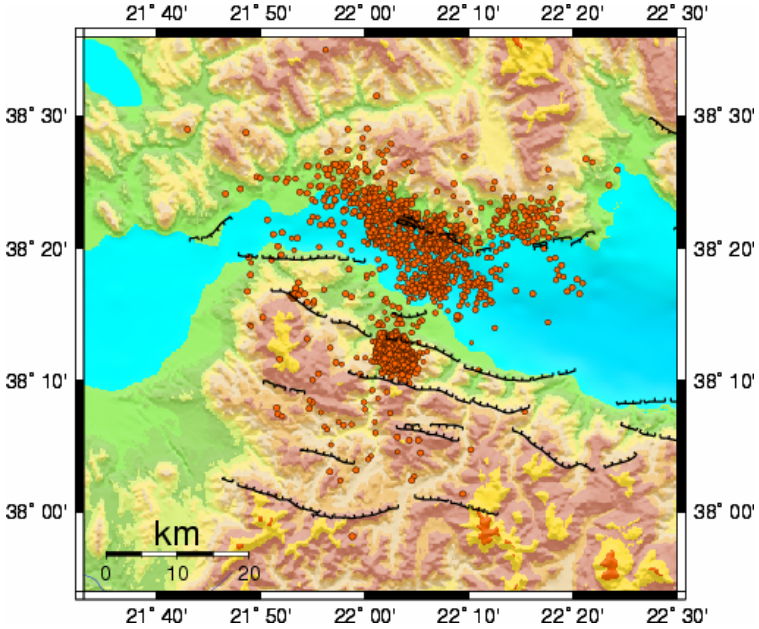

Fig.1: Seismicity located by the CRL seismological network.

The best constrained focal mechanisms, that were calculated using the P wave first motions, are presented in Figure 2. These fault plane solutions represent normal faulting, mainly oriented in E-W direction and dipping north. At the same figure the active faults are presented. The area is characterized by normal faults with an almost E-W direction and dipping NNE. The microseismic activity can be correlated to these faults, as the Eliki´s and Aigion´s faults, which have already been activated in the past.

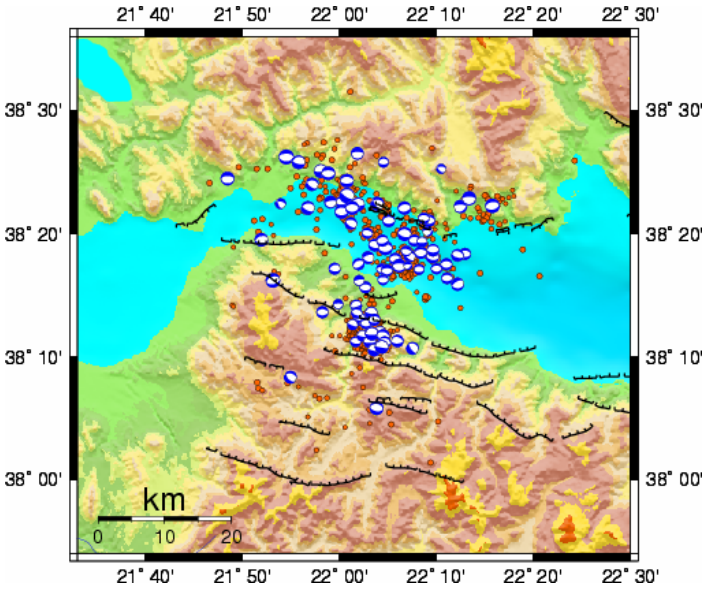

Fig.2: Best constrained focal mechanisms

The correlation between the microseismic activity and the active normal faults of the area can be proved by seismic cross-sections. For that purpose, 8 parallel cross-sections were constructed within the area, in NNE direction. The distance between them was 3km. In Figure 3 the central cross-section (Aigion area) is presented. The above mentioned cluster, located southern of the city of Aigion, can clearly be distinguished at depths between 4 and 10km at a distance of about 25 km from the south origin of the cross-section. If the representation in depth of the observed active faults is correct, seismicity can be related to the movement of more than one active fault. This is an important result that must be further investigated.

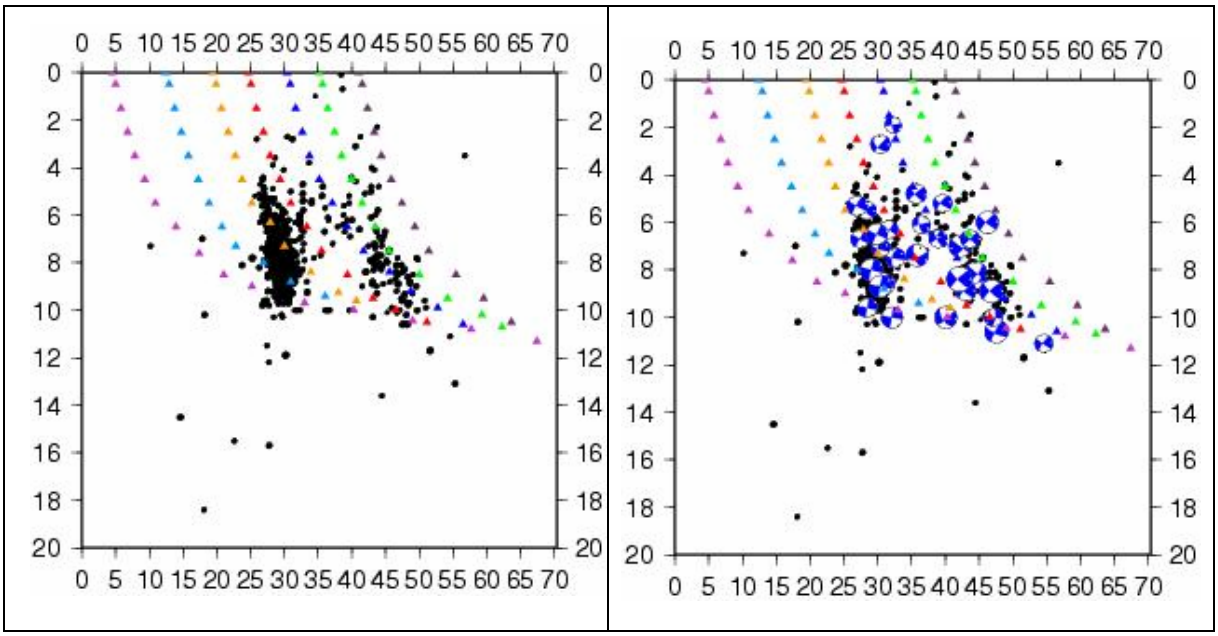

Fig. 3: Central cross-section.

The left one represents the spatial distribution of the events, while on the right one focal mechanisms were also added. Triangles represent the hypothetical cross-sections of the observed active faults on surface.

During the analysis of the recorded seismicity, the shear-wave splitting phenomenon was observed. An anisotropy study has been performed using both the polarigram and the hodogram method. The selected events have clear and impulsive S wave arrival phases on the horizontal components. In addition the amplitude of the S wave phase on the vertical component is smaller than on the horizontal ones. Visual inspection of seismograms was used to select the events that match the criteria mentioned above. Some of the selected recordings were filtered using a band-pass filter in order to obtain a better representation of the waveform.

In Figure 4 an example for the Dafnochori station is presented. The angle between the north and the fast axis direction is the polarization direction, which is equal to N93°, as shown in Figure 4a. Then the seismograms are rotated in the fast and slow direction and the obtained polarigram is presented in Figure 4b. In this Figure the obtained polarization vector is oriented almost parallel to the fast component. The measured time delay is equal to 0.088 sec and is removed (Figure 4c) in order to obtain the polarization direction of the source, which is equal to N165° (Figure 4d). The same procedure was also applied for the other station of the CRL network.

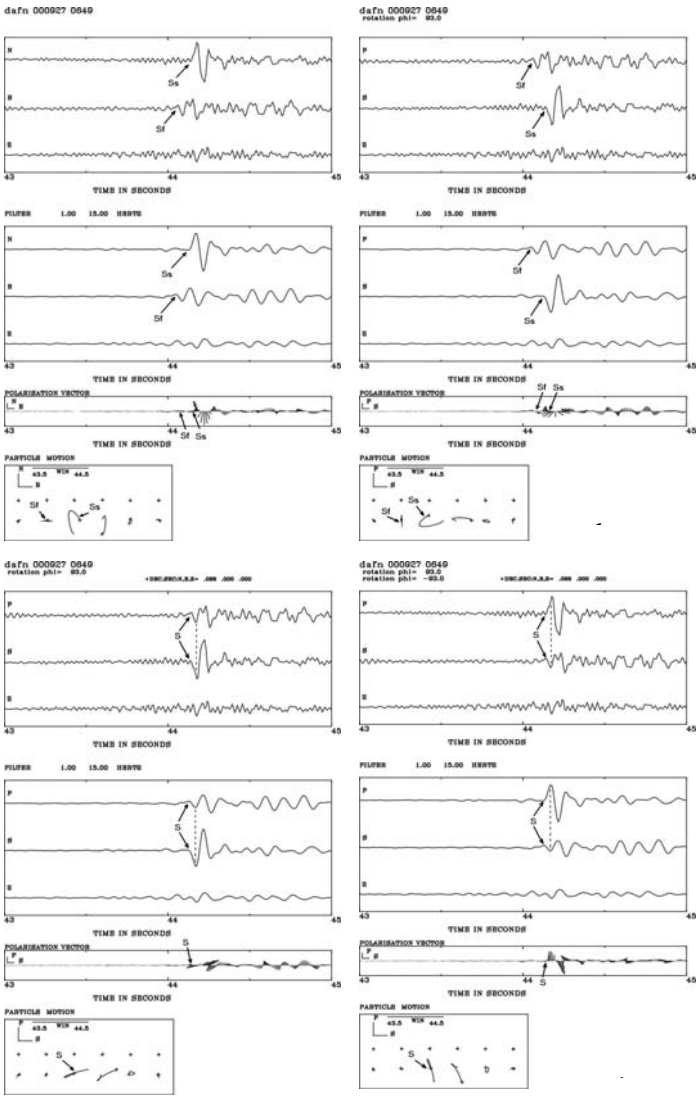

Figure 4. (a) Original traces of three component seismograms of an earthquake recorded at Dafn station, filtered traces, polarigram and hodogram in the north-east plane. (b) Traces rotated parallel and orthogonal to the polarization direction of the fast shear waves, filtered waveforms of the rotated traces, polarization vector and hodogram in the fast-slow plane where the time delay is measured. (c) Traces rotated parallel and orthogonal to the polarization direction of the fast shear waves after the correction of the time delay, filtered waveforms, polarigram and hodogram. (d) Traces rotated back to the North and East directions, filtered waveforms of the back rotated traces, polarization vector and hodogram from which the polarization of the source is estimated.

Time delays vary between 0.016 and 0.128 sec. Polarization directions of the fast shear wave on equal-area projections and rose diagrams for all the selected events were plotted for each station. From these projections it was obvious that the S_{fast} polarization directions are independent of the azimuth of each event. Mean anisotropy directions at the stations used for the anisotropy study vary between 90° and 120°.

CONCLUSIONS

1. A catalogue of seismicity was created.
2. Seismicity is mainly concentrated between 4 and 12 km depth.
3. Fault plane solutions were constrained revealing normal faulting, striking mainly in E-W direction and dipping north.
4. Several cross-sections were performed, in order to correlate the observed active faults, the located seismicity and the constrained focal mechanisms.
5. Anisotropy study was performed. Mean anisotropy directions are almost perpendicular to the general NNE-SSW direction of extension of the Gulf of Corinth, as deduced by fault plane solutions and GPS measurements.

6.2 PERMANENT INSTRUMENTATION OF AIGION FAULT (IPG-P)

This work was completed by IPG-P with the participation of the Technical Division of Institut National des Sciences de l'Univers (DT-INSU). Initial plans were to set up a dipole across the fault, i.e. two boreholes intersecting the fault at different depths, in order to investigate the fault hydraulic properties through hydraulic interference tests. But, as explained in section 1, only one well could be drilled and only one well has been instrumented. This well has intersected a very significant aquifer below the Aigion fault and the AIG10 instrumentation is aimed at better understanding interactions between this aquifer and the fault.

6.2.1 The AIG10 well instrumentation system

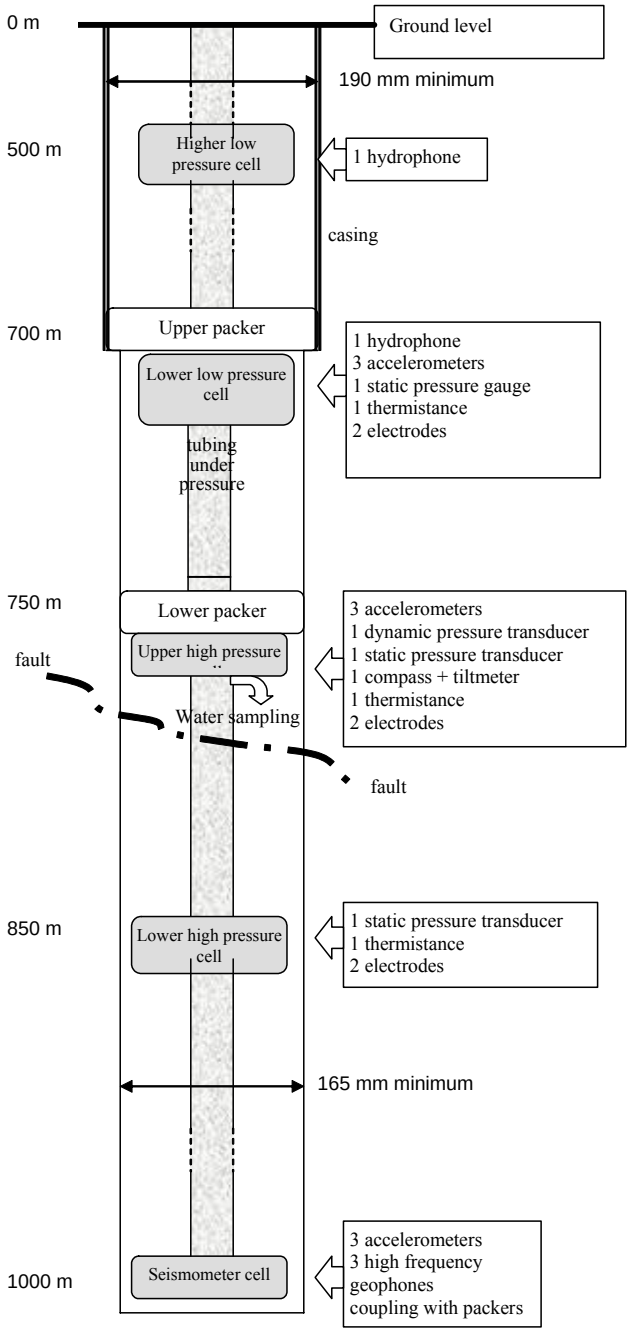

Figure 1: Schematic diagram of the permanent instrumentations planned for AIG10

Figure 2 : From left to right are shown the seismometer cell, the lower high pressue cell, the upper high pressure packer with its high pressure cell, the lower low pressure packer with lower low pressure cell and the upper low pressure cell

Figure 3 : In the foreground : the seismometer cell with its two packers for downhole coupling; in the background : the two high pressure packers

Figure 4 : Close up view showing the electrodes for water conductivity

Cell	Sensor	Sampling Rate (samples/s)	LTO (bytes)	Disk (SEED)
Seismometer	Accelerometre (X)	150	2	0,5
	Accelerometre (Y)	150	2	0,5
	Accelerometre (Z)	150	2	0,5
	Sismometre X	2501	2	0,5
	Sismometre Y	2501	2	0,5
	Sismometre Z	2501	2	0,5
	Actual Gain	1	6	3
	Case Temperature	1	2	3
	48V Alimentation Voltage	1	2	3
	Analogic Alim. Voltage	1	2	3
	Tension alim capteurs	1	2	3
Lower high pressure	Static Pressure	150	2	0,5
	Thermistor	50	2	0,5
	Electrodes	150	2	1
	Case Temperature	1	2	3
	48V Alimentation Voltage	1	2	3
	Analogic Alim. Voltage	1	2	3
Upper high pressure	Accelerometre Si (X)	150	2	0,5
	Accelerometre Si(Y)	150	2	0,5
	Accelerometre Si (Z)	150	2	0,5
	Orientation (mag X)	1	2	0,5
	Orientation (mag X)	1	2	0,5
	Orientation (mag X)	1	2	0,5
	Orientation(Pitch)	1	2	0,5
	Orientation(roll)	1	2	0,5
	Orientation (T)	1	2	0,5
	Dynamic Pressure(*)	1	600	4
	Pression statique	150	2	0,5
	Thermistor	50	2	0,5
	Electrodes	150	2	0
	Case Temperature	1	2	3
	48V Alimentation Voltage	1	2	3
	Analogic Alim. Voltage	1	2	3
	Tension alim capteurs	1	2	3
Lower low pressure	Accelerometre Si (X)	150	2	0,5
	Accelerometre Si(Y)	150	2	0,5
	Accelerometre Si (Z)	150	2	0,5
	Hydrophone	2501	2	1
	Actual Gain	1	6	3
	Pression statique	150	2	0,5
	Thermistor	50	2	0,5
	Electrodes	150	2	1
	Case Temperature	1	2	3
	48V Alimentation Voltage	1	2	3
Upper low pressure	Hydrophone	2501	2	1
	Actual Gain	1	1	3
	Case Temperature	1	2	3
	48V Alimentation Voltage	1	2	3
	Analogic Alim. Voltage	1	2	3
Surface	Packer pressure	150	2	1
	Temperature	50	2	1
	Case Temperature	1	2	3
	48V Alimentation Voltage	1	2	3

Table 1: List of sensors and their sampling rate (altogether about 3 Gigabytes per day).

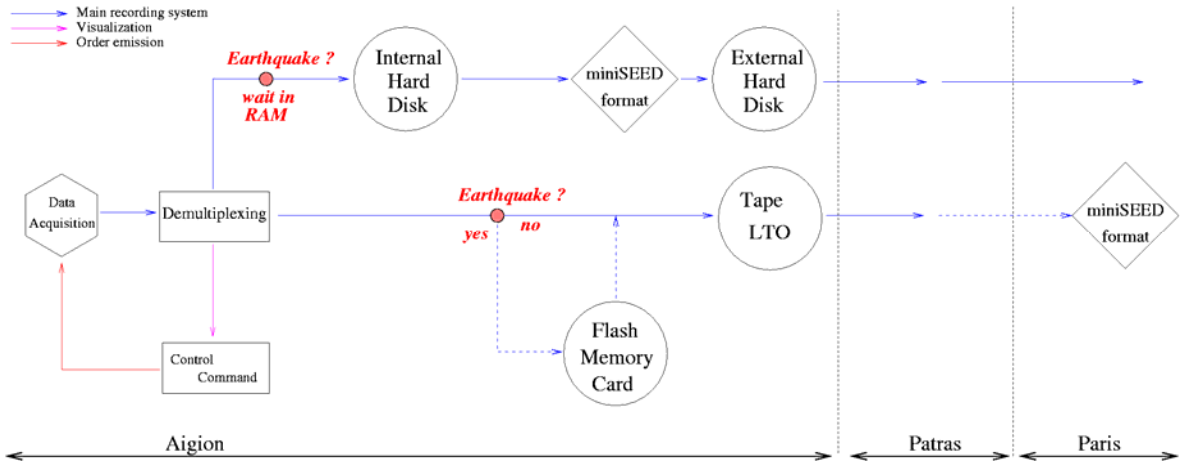

Fig. 5 : Schematic diagram of the data acquisition system

The data acquisition system has been planned with two different permanent recording systems, for safety purposes. The first one records all data as they are and store them on a tape (LTO). The second one compress the data with the miniseed format before storing them on a hard disk. The system can be autonomous for 4 weeks. In the present preliminary phase, an engineer from Patras University goes every three weeks on site for changing the tape and the hard disk. Later, it is planned to connect directly the system with the CRL data base for permanent storage.

Figure 6. The data acquisition system as installed in the shelter in Aigion. Presently the structure is tightened to the shelter frame in order to prevent it from falling in case of strong earthquake.

6.2.2 Equipment deployment and first results

Equipment deployment

As already mentioned in section 3.2, the permanent instrumentation system was to be installed after building a water evacuation system designed to accommodate flows of the order of 75 m^3/h. The program included first a series of straddle packer tests for stress determination purpose, followed by the lowering of the complete instrumentation system. But AIG10 produced flows with rates, of the order of 450 m^3/h, together with a very significant production of solid particles. Figure 7 exhibits samples of the largest pieces of rock produced when flow was at its maximum.

Figure 7 : Samples of rock pieces eroded from the fault gouge because of the high production flow rate.

Although the flow was fairly high, the lowering of the stress measurement tool was undertaken. However, when the packers were inflated in the casing for tool testing, the water pressure displaced the tool (380 kg) upward and some damage was done to the flexible hose. Hence no measurements could be undertaken later on. It was also felt that the solid particle production was too large and was dangerous for operating the tool in the smaller diameter open-hole section. Indeed, it was feared that the rock particles of various sizes would block the straddle packer tool used for stress measurements.

Then the lowering of the permanent instrumentation system was undertaken. But when the seismometer was lowered with a drill rod, the upward force generated by the upward flow was large enough to compensate the weight of the tool. Although we contemplated adding some weight to the equipment, here again it was felt that the solid production would jeopardize the equipment.

It was decided to install only the high pressure packer within the upper part of the casing. This would block the flow and set the dynamic pressure transducer in place for recording the downhole pressure, i.e. the pressure from below the fault. This would also lead to re-injecting the fluid produced below the fault into the formation just above the fault but below the impervious radiolarites. This was done with some difficulty because of the 2.5 tons upward force exerted onto the equipment when the packer started to plug the casing. However, the operation was successful and presently the downhole pressure is being monitored since September 25, 2003, i.e. nearly 3 months after the official end of the DGLab contract. This recording is associated with that of signals produced by the hydrophone and by the low sensitivity accelerometer set on this equipment.

First results

Despite some initial difficulties with running, from Paris, a continuous recording system in Aigion, a fair amount of data has already been obtained during the nearly two months of operation. It is quite premature to provide a detailed analysis of observed signals, but results illustrate the potential of the tool. Different kinds of results have been observed.:

1. While during the months of September and October the mean daily pressure value decreased regularly by more than 10^4 pascal, the trend seems to stabilize in November with the start of the rainy season. This lets us anticipate seasonal variations. Correlation with the rain and snow fall in the Peloponnesus will provide useful information on the aquifer recharge process, and possibly with the occurrence of microseismicity.

2. Periodic pressure variations associated with earth and ocean tides are recorded with excellent resolution. These data will help to ascertain the hydraulic characteristics of the aquifer. Indeed tide gage have been installed in the context of CORSEIS and provide an excellent definition of the exact variations of mean sea level (fig. 8).

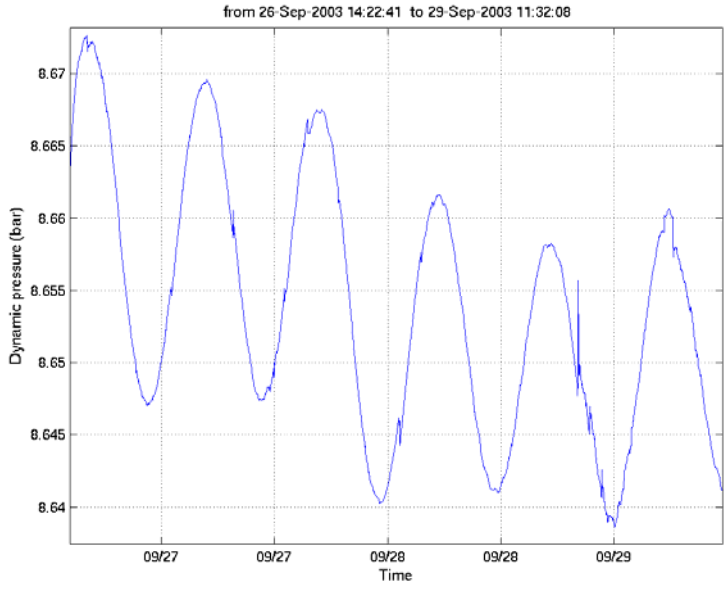

Figure 8 ; Records of pressure variations below 710 m. The periodic variation is induced by earth and ocean tides. Note the overall decrease of pressure with time. Note also the teleseismic (Okaido) event seen on September 28. A similar event is shown with more details on figure 9.

3. Teleseismic events have been recorded simultaneously with the strain meter installed 150 m deep in a borehole in Trizonia Island. The good resolution of the signal will help characterize the aquifer response for periods ranging from a few seconds to tens of minutes (Fig. 9).

4. Signals associated with local earthquakes have also been identified (fig. 11).

5. Finally the hydrophone has recorded some very high frequency signals while the pressure dropped suddenly (fig. 12).

Hence, this equipment yields data on hydro-mechanical coupling effects for periods ranging from a few hundredths of seconds to a few months. Given the karstic characteristics of the aquifer, these should constitute a very unique dataset which may provide useful clues on the regional deformation process.

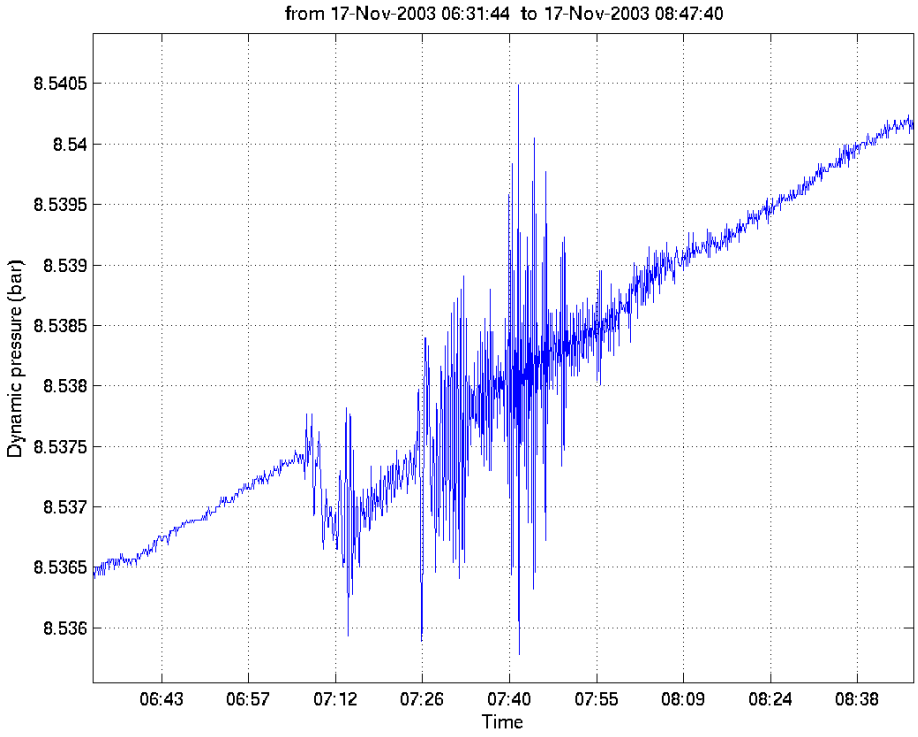

Figure 9. Example of teleseismic (Aleutian) record obtained with the dynamic pressure transducer. Note the sharp decrease of pressure slightly after the onset of the record. Although this may be purely coincidental, similar results have been reported in observatory of the West Coast of the USA. Existing models proposed for explaining this phenomenon will be investigated with the Aigion data set.

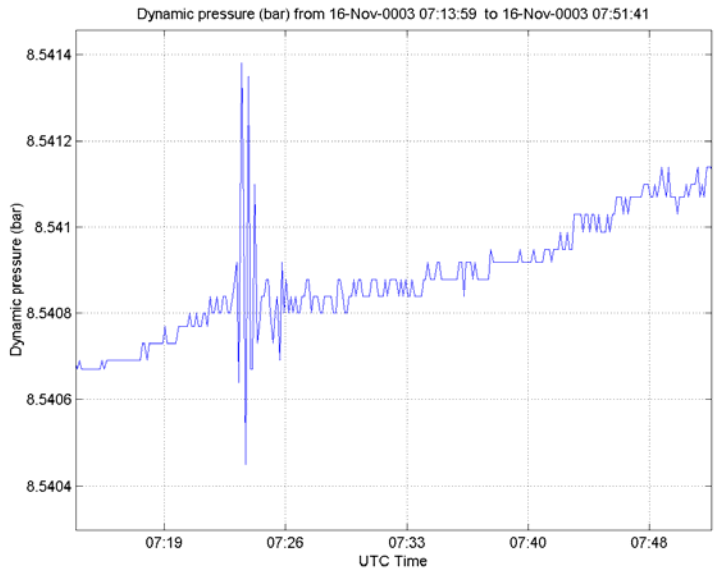

Figure 10 : Example of a pressure signal induced by a local earthquake (Magitude 3.9, located west of Patras). This signal illustrates the dynamic response of the pressure transducer. Its sampling frequency may be increased up to 150 Hz, but then its resolution decreases drastically. An optimization is required, which will be part of the learning process undertaken with this instrumentation.

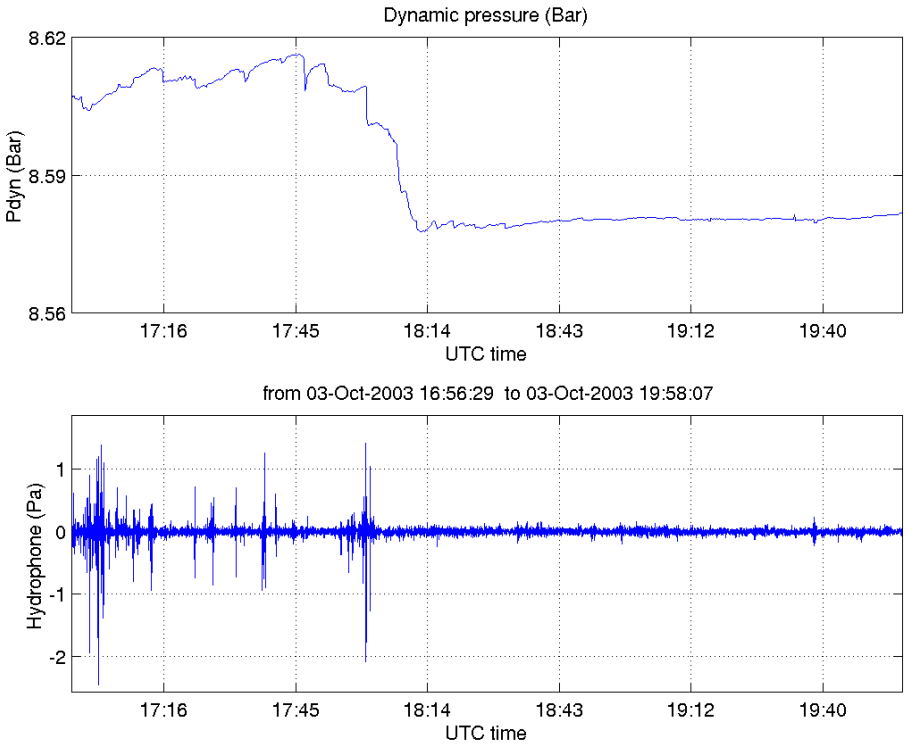

Figure 10 : Variation of downhole pressure observed on October 3, together with the signals seen on the hydrophone. Interestingly, a short drop in pressure is observed simultaneously with an acoustic event. The long term pressure variation is shown on figure 11

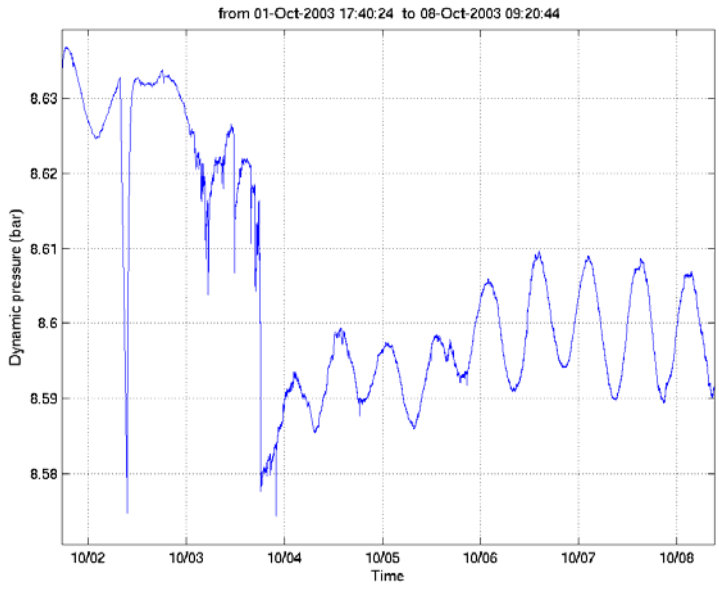

Figure 11 : Downhole pressure variation around October 3. The sudden decrease of pressure is shown in Figure 10. This figure shows the progressive build up of pressure after a deformation process that involved temporary high frequency instabilities.